Real time visualization of cGMP and cAMP dynamics in intact adult cardiomyocytes using new transgenic mice

Doctoral thesis

In partial fulfillment of the requirements for the degree
“Doctor rerum naturalium (Dr. rer. nat.)”
in the Molecular Medicine Study Program
at the Georg-August University Göttingen

submitted

by

Konrad Götz

Born 01.05.1984

Bad Neustadt a. d. Saale

Göttingen 2014

Members of the thesis committee:

Supervisor
Name, Institute: **Dr. rer. nat. Viacheslav O. Nikolaev**, Department of Cardiology and Pneumology, Georg-August University Medical Center Göttingen

Second member of the thesis committee
Name, Institute: **Prof. Dr. med. Michael P. Schön**, Department of Dermatology, Georg-August University Medical Center Göttingen

Third member of the thesis committee
Name, Institute: **Prof. Dr. rer. nat. Peter Rehling**, Department of Cellular Biochemistry, Georg-August University Göttingen

Date of disputation:

Affidavit

Here I declare that my doctoral thesis entitled “Real time visualization of cGMP and cAMP dynamics in intact adult cardiomyocytes using new transgenic mice.” has been written independently with no other sources and aids than quoted.

Furthermore, I confirm that this thesis has not yet been submitted as part of another examination process neither in identical nor in similar form.

Konrad Götz

Göttingen, August 2014

Table of Contents

List of publications

Götz, K.R., Sprenger, J.U., Perera, R.K., Steinbrecher, J.H., Lehnart, S.E., Kuhn, M., Gorelik, J., Balligand, J.L., and Nikolaev, V.O. (2014). Transgenic mice for real-time visualization of cGMP in intact adult cardiomyocytes. **Circulation research** *114*, 1235-1245.

Götz, K.R., and Nikolaev, V.O. (2013). Advances and techniques to measure cGMP in intact cardiomyocytes. **Methods in molecular biology** (Clifton, NJ) *1020*, 121-129.

Belge, C., Hammond, J., Dubois-Deruy, E., Manoury, B., Hamelet, J., Beauloye, C., Markl, A., Pouleur, A.C., Bertrand, L., Esfahani, H., Jnaoui K, **Götz K.R.**, Nikolaev VO, Vanderper A, Herijgers P, Lobysheva I, Iaccarino G, Hilfiker-Kleiner D, Tavernier G, Langin D, Dessy C, Balligand JL (2014). Enhanced expression of beta3-adrenoceptors in cardiac myocytes attenuates neurohormone-induced hypertrophic remodeling through nitric oxide synthase. **Circulation** *129*, 451-462.

Lowther, K.M., Uliasz, T.F., **Götz, K.R.**, Nikolaev, V.O., and Mehlmann, L.M. (2013). Regulation of Constitutive GPR3 Signaling and Surface Localization by GRK2 and beta-arrestin-2 Overexpression in HEK293 Cells. **PloS one** *8*, e65365.

Sprenger, J.U., Perera, R.K., **Götz, K.R.**, and Nikolaev, V.O. (2012). FRET microscopy for real-time monitoring of signaling events in live cells using unimolecular biosensors. **Journal of visualized experiments : JoVE**, e4081.

Acknowledgements

Most of all I would like to thank Slava Nikolaev for giving me the opportunity to come to Göttingen and do a PhD in your laboratory. Thank you for your immense scientific advice, excellent guidance, continuous support and enormous patience during the last 4 years. I highly appreciate the way you leaded your group, supervised my PhD thesis and gave me the opportunity to follow own ideas. I honestly could not have imagined having a better supervisor and mentor.

I am grateful to my thesis committee members Prof. Michael Schön and Prof. Peter Rehling for constructive comments, inspiring discussions and for letting our thesis committee meetings be enjoyable moments.

I am gratefully indebted to Prof. Susanne Lutz, Prof. Kaomei Guan and Prof. Walter Stühmer for accepting to participate in the examination committee.

I am particular thankful to Prof. Michaela Kuhn and Birgit Gassner for advice and great support, especially for the RIA measurements and working heart preparations.

I am gratefully indebted to Joe Greenmann for help with English grammar.

For their excellent technical assistance I would like to thank Anke Rüttgeroth, Karina Zimmermann and Tobias Goldak. Special thanks go to Karina for the histology work, I highly appreciate your social competence, you were the “heart” of our cardiology group. Thanks for organizing the birthday dinners, Betriebsausflüge, christmas parties and so on. Thank you Tobias for great support during the revision of the paper, I deeply apologize for my poor baking qualities.

My special thanks go to my workmates at the Nikolaev group, Julia Sprenger, Ruwan Perera, Zeynep Bastug, Alexander Fröse, Anke Fabian, Daniela Hübscher, Sandra Hofmann and Uta Krieger for the good working atmosphere. I would like to thank all colleagues from the Departments of Pharmacology and Clinical Pharmacology for support and companionship.

Finally, my dearest thanks go to my parents and brother for continuous support and patience with my thesis.

My warmest thanks go to Anita Ongherth for reading and commenting on this work and for your enormous patience with me during the last months.

Abstract

cAMP and cGMP are important second messengers in the cardiovascular system. Previously, it has been demonstrated that the cardiac ryanodine receptor (RyR2) forms a microdomain associated with key contributors of cAMP signaling such as PKA, PDE4D3 and various phosphatases. Its calcium release channel function is highly regulated by cAMP and its effector kinase PKA; hyperphosphorylation of the channel occurs in heart failure and causes arrhythmias. A transgenic mouse model was generated with cardiomyocyte specific expression of the FRET-based cAMP indicator Epac1-camps-JNC. Epac1-camps-JNC is a targeted version of the cytosolic cAMP sensor Epac1-camps by its fusion with junctin protein, which forms a complex with calcium release units to permit locally restricted real time visualization of cAMP dynamics in vicinity of the RyR2. Stimulation of the β_1-adrenergic receptor strongly increased cAMP levels, while the β_2-induced signals were hardly detectable in this microdomain. Furthermore, it was found that PDE3 and PDE4 are the major contributors to local cAMP catabolism. cAMP dynamics recorded with the localized Epac1-camps-JNC were compared with cAMP signaling in the bulk cytosol using cardiomyocytes isolated from Epac1-camps mice. Yet there were no significant differences detectable in cAMP signaling between the cytosol and the RyR2 compartment.

cGMP is another important second messenger which is considered cardioprotective, and the agents that raise cGMP are under investigation in clinical trials for hypertension and heart failure. However, little is known about the spatio-temporal dynamics of cGMP in adult cardiomyocytes. Therefore, a new transgenic mouse model with cardiomyocyte-specific expression of the FRET-based biosensor red cGES-DE5 was generated to allow real time visualization of cGMP dynamics with nanomolar sensitivity in living adult cardiomyocytes. In these cells, basal cGMP levels were amounted to ~10 nmol/L. It was found that they are generated by NO-GC activity and β_3-adrenergic receptors are involved in the regulation of unstimulated cGMP levels. A strong increase upon stimulation of GC-B with CNP was observed, while ANP which stimulates GC-A evoked only minor effects. In contrast, NO donors such as SNAP failed to raise cGMP via activation of NO-GC, most likely due to low expression levels of NO-GC in adult cardiomyocytes. Surprisingly, cGMP degradation was mainly mediated by PDE3 hydrolytic activity, while PDE1, 2 and 5 seemed to be not involved in cGMP turnover. In a model of compensated cardiac hypertrophy, PDE3 remained the major cGMP-PDE and PDE5 activity was upregulated. PDE3 is well known as a major cAMP-PDE and regulator of myocyte contractility. However, it is also established that PDE3 is inhibited by cGMP, since it degrades both cyclic nucleotides with high affinity but has a 10-fold higher catalytic activity for cGMP compared to cAMP. To elucidate the role of PDE3 is

cyclic nucleotide interplay, cardiomyocytes isolated from transgenic mice expressing the cytosolic cAMP sensor Epac1-camps were subjected to FRET-based measurements of cAMP. After β-adrenergic stimulation, application of CNP increased cAMP levels due to cGMP-mediated PDE3 inhibition, thus confirming the major role of PDE3 in cGMP/cAMP crosstalk.

List of figures:

List of tables

Abbreviations

AC	adenylyl cyclase
AngII	angiotensin II
ANP	atrial natriuretic peptide
β-AR	β-adrenergic receptor
ATP	adenosine triphosphate
AWTD	anterior wall thickness in diastole
AWTS	anterior wall thickness in systole
BAY	BAY 60-7550
BCA	Bicinchoninic Acid
BD	binding domain
BDM	2,3-butanedione monoxime
BNP	B-type natriuretic peptide, brain natriuretic peptide
BSA	Bovine serum albumin (BSA)
CaM	calmodulin
CaMKII	Ca^{2+}/calmodulin-dependent kinase II
cAMP	3´,5´-cyclic adenosine monophosphate
CFP	enhanced cyan fluorescent protein
CHD	cyclase homology domain
cGMP	3´,5´-cyclic guanosine monophosphate
cGK	cGMP-dependent kinase
cGKI	cGMP-dependent kinase isoform I
CGP	CGP-20712A
CICR	calcium- induced calcium release
CIL	cilostamide
CNG	cyclic nucleotide-gated ion channel
CNP	C-type natriuretic peptide
CNBD	cyclic nucleotide binding domain
cpEGFP	circularly permuted enhanced GFP
CSQ	calsequestrin
Da	dalton
DEA/NO	Diethylamine NONOate
E. coli	Escherichia coli
EF	ejection fraction
Epac	exchange protein directly activated by cAMP
Epac1-camps	Epac1-camp-sensor

FAS	fractional area shortening
FS	fractional shortening
GFP	green fluorescent protein, T-Sapphire
FlincG	fluorescent indicator of cGMP
Forsk	Forskolin
FRET	Förster resonance energy transfer
GC	guanylyl cyclase
GC-A	guanylyl cyclase A, natriuretic peptide receptor A
GC-B	guanylyl cyclase B, natriuretic peptide receptor B
GC-C	guanylyl cyclase C, receptor for guanylin
GPCR	G-protein coupled receptor
GTP	guanosine triphosphate
HEK cell	Human embryonic kidney 293A cell
HRP	horseradish peroxidase
HW/BW	heart weight body weight ratio
HW/TL	heart weight tibia length ratio
IBMX	3-Isobutyl-1-methylxanthine
ICI	ICI 118,551
ICER	inducible cAMP early repressor
ISO	isoproterenol
KHD	kinase-homology domain
LB	Luria-Bertani
L-NAME	N-Nitro-L-arginine methyl ester
LTCC	L-type Ca^{2+} channel
LV-ESD	left ventricular end-systolic dimension
LV-EDD	left ventricular end-diastolic dimension
mAKAP	muscle A kinase-anchoring protein
8-MMX	8-methoxymethyl-3-isobutyl-1-methylxanthine
min	minute
NPRC	natriuretic peptide clearance receptor
NCX	Na^{+}/Ca^{2+} exchanger
NO	nitric oxide
NO-GC	NO-responsive gunylyl cyclase, soluble guanylyl cyclase
NOS	nitric oxide synthase
ODQ	1H-[1,2,4]oxadiazolo-[4,3-a]quinoxalin-1-one
PCR	Polymerase chain reaction
PDE	phosphodiesterase

PKA	protein kinase A
PLB	phospholamban
PP1	phosphatase 1
PP2A	phosphatase 2a
PROLI-NO	PROLI-NONOate
PWTD	posterior wall thickness in diastole
PWTS	posterior wall thickness in systole
RFP	red fluorescent protein, Dimer2
RIA	radioimmunoassay
ROS	reactive oxygen species
RyR2	cardiac ryanodine receptor
s	second
SR	sarcoplasmic reticulum
SE	standard error
SERCA2a	sarcoplasmic or endoplasmic reticulum Ca^{2+}-ATPase 2a
SNAP	S-Nitroso-N-Acetyl-D,L-Penicillamine
SNP	sodium nitroprusside
TAC	transverse aortic constriction
TAD	tadalafil
TnI	Troponin I (inhibitory)
V_{max}	maximum enyme activity
WGA	wheat germ agglutinin
YFP	enhanced yellow fluorescent protein

1 Introduction

1.1 Cyclic nucleotide signaling and its relevance for physiology

3´,5´-cyclic adenosine monophosphate (cAMP) and 3´,5´-cyclic guanosine monophosphate (cGMP) are ubiquitous second messengers that are involved in the regulation of numerous physiological functions. Since its discovery in 1957,[1] it has been demonstrated that cAMP regulates secretion of insulin in pancreatic β-cells,[2] immune function,[3, 4, 5] learning and memory,[6, 7] gene expression[8, 9] and division of cells.[10] In the heart, cAMP mainly mediates excitatory effects of β-adrenergic receptors on cardiac function.[11] Formation of cAMP is modulated via G-protein coupled receptors (GPCRs), which induce cAMP synthesis through stimulatory G-proteins (G_s) or inhibit cAMP generation via inhibitory G-proteins (G_i). These G-proteins affect adenylyl cyclases (ACs), which catalyzes the conversion of adenosine triphosphate to cAMP. As cAMP effector proteins, cyclic nucleotide gated ion channels (CNGs),[12] exchange protein directly activated by cAMP (Epac),[13] and protein kinase A (PKA)[14] were identified.

cGMP regulates visual and olfactory transduction,[15] renal function by inhibition of aldosterone and renin secretion,[16-18] bone growth,[19] gastrointestinal motility,[20, 21] bladder function,[22] as well as penile erection,[23] metabolism[24, 25] and brown fat cell differentiation.[26] In the central nervous system, cGMP is considered to control a wide range of functions, such as axon guidance[27] and synaptic plasticity.[18, 28] cGMP plays an important role in the cardiovascular system, where signaling by cGMP is involved in the regulation of cardiac contractility,[29] pathological remodeling,[30] platelet function,[31] vascular smooth muscle tone and hence blood pressure.[32] Formation of cGMP is catalyzed by guanylyl cyclases (GCs), in particular by the soluble guanylyl cyclase (NO-GC), which is mainly located in the cytosol and signals through nitric oxide (NO). Membrane-associated guanylyl cyclases (particulate guanylyl cyclases) are the receptors for the hormones atrial (ANP), B-type (BNP), and C-type natriuretic peptides (CNP), and the intestinal peptide guanylin. ANP and BNP are agonists for GC-A, CNP binds to GC-B, and guanylin was demonstrated to affect GC-C activity.[25] However, the family of particulate guanylyl cyclases consists of seven isoforms (GC-A through GC-G), while ligands were identified only for the first four isoenzymes.[33] Three major cGMP binding partners have been identified, namely several phosphodiesterases (PDEs), cyclic nucleotide gated ion channels (CNGs) and cGMP-dependent kinases (cGKs). It was demonstrated that cGMP binds to cyclic nucleotide binding domains present in various PDEs (so called GAF domains, found in such PDEs as PDE2, PDE5, PDE10, and PDE11) to regulate PDE catalytic activity.[34] For instance, it was shown that cGMP, via binding to GAF-B domain, stimulates

PDE2 hydrolytic activity and thus cAMP catabolism by an allosteric process.[35] This mechanism allows interplay of cAMP and cGMP signaling. In addition, cGMP activates CNGs, a mechanism most prominent in the visual and olfactory systems.[36] Last but not least, cGMP mediates phosphorylation of substrates via cGMP-dependent kinases (cGKs).[25]

1.2 cAMP signaling in cardiomyocytes

1.2.1 Cardiac excitation-contraction coupling and its regulation by PKA

In cardiomyocytes, the movement of Ca^{2+} between various subcellular compartments and between cell cytosol and extracellular space facilitates contraction and relaxation of the heart. Myocyte contraction involves electric and contractile components (excitation-contraction coupling).[37] Initially, an electric signal (action potential) depolarizes the surface membrane of a cardiomyocyte (sarcolemma) and activates voltage-gated Ca^{2+} channels (L-type Ca^{2+} channels, LTCCs) to cause an inward Ca^{2+} current (I_{Ca}). LTCCs are located in invaginations of the sarcolemma (T-tubules) in close proximity to the Ca^{2+} release channel (cardiac ryanodine receptor isoform, RyR2) to permit the formation of a local Ca^{2+} signaling complex (couplon).[38] A single couplon contains 10-25 LTCCs and 100-200 RyRs,[39] to allow the calcium-induced calcium release (CICR) from the sarcoplasmic reticulum (SR), which serves as Ca^{2+} storage organelle in cardiomyocytes. However, activation of a single couplon does not affect contractility; it is necessary that all couplons are activated at the same time by an action potential to induce a robust Ca^{2+} transient that activates the contraction machinery.[39] During myocyte contraction (systole), cytosolic Ca^{2+} levels are elevated due to Ca^{2+} influx via LTCCs and Ca^{2+} release from the SR through RyRs. To permit relaxation (diastole), Ca^{2+} is restored into the SR by the sarcoplasmic/endoplasmic reticulum Ca^{2+} ATPase 2a pump (SERCA2a), which is negatively regulated by phospholamban (PLB) and extruded by the Na^{+}/Ca^{2+} exchanger (NCX).[39] A small amount of the Ca^{2+} is extruded by sarcolemmal Ca^{2+}-ATPase and mitochondrial Ca^{2+} uniporter.[38, 40] The amplitude and velocity of Ca^{2+} cycling is ultimately translated into cardiac performance and regulated by catecholamines, which stimulate β-adrenergic receptors (β-AR) and mediate the “fight-or-flight” mechanism.[11] In particular, stimulation of the β_1 subtype results in strong cAMP formation and activation of PKA, which phosphorylates proteins involved in Ca^{2+} cycling. Phosphorylation of the LTCC,[41] PLB,[42] RyR2,[43] and troponin I (TnI)[44] occurs and results in enhanced I_{ca}, increased Ca^{2+} reuptake mediated by SERCA2a, increased Ca^{2+} release from the SR, and altered Ca^{2+} sensitivity of the myofilaments to increase cardiac performance and output (Fig. 1A).

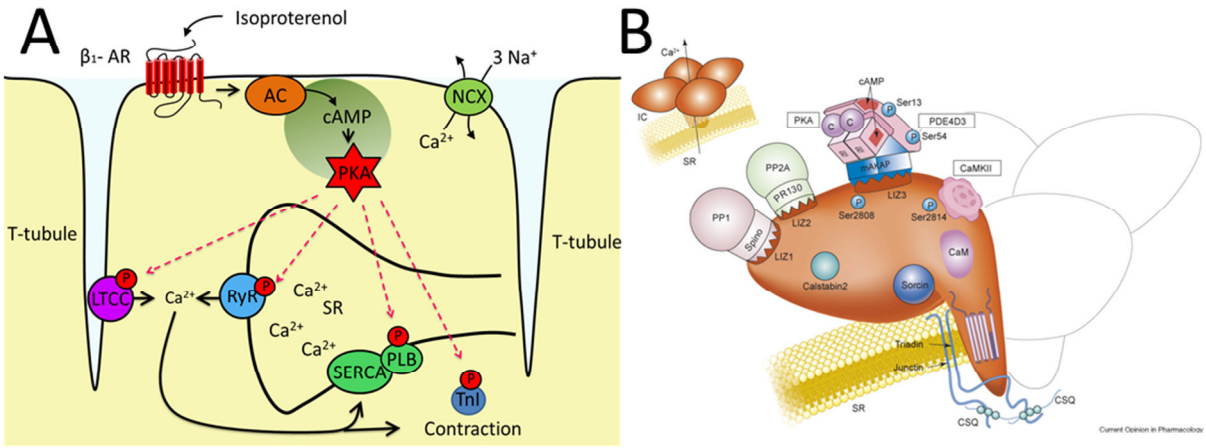

Figure 1. Ca^{2+} cycling and β-adrenergic regulation in cardiomyocytes; the RyR2 signaling complex. (A) Ca^{2+} transients regulate myocyte contraction and relaxation. Cytosolic Ca^{2+} is increased by Ca^{2+} influx through the LTCC (L-type Ca^{2+} channel) and Ca^{2+} release from the SR (sarcoplasmic reticulum) through the RyR (ryanodine receptor). Ca^{2+} is removed to the SR by SERCA (sarcoplasmic/endoplasmic reticulum Ca^{2+}-ATPase), which is regulated by its endogenous inhibitor PLB (phospholamban). Na^{+}/Ca^{2+} exchanger (NCX) is also involved in the regulation of myocyte Ca^{2+} homeostasis. Ca^{2+} cycling itself is modulated by catecholamines (the synthetic catecholamine isoproterenol is shown) to mediate the "fight-or-flight" mechanism mainly via activation of β_1-adrenergic receptors (β_1-AR). PKA phosphorylates the LTCC, RyR, PLB and TroponinI (TnI). Phosphorylation of TnI affects Ca^{2+} sensitivity of the myofilaments (myoficaments are not shown in the cartoon). **(B)** The RyR2 is a tetrameric ion channel and consist of 4 identical subunits arranged around a pore region. Each subunit contains a short C-terminal transmembrane segment, associated with junctin, triadin and calsequestrin (CSQ), and a cytosolic foot-shaped domain that serves as a scaffold to complex regulatory proteins and enzymes. Calstabin2, protein kinase A (PKA), Ca^{2+}/calmodulin-dependent kinase II (CaMKII), PDE4D3, phosphatases 1 and 2a (PP1 and PP2A), calmodulin (CaM), and sorcin are associated with the N-terminal domain. PKA and CaMKII phosphorylation sites are shown at serine 2808 and 2814, respectively. The schematic illustration of the RyR2 signaling complex was taken from Lehnart *et al.*[45]

1.2.2 Local cAMP signaling at the RyR2

In cardiomyocytes, the concept of cAMP microdomains is highly relevant since cAMP is not uniformly distributed within the cell but is rather organized in subcellular compartments. Initially, it was found that agonists of β-adrenergic and prostaglandin receptors both caused an increase in cAMP and PKA activity in the cytosolic fraction of homogenates from rabbit myocytes. In contrast, only β-AR agonists affected cAMP and PKA activity in the particulate fraction, while stimulation of prostaglandin receptors could not, although both agonists led to comparable cAMP amounts produced in whole cell lysates.[46] Since then, a wealth of information has provided proof for the existence of subcellular cAMP compartments or microdomains (there are also few studies on cGMP microdomains), where cyclic nucleotide signaling occurs in a spatially and temporally highly defined manner.[47-49] Key components involved in the formation of cAMP microdomains are PDEs and local pools of effector

kinases and receptors. The RyR2 has been associated with various regulatory proteins and assumed to be highly regulated by local cAMP levels.[43, 50, 51] The concept of cAMP compartmentation will be illustrated by dissection of the RyR2 signaling complex (Fig. 1B).

The cardiac RyR2 is a homotetrameric ion channel and consists of 4 identical subunits of ~565 kDa each (and ~2 mega Da size for the entire channel), which are arranged around a pore region to gate Ca^{2+} ions.[37, 45] Each subunit consists of a relatively short C-terminal transmembrane segment and a huge cytosolic foot-shaped domain, which serves as a scaffold for a complex of regulatory proteins and enzymes.[37, 52] The C-terminus in the SR lumen has been associated with triadin and junction, which anchor the Ca^{2+} binding protein calsequestrin (CSQ) to the RyR2 to form a quaternary complex, termed Ca^{2+} release unit.[37, 53, 54] It was demonstrated that calstabin2,[55] PKA,[43] Ca^{2+}/calmodulin-dependent kinas II (CaMKII),[56] phosphodiesterase 4D3 (PDE4D3),[50] phosphatases 1 and 2a (PP1 and PP2A), calmodulin protein (CaM), and sorcin are associated with the N-terminal domain.[37] Calstabin2 is a 12.6 kDa polypeptide that binds to the RyR2 and stabilizes the closed state of the channel. One calstabin2 molecule can bind per RyR2 subunit.[45] The PKA is associated to the RyR2 macro complex via muscle A kinase-anchoring protein (mAKAP).[37] The cytosolic RyR2 domain provides leucine/isoleucine zipper motifs to facilitate binding of mAKAP. PKA phosphorylates the RyR2 at serine position 2808 (Ser2809 in the human sequence), whereas another phosphorylation site at serine 2030 is discussed.[57] In addition, PDE4D3[50] and phosphatases[58] are targeted to the RyR2 signaling complex and locally regulate cAMP levels and PKA activity, respectively. CaMKII-mediated phosphorylation of the RyR2 at serine 2814 has been demonstrated.[56] It is worth mentioning that channel phosphorylation regulates the RyR2, without directly opening or closing the channel, but modifies the sensitivity of the channel to its physiological ligand Ca^{2+}. Finally, calomdulin and the 22 kDa protein sorcin have been found to inhibit RyR2-dependent Ca^{2+} release[59] and to be involved in channel closure after Ca^{2+} release.[37, 60, 61]

1.2.3 PKA-mediated Ca^{2+} leak hypothesis

Over the past 15 years, diastolic Ca^{2+} leak through dysfunctional RyRs has been recognized as an important mechanism in heart failure. Initially, Marks and colleagues postulated that chronic hyperphosphorylation of serine 2808 by PKA causes depletion of calstabin2 from the RyR2, which results in increased sensitivity to Ca^{2+} and open probability of the receptor during diastole.[43] Thus, PKA-dependent hyperphosphorylation causes leaky RyRs, which decrease SR Ca^{2+} content and cause arrhythmias during heart failure. Indeed, catecholaminergic overstimulation is a hallmark of heart failure,[11, 62] but it is also a dogma that β-adrenergic receptors are downregulated and cAMP levels are decreased during heart

failure.[63, 64] A possible explanation is that remodeling causes local depletion of PDE4D3 and phosphatases from the RyR2 macrocomplex[50], leading to increased phosphorylation of the RyR2, while global cAMP levels are decreased. However, this hypothesis is highly controversial, and hyperphosphorylation of Serine 2808, which causes calstabin2 dissociation from the RyR2, has been challenged by several other studies.[65-67]

1.3 cGMP signaling in cardiomyocytes

1.3.1 cGMP formation by guanylyl cyclases

cGMP formation is catalyzed by guanylyl cyclases, located in the cytosol or associated with the cellular membranes. The major role of gaseous NO and its receptor NO-GC is highly appreciated in the vascular system, but it became obvious that the NO/NO-GC/cGMP signaling pathway also directly affects cardiomyocyte function. In such a setting, NO derived from cardiac endothelial cells, diffuses into surrounding cardiomyocytes or NO generation occurs within cardiomyocytes.[68] Although, NO donor effects on heart function have been controversial, there is a growing body of evidence that suggests positive effects on contractility after stimulation with low amounts of NO,[69-71] while higher levels exert a negative inotropic response.[72-74] The postulated mechanism for the negative inotropic response includes cGKI-dependent phosphorylation of TnI, causing a decreased responsiveness of the myofilaments to Ca^{2+}.[75] It was recently demonstrated that stimulation of β_3-adrenoceptors causes a negative inotropic response in the human or mouse ventricle that is mediated via an NO-dependent mechanism.[76, 77] Finally, NO donor-derived cGMP attenuates β-adrenergic responses[75] and signaling of cGMP is thought to induce a protective brake for the heart after catecholaminergic stimulation.

In general, NO is released from NO-generating drugs (NO-donors) or is endogenously synthetized by oxidation of the amino acid L-arginine to L-citrulline and NO, which is catalyzed by NO synthase activity (NOS).[78, 79] The family of NOS enzymes consist of 3 isoforms, including neuronal NOS (nNOS or NOS1), inducible NOS (iNOS or NOS2) and endothelial NOS (eNOS, NOS3), with all of them expressed in cardiac myocytes.[80] eNOS and nNOS are activated by Ca^{2+}/calmodulin complex, while iNOS activation is mediated by cytokines.[78, 81] NO stimulates NO-GC catalytic activity a several hundred-fold, causing an increase in cGMP concentrations. NO-GC is a heterodimeric enzyme that consists of one α and one β subunit, the α1 β1 heterodimer is the most highly abundant isoform and physiologically relevant.[82] The heterodimer contains a prosthetic heme group with a ferrous iron, located at the N-terminus of the β1 subunit. NO coordinates to the heme moiety and activates NO-GC in a rapid manner at nanomolar concentrations.[79] Regulation of NO-GC

activity is complex, and it has been shown that NO binds to the heme to form a six-coordinate complex (His105-Fe^{II}-NO), which is not stable and turns into a five-coordinate complex (Fe^{II}-NO).[83] Breakage of the bond between histidine 105 of the β subunit and ferrous iron of the heme cofactor leads to a conformational change in the catalytic domain of the protein and causes an increase in cGMP formation.[79, 84] A low-activity complex has been identified at low NO concentrations and a high-activity complex at elevated NO.[79, 85] In the presence of Mg^{2+} and guanosine triphosphate (GTP) or the reaction products (Mg^{2+}, cGMP, pyrophosphate PP_i), the high-activity complex is preferentially formed,[86] while the presence of adenosine triphosphate (ATP) benefits the formation of the low-activity complex.[87] However, functional NO-GC activity and effective cGMP synthesis is strongly dependent on nitroso-redox balance.[88] Oxidative stress is associated with cardiovascular disease and causes the formation of reactive oxygen species (ROS). NO reacts with superoxide radical (O_2^-) to form peroxynitrite ($ONOO^-$), which has been shown to decrease NO-GC sensitivity.[89, 90] Hence, ROS interferes with NO-GC/cGMP signaling via scavenging of NO and causes insensitive NO-GC.[91] In addition, other mechanisms explaining depressed NO-GC/cGMP signaling have been proposed.[84, 91-93] It was demonstrated that oxidized NO-GC loses its heme group and is susceptible to degradation. Stasch *et al.* introduced the compound BAY 58-2667 (Cinaciguat), which is capable of activating oxidized NO-GC in a heme-independent manner.[91]

The natriuretic peptide hormones ANP, BNP and CNP induce cGMP generation through binding to its membrane-associated guanylyl cyclase receptors that catalyze cGMP formation.[94] These enzymes form the family of particulate guanylyl cyclases, which comprise a common topology[33] that includes an extracellular ligand-binding domain, a short hydrophobic membrane-spanning region, and an intracellular region. The intracellular region contains a kinase-homology domain (KHD), a hinge region, and a C-terminal cyclase homology domain (CHD).[95] The role of the KHD is incompletely understood, the hinge region is involved in the formation of dimers and higher oligomers, which are required for an active enzyme. Finally, the CHD catalyzes the conversion of GTP into cGMP.[95]

ANP is synthesized and stored as a pre-hormone, mainly in atrial myocytes and released as mature hormone upon atrial wall stretch.[96] In the circulation, ANP is strongly involved in the regulation of arterial blood pressure and blood volume in an endocrine manner through stimulation of GC-A activity in various tissues.[95] The main effects include relaxation in specific vascular beds,[97] counteraction of the renin-angiotensin-aldosterone- and sympathetic system and stimulation of renal diuresis.[95 98] Mice with absent ANP or lacking the GC-A receptor showed salt-resistant hypertension,[32, 99] while transgenic mice with elevated ANP levels or global overexpression of GC-A revealed an opposing effect; namely,

a decrease in arterial blood pressure.[100, 101] However, it became clear that ANP also directly influences cardiac myocytes, which is relevant in cardiovascular disease such as heart failure, where ANP and BNP levels are highly elevated.[95] BNP is mainly synthesized in ventricular myocytes,[96] circulating BNP plasma levels are significantly lower than those of ANP,[102] and BNP shows lower affinity for GC-A receptor compared with ANP.[103] Despite the fact that both peptides share the same receptor, mice with targeted disruption of BNP lacked hypertensive and hypertrophic phenotypes but revealed severe cardiac fibrosis.[104] Given the fact that cardiac fibroblasts express high levels of GC-B,[105] BNP is most likely induced to counterbalance fibrosis during heart failure and is less involved in the regulation of blood pressure homeostasis.

CNP is mainly synthesized in the vascular endothelium[106] and exerts effects through its receptor GC-B. In contrast to ANP, CNP has only little effect on the blood pressure[107] and is found only in trace amounts in the blood. Hence its endocrine function might be minor, and more local paracrine effects have been postulated for CNP. GC-B is abundant in the vasculature, bone, brain, at high levels in cardiac fibroblasts,[95 108] and is also expressed in cardiomyocytes.[109-111] Disruption of the CNP encoding gene caused severe dwarfism in mice,[19] while mice lacking the natriuretic peptide clearance receptor (NPRC), showed bone overgrowth due to decreased CNP degradation.[112] CNP synthesis was reported in the hearts of patients with chronic heart failure,[113] and GC-B-mediated cGMP formation was detected in myocardium from heart failure patients.[114] Finally, CNP has been shown to affect heart contractility, whereas ANP does not.[29, 78, 115, 116]

1.3.2 cGMP degradation by phosphodiesterases

Degradation of cGMP levels is mediated via PDE hydrolytic activity. PDEs are grouped into 11 families, expression and functional roles in cGMP signaling has been described for PDE1, 2, 3 and 5 in cardiomyocytes.[117, 118]

Isoform	Substrate Specificity	K_m (µmol/L)		V_{max} (purified) (µmol/min/mg)		Reference
		cGMP	cAMP	cGMP	cAMP	
PDE1A	cAMP<cGMP	2.6-3.5	72.7-124	50-300	70-450	119-122
PDE1B	cAMP<cGMP	1.2-5.9	10-24	30	10	123, 124
PDE1C	cAMP=cGMP	0.6-2.2	0.3-1.1	-	-	125, 126
PDE2A	cAMP=cGMP	10	30	123	120	127, 128
PDE3A	cAMP>cGMP	0.02-0.15	0.18	0.34	3.0-6	129, 130
PDE3B	cAMP>cGMP	0.28	0.38	2.0	8.5	131
PDE5A	cAMP<cGMP	2.9-6.2	290	1.3	1.0	132-134

Table 1. Biochemical characterization of PDE enzyme kinetic properties; K_m is the Michaelis-Menten constant, V_{max} describes the maxiumum enzyme activity, - no information available; modified from Bender *et al.*[118]

The PDE1 family (often referred as the "Ca^{2+}/calmodulin-dependent PDE") constitutes 3 isoforms (PDE1A, PDE1B and PDE1C), with all of them showing dual substrate specificity. PDE1A and PDE1B preferentially degrade cGMP over cAMP, while PDE1C hydrolyzes both cyclic nucleotides with equal affinity.[135] PDE1 is unique due to the fact that it can be activated by Ca^{2+}/calmodulin (Ca^{2+}/CaM) complex and thereby decreases cyclic nucleotide levels.[80] The PDE1 enzymes contain an inhibitory domain which, when interacting with the catalytic domain, causes less active enzyme. Binding of Ca^{2+}/CaM releases the catalytic domain and relieves the inhibition of cyclic nucleotide hydrolysis.[121] In addition, its catalytic activity is negatively influenced by phosphorylation through PKA and CaMKII, leading to decreased recruiting of Ca^{2+}/CaM and hence slower cyclic nucleotide degradation.[121, 136] PDE1C is highly expressed in human cardiomyocytes,[137] while PDE1A is the predominant isoform in rodent myocytes.[138] Despite the fact that PDE1 is strongly involved in cyclic nucleotide breakdown in human myocardium,[137, 139] little is known about its physiological effects in the heart, mainly due to the lack of highly specific PDE1 inhibitors.[78]

The PDE2 family (often referred as the "cGMP-stimulated PDE") is encoded by a single gene and consists of 3 isoforms (PDE2A1-3), which differ in their subcellular localization. PDE2A2 and PDE2A3 are membrane associated, whereas PDE2A1 lacks an N-terminal localization motif and is cytosolic.[117] PDE2 can hydrolize cAMP and cGMP with high catalytic activity (high V_{max}), while it shows low affinity (low K_m) for both cyclic nucleotides.[118] Highly remarkable is the fact that cGMP can activate PDE2 catalytic activity, which is mediated through binding of cGMP to regulatory GAF-B domains.[34] Therefore, PDE2 is often referred to as the cGMP- stimulated PDE. Its contribution to total cGMP hydrolysis is considered to be moderate, but it has been shown that PDE2 is strongly involved in cGMP/cAMP interplay

after β-adrenergic activation. Thus, cAMP levels induced by catecholamines can be counterbalanced by PDE2 cAMP catabolism, which is strongly regulated by cGMP. Initially, it was reported that cGMP does not affect LTCC-gated Ca^{2+} currents in cells from frog ventricle at basal state, but decreases these after β-adrenergic stimulation, and this effect is mediated by stimulation of PDE2.[140] Mongillo *et al.* showed that catecholamines increase cAMP through stimulation of $\beta_{1/2}$-adrenergic receptors, in parallel cGMP is synthetized due to activation of the β_3-AR, and this specific pool of cGMP activates PDE2 hydrolytic activity and shapes the concomitant cAMP signal.[35] Furthermore, PDE2 has been associated with the plasma membrane in neonatal rat cardiomyocytes[35], and it was demonstrated that PDE2 is a key regulator of cyclic nucleotide compartmentation in neonatal and adult rat cardiomyocytes. Castro *et al.* showed that PDE2 regulates cGMP levels, produced by GC-A.[49, 141]

The PDE3 family contains PDE3A1/2/3 and PDE3B isoforms. PDE3B is associated with the particulate fraction, and PDE3A is found in the soluble and particulate fractions. Both isoenzymes are regulated by PKA phosphorylation to increase its catalytic activity.[118] PDE3 is a dual substrate enzyme and shows high affinity for both cyclic nucleotides but hydrolyzes cAMP with a 10-fold higher catalytic activity compared to cGMP. Thus cGMP can act as a competitive inhibitor to cAMP catabolism and PDE3 is often referred as “the cGMP-inhibited PDE”.[118] It has been established that PDE3 is a major contributor to total cAMP breakdown in cardiomyocytes, and is strongly involved in the regulation of contractility.[142] Indeed, peripheral vasodilating actions and positive inotropic effects made inhibition of PDE3 a promising target for heart failure drugs. However, despite positive actions on hemodynamics and heart function, long-term treatment with inhibitors of PDE3 caused increased mortality in heart failure patients mainly due to arrhythmias and sudden cardiac death.[143] So far, milrinone in intravenous dosage form is approved for short-term treatment of acute cardiogenic shock. Importantly, downregulation of PDE3 was reported in a mouse model of pressure overload and in heart failure patients, which was associated with increased cardiomyocyte apoptosis. As a possible mechanism, an upregulation of the proapoptotic transcriptional repressor ICER (inducible cAMP early repressor) due to PDE3 downregulation was postulated.[144] Furthermore, a cardioprotective role of PDE3A was observed after ischemia/reperfusion injury in mice.[145]

PDE5 (also referred as the “cGMP-specific PDE”) is probably the most well characterized cGMP-PDE, and its selective inhibitors (sildenafil, tadalafil, vardenafil) are approved for the treatment of erectile dysfunction and pulmonary hypertension. PDE5A is highly abundant in the lung, corpus cavernosum, platelets and vascular smooth muscle cells.[117] In the heart muscle, PDE5 expression and cGMP turnover is low,[146] but becomes elevated during

hypertrophy and heart failure.[30] The PDE5 family consists of 3 isoforms (PDE5A1-3) and hydrolyzes exclusively cGMP, with high affinity and selectivity. PDE5 hydrolytic activity is tightly modified by its substrate cGMP, which acts as an activator of enzyme catalytic activity. Association of cGMP to its specific binding domains (GAF-A domain) results in a ~10-fold increase in the catalytic activity of PDE5.[118, 147] At high cGMP, cGKI phosphorylates the PDE5 to further raise catalytic activity and cGMP affinity of cGMP to the allosteric binding site (GAF-A domain).[117] There is good evidence that PDE5 is an important mediator in cGMP compartmentation. Takimoto and colleagues showed that PDE5 activity is tightly associated with NOS3, and this specific coupling of cGMP generation and degradation is required to affect contractility. Inhibition of PDE5 in mice had minimal impact on basal heart function. However, after β-adrenergic stimulation, sildenafil markedly blunted inotropic response. This effect was strongly dependent on NOS3 activity, since sildenafil failed to attenuate contractility in mice with deleted NOS3. The mechanism included cGKI-dependent phosphorylation of TnI, to counterbalance contractility. Finally, it was demonstrated that the majority of PDE5 enzymes are localized to the Z-bands of the sarcomere, in close proximity to NOS3. NOS3 KO mice and treatment with a NOS inhibitor caused a diffuse PDE5 expression pattern. Notably, inhibition of the redistributed PDE5 failed to suppress catecholamine-induced contractility.[148] Castro *et al.* showed that NO-GC-induced cGMP pools are regulated by PDE5 hydrolytic activity in adult rat cardiomyocytes *in vitro*, while cGMP generated by GC-A activity were controlled by PDE2, further supporting the major role of PDE5 in compartmentalized signaling of cGMP.[49]

1.3.3. cGMP-dependent kinase

cGMP activates its effector kinase cGK, which mediates phosphorylation of proteins (see Fig. 2). Most prominent are phosphorylation of TnI and PLB, which are strongly involved in the regulation of myocyte contraction and relaxation (see Fig. 1A).[149, 150] The cGK belongs to the family of serine/threonine kinases, and cGKI is the predominant isoform in the cardiovascular system. The architecture of cGKs includes an N-terminal domain, a regulatory domain (cGMP binding domain) and a C-terminal catalytic domain. The N-terminus is encoded by 2 exons that are translated into cGKIα and cGKIβ splice variants, whith the cGKIα the dominant isoform expressed in cardiomyocytes.[18] However, the N-terminal domain is involved in the formation of dimers (cGKIs are homodimers) and subcellular localization. The regulatory domain contains two in-tandem cGMP binding sites (A+B). Binding of cGMP induces a conformational change that results in a more elongated structure of the kinase, a feature that has been exploited for the generation of several cGMP biosensors. The catalytic domain mediates phosphorylation of serine and threonine residues in target proteins.[18]

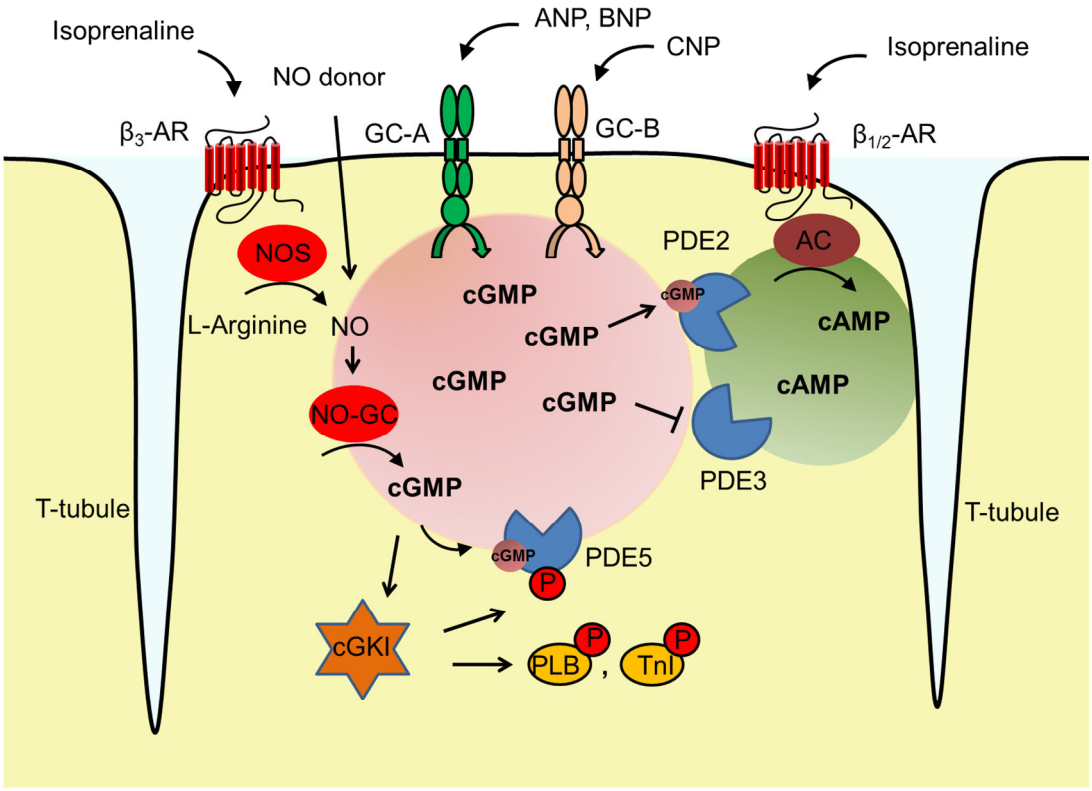

Figure 2. cGMP dynamics in cardiomyocytes. Guanylyl cyclases (GCs) catalyze the formation of cGMP. Natriuretic peptides ANP, BNP activate GC-A; GC-B is the receptor for CNP. NO binds to NO-GC, the β_3-adrenergic receptor (β_3-AR) is associated with eNOS (NOS) which catalyzes the conversion of L-arginine to NO. cGMP activates its effector kinase cGKI which phosphorylates phospholamban (PLB), troponin I (TnI) and PDE5 (more targets of cGKI have been identified such as VASP, but are not shown in the cartoon). cGMP synthesis is counterbalanced by phosphodiesterase (PDE) hydrolytic activity. Finally, cGMP modifies cAMP levels via PDE2 and PDE3 to facilitate a crosstalk between both cyclic nucleotides; cAMP is generated by adenylyl cyclase (AC) activity.

1.3.4 cGMP signaling in cardiac hypertrophy

Cardiac hypertrophy is a mechanism of the heart to adapt to wall stress. Increased hemodynamic overload or decreased contractile force after myocardial infarction causes wall stress and elevated oxygen consumption, which is counterbalanced by cardiac growth and results in compensative thickening of the walls to sustain cardiac performance. However, the initially adaptive process can become maladaptive and ultimately leads to cardiac disease. The so-called fetal gene program is induced which leads to increased protein generation, changes in the organization of the sarcomere and enhanced cardiomyocyte size.[151] On the molecular level, various signaling and transcription pathways are activated during hypertrophy.[30] For instance, stimulation of angiotensin II, endothelin 1 and α-adrenergic receptors, which are coupled to $G_{q/11}$-proteins causes cardiac hypertrophy.[152] These pathways stimulate a remodeling process that induces disturbed Ca^{2+} cycling and morphological alterations; and is directly translated into heart failure and malignant

arrhythmias. However, it is widely appreciated that signaling of cGMP inhibits hypertrophy, and thereby protects the heart from pathological myocyte remodeling.

Initially, Calderone *et al.* found that ANP and NO donor attenuate norepinephrine-induced hypertrophy in cultured neonatal rat cardiomyocytes and fibroblasts, and that the ANP and NO effects on hypertrophic growth were mimicked by the cGMP analogue 8-bromo-cGMP.[153] Following these observations, a growing body of evidence suggests that cGMP formation after natriuretic peptide and NO stimulation, or after inhibition of its degradation, blunts pathological hypertrophy. Recently, β_3-adrenoceptors, which are well known to regulate metabolism,[154] gained great attention in the cardiovascular field and were proposed as potential targets to counterbalance hypertrophy and heart failure.[155] This was based on the remarkable finding, that stimulation of β_3-adrenoceptors causes a negative inotropic response[76] and on the observation that this receptor is upregulated in human heart failure.[156] Furthermore, receptor activation requires high amounts of catecholamines (which are a hallmark of heart failure), and the β_3-adrenoceptor is resistant to downregulation.[157] These characteristics are in clear contrast to those of the β_1-AR, which is considered to induce a short-term positive effect on contractile force and heart beating frequency, while an overload of catecholamines is associated with receptor downregulation and detrimental effects on the long-term goal.[11] Very recently, it was demonstrated that overexpression of the β_3-AR attenuates catecholamine- and angiotensin II-mediated hypertrophy via NOS mechanism.[158]

Global GC-A knock-out mice develop a hypertensive phenotype, which is associated with cardiac hypertrophy.[159] Therefore, transgenic mice with cardiomyocyte-restricted deletion of GC-A were developed to elucidate anti-hypertrophic effects of ANP independent of blood pressure. These mice showed mild cardiac hypertrophy at baseline and inflated hypertrophic growth reaction after transverse aortic constriction[160] and treatment with angiotensin II.[161] In line with these observations, transgenic mice expressing a constitutively active GC-A mutant had increased cGMP levels within cardiomocytes and were protected against isoproterenol treatment and aortic banding.[162] Antifibrotic and, more recently antihypertrophic characteristics have also been attributed to CNP, since *in vitro* data in cultured cardiomyocytes showed that CNP locally counter-regulated hypertrophy in adult rat cardiomyocytes.[111] These observations were confirmed by *in vivo* studies using a myocardial infarction model in CNP-overexpressing mice[163] and in rats with CNP infusion via osmotic mini pumps.[164] Frantz *et al.* reported that deletion of cGKI in cardiomyocytes causes dilated cardiomyopathy after transverse aortic constriction and angiotensin II treatment. A depressed Ca^{2+} cycling was observed in the cGKI knock-out mice, mainly due to reduced CNP-mediated PLB phosphorylation. These observations suggest that GC-B/cGMP/cGKI signaling

attenuates remodeling and pathological transformation into heart failure by maintaining myocyte Ca^{2+} handling and contractility during hypertrophy.[165]

It has been shown that expression and cGMP catabolism of PDE1[138] and PDE5[166-168] are increased in human heart failure. Thus, it is widely accepted that inhibition of cGMP degradation to elevate cGMP levels is an attractive strategy to antagonize pathological hypertrophy and remodeling. Takimoto *et al.* demonstrated in a landmark paper that the PDE5 inhibitor sildenafil prevents cardiac hypertrophy after aortic banding *in vivo*. Sildenafil was even able to reverse pre-established mild hypertrophy.[30] Cardioprotective effects of PDE5 inhibition were also reported in rodent models of doxorubicin cardiotoxicity[169, 170] and ischemic injury.[171-174] Still, the relevance of cardioprotective sildenafil effects for human heart is controversial, since the main cGMP turnover in human myocardium is attributed to PDE1 and PDE3, and some sildenafil effect might be due to its low selectivity and concomitant inhibition of PDE1.[175] Recently, the results from the RELAX trial revealed that in heart failure patients with preserved ejection fraction, sildenafil treatment showed no significant benefits versus placebo.[176] However, ongoing clinical trials will further elucidate the usefulness of PDE5 inhibition using available oral drugs to treat heart failure. In this context, it is important to mention that the role of PDE1 was further studied, and it has been shown that PDE1A expression is strongly upregulated in various rodent models of cardiac hypertrophy. Likewise, the selective PDE1 inhibition attenuated cardiac hypertrophy *in vitro* and *in vivo*.[138]

1.4 Methods for the visualization of cAMP and cGMP dynamics

1.4.1 Challenges in the detection of cyclic nucleotide fluctuations

Classical measurements of cGMP levels use biochemical techniques such as radioimmunoassays, enzyme-linked immunosorbent assays, and indirect detection of cyclic nucleotides using western blot analysis of substrate phosphorylation by effector kinases.[177, 178] These techniques require cell and tissue lysis and therefore lack information on the subcellular localization of cyclic nucleotide signaling events. In addition, total cyclic nucleotide amounts are detected despite physiologically relevant unbound cyclic nucleotides. Finally, it is worth mentioning that preincubation with IBMX is required in most cases to block cGMP degradation and enhance cGMP amounts to a detectable level during biochemical assays. This is highly relevant for cardiomyocytes, which produce low amounts of cGMP. It is also important to consider that signaling of cAMP and cGMP follows fast kinetics, and cyclic nucleotide fluctuations can occur rapidly and are transient.[179-181] Excessive re-probing is necessary to gain insights into the temporal dynamics using classical biochemical assays and these measurements typically resolve cyclic nucleotide dynamics with a poor resolution

(for instance cGMP amount 1, 2, 5 min after stimulation). To resolve those issues, a number of optical and non-optical techniques which allow visualization of spatiotemporal cAMP or cGMP dynamics in living cells have been described in recent years.

1.4.2 Principle of fluorescence resonance energy transfer

In the past ten years, the Förster/Fluorescence Resonance Energy Transfer (FRET) technique has gained great popularity in the study of biochemical events and protein-protein interactions in living cells (see Fig. 3).

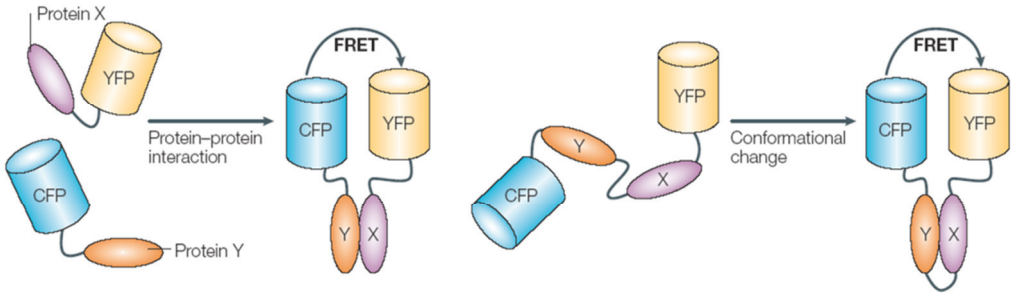

Figure 3. The FRET technique is applied to track cellular events. If donor (CFP) and acceptor fluorescent protein (YFP) come into close proximity, FRET occurs. FRET allows visualization of dynamic protein-protein interactions and conformational changes within a single protein; cyan fluorescent protein (CFP), yellow fluorescent protein (YFP). Figure from Zhang *et al.*[182]

FRET describes a non-radiative energy transfer between two fluorophores. The energy flows from an excited donor fluorescent protein to a nearby acceptor fluorophore through dipol-dipol interactions which results in decreased (quenched) donor- and increased acceptor emission intensity. The occurrence of FRET strongly depends on three conditions. Namely, donor and acceptor have to be in closed proximity to each other, a beneficial orientation of the dipoles is essential, and donor emission spectrum and acceptor excitation spectrum need to overlap.[183] In detail, the efficiency of the energy transfer strongly depends on the distance between the donor and acceptor molecules and varies as the inverse of the sixth power of the distance,[183] as described by the Förster equation:

$$E_{FRET} = 1/[1 + (r/R_0)^6]$$

R_0 is the distance between donor and acceptor fluorescent protein, where 50 % energy transfer occurs, this value can be calculated for each specific pair of fluorescent proteins. Highly notable is the fact that the FRET efficiency falls off with the sixth power, which indicates that FRET happens only within a highly defined distance, and thus FRET can be used as a molecular ruler, i.e. to monitor distances.[184]

R_0 is specific for each FRET pair of fluorescent proteins and is calculated for aqueous solutions as follows:

$$R_0 = \left[2.8 \times 10^{17} \cdot \kappa^2 \cdot Q_D \cdot \varepsilon_A \cdot J\,(\lambda)\right]^{1/6} nm$$

κ^2 is the orientation angle variable and describes the angle between the two dipoles of the fluorophores. FRET efficiency strongly depends on the alignment of the fluorophores to each other. Parallel orientated dipoles of the fluorophores show higher FRET efficiencies compared with a perpendicular orientation. Values from 0 to 4 are theoretically possible, but in general, the value is fixed and close to 2/3. Q_D is the donor quantum yield, ε_A the maximal acceptor extinction coefficient, both values are constants. $J\,(\lambda)$ is the spectral overlap integral, which describes the region between the normalized donor emission spectrum $F_D(\lambda)$ and the acceptor excitation spectrum $E_A(\lambda)$:

$$J\,(\lambda) = \int F_D(\lambda) \cdot E_A(\lambda) \cdot \lambda^4 d\lambda$$

In theory, for an optimal FRET pair, one has to choose a donor with high quantum yield, an acceptor with a strong extinction coefficient, and the donor emission and acceptor excitation spectra have to overlap (Fig. 4).[185]

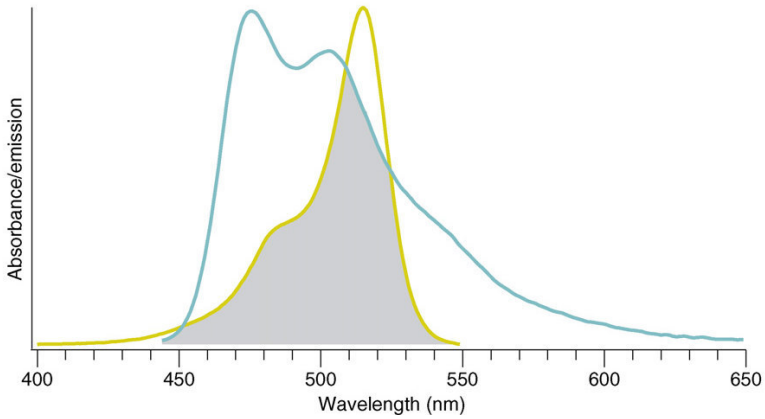

Figure 4. Overlap of CFP emission spectrum and YFP excitation spectrum. The CFP emission spectrum (cyan line) overlaps with the YFP absorption spectrum (yellow line) to allow FRET. The grey area indicates the spectral overlap. Figure from Piston and Kremers.[185]

1.4.3 Biosensors for the visualization of cAMP dynamics

Over the past 20 years, a large number of genetically encoded biosensors have been developed to allow visualization of cAMP dynamics in living cells. The great majority of cAMP indicators are based on the principle of FRET and contain a conformationally sensitive domain (cAMP binding domain) sandwiched between two fluorescent proteins to allow FRET. In most cases, cyan and yellow fluorescent proteins are selected as a FRET pair, but also other variants of green fluorescent protein (GFP) have been used. Biosensors based on PKA,[142, 186, 187] cyclic nucleotide gated ion channels[188] and Epac[189-191] have been developed. These biosensors are introduced into living cells using conventional transfection techniques or viral gene transfer (which is necessary for cardiomyocytes).[48] The probes were extensively used and largely improved the understanding of cAMP signaling and its compartmentation in cardiomyocytes. Highly notable is a transgenic mouse model with ubiquitous expression of the cytosolic cAMP indicator Epac1-camps.[192] This cAMP indicator molecule contains a cAMP binding domain derived from Epac1 sandwiched between CFP and YFP as a FRET pair (Fig. 5).

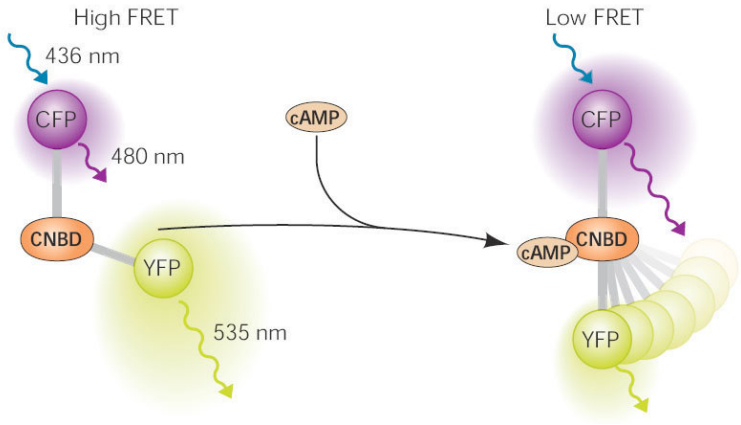

Figure 5. Principle of the Epac1-cAMP-sensor (Epac1-camps). The Epac1-camps is based on a single cAMP binding domain (CNBD) from Epac1 flanked by cyan and yellow fluorescent proteins. At low cAMP levels, donor (CFP) and acceptor (YFP) are in close proximity and FRET occurs. Binding of cAMP to the CNBD induces a conformational change and a concomitant decrease in FRET. Excitation of CFP is at 436 nm, CFP and YFP emission are collected at 480 and 535 nm, respectively. The figure is from Nikolaev and Lohse.[193]

1.4.4 Biosensors for the visualization of cGMP dynamics

In contrast to extensive studies on cAMP dynamics using biosensors for cAMP, far less is known about cGMP, especially in cardiomyocytes. In the following, major cGMP biosensors and some of novel findings obtained using them in the cardiovascular system are briefly reviewed to illustrate the power and potential usefulness of these probes (Table 2).

Sensor	cGMP-binding domain (cGMP- BD)	Fluoro-phores	EC_{50} cGMP (µmol/L)	EC_{50} cAMP (µmol/L)	Selec-tivity	Ref.
δFlincG	Truncated cGKI (cGMP-BD A+B)	cpEGFP	0.17	48	280	[194]
CGY-Del1	Truncated cGKI (cGMP-BD A+B)	CFP/YFP	0.02	0.152	7.6	[195, 196]
Cygnet 2	Truncated cGKI (cGMP-BD A+B)	CFP/YFP	1.9	185	100	[197]
cGi-500 **cGi-3000** **cGi-6000**	Truncated cGKI (cGMP-BD A+B)	CFP/YFP	0.5 3 6	>100 >100 >1000	>200 >30 >166	[180]
cGES-GKIB	Truncated cGKI (cGMP-BD A+B)	CFP/YFP	5	485	97	[196]
cGES-DE2	PDE2 GAF-B domain	CFP/YFP	0.9	115	128	[196]
cGES-DE5	PDE5 GAF-A domain	CFP/YFP	1.5	630	420	[196]
Red cGES-DE5	PDE5 GAF-A domain	GFP/RFP	0.04	>100	>1000	[198]

Table 2. Comparison of various fluorescent cGMP biosensors, EC_{50} and selectivity values are *in vitro* data using recombinant protein. For simplicity, ECFP, EYFP, T-Sapphire and Dimer2 are termed as CFP, YFP, GFP and RFP, respectively. Table has been modified from[196, 199].

Recently, the development of non-FRET-based fluorescent cGMP indicators, termed FlincGs (fluorescent indicators of cGMP) has gained great attention.[194] These biosensors have a single circularly permuted enhanced GFP (cpEGFP) N-terminally fused to a regulatory domain fragment from cGKI. Association of cGMP induces a conformation change that causes an increase in fluorescence intensity of cpEGFP. Initially, two constructs, with regulatory domains from cGKIα and cGKIβ were created and termed α-, β-FlincG. These constructs showed strong increases in fluorescence intensities upon stimulation of recombinant proteins with cGMP, but the signals were strongly reduced after sensor expression in vascular smooth muscle cells (1.2-fold intensity change). However, a truncated version of α-FlincG has an absent N-terminal domain fragment, which mediates the formation of dimers. Thus, δFlincG did not interact with endogenous kinases, leading to a robust change in intensity (3.5-fold increase), even when expressed in primary cells, which makes the δFlincG superior to the other variants. The δFlincG showed high sensitivity, selectivity for cGMP over cAMP and rapid kinetics (see Table 2). The combination of live cell imaging with confocal microscopy was able to unravel spatio-temporal dynamics of cGMP. It was shown that in vascular smooth muscle cells, GC-A induced a cGMP pool that was located at the plasma membrane, while NO-GC evoked global elevations in cGMP. The spatial confined ANP signal could be transformed into a cytosolic one by inhibition of PDE5. Finally, it should be mentioned that these imaging experiments can be carried out at one single emission

wavelength (510 nm), whereas FRET-based biosensors necessitate collecting emission light at two wavelengths using a more sophisticated detection system.[194]

Nevertheless, most of the cGMP indicators are based on the principle of FRET and contain a cGMP-binding domain that is sandwiched between two fluorescent proteins. Two types of cGMP binding domains are known, those found in cGK and cGMP regulated ion channels and cGMP binding domains from PDEs termed GAF domains. Interestingly, the cGMP binding domains are universally grouped in tandem pairs.[180] The first engineered cGMP indicators contained partially truncated cGKI sandwiched between CFP and YFP. The sensor backbone, derived from cGKI contained almost the entire cGKI molecule including the two cGMP binding domains (A and B) and the catalytic domain, with only the N-terminal dimerization domain being deleted. In particular, Sato *et al* described an increase in fluorescence energy transfer upon stimulation in HEK 293 cells using CGY-Del1 probe,[195] while biosensors termed Cygnets, showed a decrease in FRET upon CNP stimulations in lung fibroblasts.[197] Cygnet 2.1, which had the inactivated catalytic domain (threonin 516 was mutated to alanin) and YFP replaced by more pH insensitive Citrine successfully visualized cGMP dynamics in neonatal rat cardiomyocytes[35, 148] and vascular smooth muscle cells.[200] Stangherlin and colleagues created targeted versions of Cygnet 2.1 to compartments where PKA-RI and PKA-RII are located. To do so, they fused the dimerization/docking domains from RIα or RIIβ to the N-terminus of soluble Cygnet 2.1 indicator, to create cGMP biosensors associated either with the soluble or particulate fraction of cell lysates. The RI_Cygnet 2.1 was homogenously distributed, and the RII_Cygnet 2.1 revealed a striated pattern when expressed in neonatal rat cardiomyocytes. Both sensors showed distinct cGMP formation patterns upon identical receptor stimulation in the two compartments.[141] It is important to mention that Cygnet 2.1 acts very slowly and cannot reflect rapid oscillations in cGMP. Nikolaev *et al* demonstrated that the Cygnet 2.1 could not resolve pulsatile stimulations, as those were seen with cGES-DE5, which is based on a single cGMP binding domain from PDE5.[196] In consequence, these “long” cGKI-based biosensors had low sensitivity and poor temporal resolution. To overcome these limitations, simpler versions of the cGKI based sensors were created, such as the cGES-GKIB. This sensor is based on a single cGMP binding domain (B domain of cGKI) but it is not superior to Cygnet 2.1.[196] Finally, a systematic approach to generating cGMP FRET biosensors based on single and tandem cGMP binding domains from cGKI and PDE5 introduced cGi500, 3000 and 6000, which contain the complete tandem cGMP binding domain (A + B domain of cGMP binding domain from cGKI) and cover a wide range of cGMP affinities.[180]

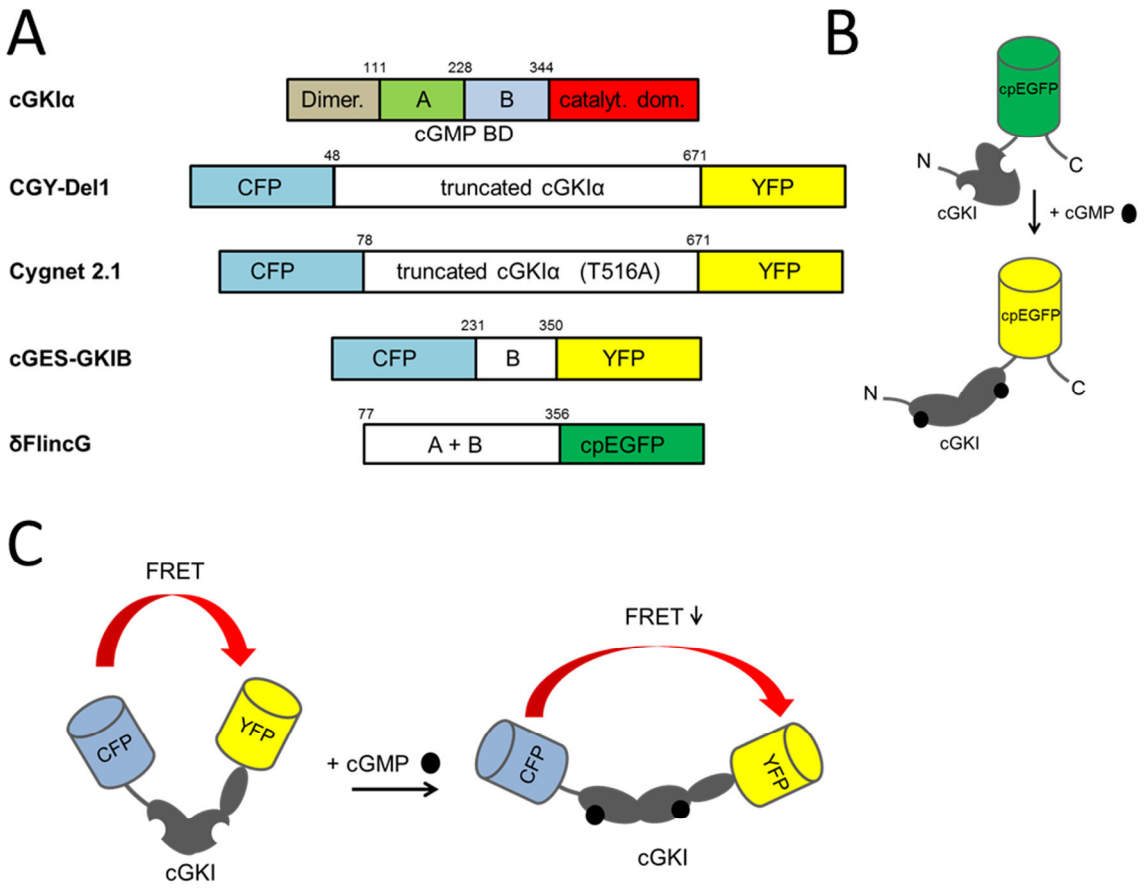

Figure 6. Fluorescent biosensors based on cGMP binding domains from cGKIα. (A) cGKI contains 3 major domains: the N-terminal domain, which is involved in dimerization; the cGMP binding domain (cGMP BD) which contains two in-tandem cGMP binding sites (A and B); and a catalytic domain (catalyt. dom.). The cartoon shows the domain structures of cGKIα, and selected cGMP indicators that are based on various fragments of cGKIα. CGY-Del1 and Cygnet 2.1 contain almost the full cGKI molecule, lacking only the dimerization domain, Cygnet 2.1 has an inactivated catalytic domain. In contrast, cGES-GKIB is based on a single cGMP binding domain, while δFlincG contains the two tandem cGMP binding sites. The information on domain structures was taken from[194-197] **(B)** The cartoon shows the schematic architecture of δFlincG and its activation by cGMP, which is not based on FRET; binding of cGMP causes an increase in fluorescence emission intensity of circularly permuted EGFP (cpEGFP), modified from Nausch *et al.*[194] In contrast, **(C)** shows the schematic structure of Cygnet 2.1, which is a FRET-based biosensor, the catalytic domain is not fully shown, this has been done to allow a better comparison between FRET-based Cygnet 2.1 and non-FRET based δFlincG, which lacks this domain. cGMP binds to the cGMP binding sites causes a conformational change that results in a more elongated molecule. The distance between FRET donor and acceptor increases and results in a decrease in energy transfer.

Biosensors based on single cGMP binding domains of PDE2 and PDE5, namely GAF domains, have been developed. The domain structure of PDEs contains a C-terminal conserved catalytic domain and regulatory domains at the N-terminus.[34] Five of the 11 PDE families have been identified as containing a tandem pair of GAF domains (N-terminal GAF-A and a more distal GAF-B domain). However, in PDE2 cGMP binds to the GAF-B domain, while in PDE5 it is the GAF-A domain. cGES-DE2 is based on the single GAF-B domain of PDE2A and showed a relatively high affinity for cGMP, but was inferior to cGES-DE5, which

showed a higher selectivity for cGMP over cAMP.[196] Finally, the replacement of the CFP/YFP FRET pair by T-Sapphire/Dimer2 led to an unexpected increase in cGMP affinity, with retained selectivity and rapid kinetics (Table 2, Fig. 7).[198]

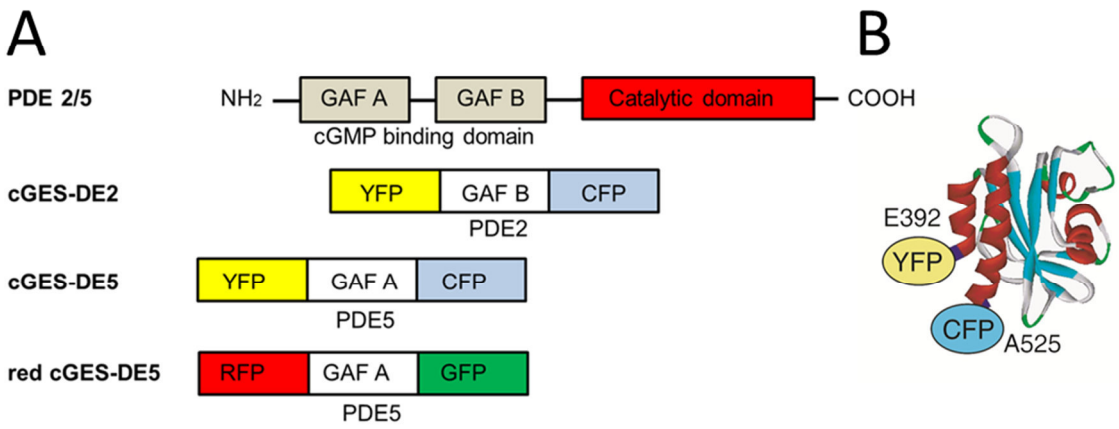

Figure 7. Fluorescent biosensors based on cGMP binding domains from PDEs. (A) PDE2 and PDE5 contain N-terminal cGMP binding domains (GAF-A and GAF-B) and a C-terminal catalytic domain. The selected biosensors are based on a single cGMP binding domain (GAF domain) from PDE2 or PDE5. Red cGES-DE5 contains Dimers2 (designated for simplicity as RFP) and T-Sapphire (GFP) as FRET pair, all shown biosensors are based on FRET. The information on domain structures was taken from [34, 196]. **(B)** The model structure of cGES-DE2 is based on a single cGMP binding domain of PDE2 (amino acids E392 to A525; the crystal structure is shown) flanked by YFP and CFP, figure from Nikoalev *et al.*[196]

Finally in 2006, Castro and colleagues reported measurements of cGMP dynamics in cultured adult rat cardiomyocytes using the α-subunit of rat olfactory cyclic nucleotide-gated (CNG) channel as a sensor for non-optical and indirect cGMP recordings. Electrophysiological measurements of cGMP-induced ion currents (I_{CNG}) were performed and revealed compartmentalized cGMP signals. In particular, it was detected that GC-B-induced cGMP resides at the plasma membrane and is regulated by PDE2, while cGMP that was synthetized by NO-GC is located in the cytosol and under control of PDE5 hydrolytic activity.[49] Moreover, the same group demonstrated that cGKI is involved in the cGMP compartmentation via a negative feedback mechanisms, using the same technical setting.[201] However, the main limitation of CNG channels as cGMP sensor remained their exclusive sarcolemmal localization and inability to monitor cGMP in various deeper parts of the cells.

1.5 Aim of the work

Previous studies have demonstrated that key components of cAMP signaling are associated with the cardiac RyR to form a local cAMP microdomain, which is involved in the regulation of channel function. It has been postulated that Ca^{2+} leak through dysregulated cardiac RyRs occurs in cardiovascular disease. Furthermore, there is a wealth of information that supports a protective role of cGMP-dependent signaling in cardiomyocytes and agents that raise cGMP are investigated in a large number of clinical trials. However, little is known about the spatio-temporal dynamics of cyclic nucleotides in functionally relevant subcellular microdomains, and there are no reports on FRET-based measurements of cGMP in adult mouse cardiomyocytes to date. The aim of the current work was to generate new transgenic mouse models for the visualization of local cAMP and global cGMP dynamics in adult cardiomyocytes. To achieve this, the dissertation contains two parts. The first part investigates local cAMP dynamics at RyRs, and the second studies global cardiomyocyte cGMP dynamics.

Major goals of the thesis:

1. Generation and characterization of a new transgenic mouse model with cardiomyocyte-specific expression of a targeted version of the cytosolic cAMP indicator Epac1-camps (Epac1-camps-JNC) designed to visualize cAMP at RyRs.
2. Monitoring cAMP dynamics in the vicinity of cardiac RyRs and comparing local signaling with cAMP changes in the bulk cytosol using Epac1-camps-JNC and Epac1-camps transgenic mice, respectively.
3. Generation and characterization of a transgenic mouse model with cardiomyocyte-specific expression of the cytosolic cGMP indicator red cGES-DE5.
4. Monitoring cGMP dynamics in adult mouse cardiomyocytes.
5. Analysis of cyclic nucleotide crosstalk.

2 Materials and Methods

2.1 Materials

All solutions were prepared using ultrapure water from Milli-Q Reference Water Purification System (EMD Millipore, Billerica, USA) if not stated otherwise.

2.1.1 Bacteria strains and cell lines

E.coli (TOP 10)	(Invitrogen)
Human embryonic kidney (HEK) 293A cell line	(Invitrogen)

2.1.2 Mouse lines

Epac1-camps	(Dr. Viacheslav Nikolaev)
Epac1-camps-JNC	(this work)
red cGES-DE5	(this work)

β_3-AR-TG and β_3-AR-KO mice were provided by Prof. Jean Luc Balligand (Brussels) and cross-bred with red cGES-DE5 mice to create double transgenic mice:

red cGES-DE5$^{+/0}$; β_3-AR$^{+/0}$
red cGES-DE5$^{+/0}$; β_3-AR$^{wt/wt}$
red cGES-DE5$^{+/0}$; β_3-AR $^{-/-\ 158}$

2.1.3 Plasmid vectors

Red cGES-DE5 in pcDNA3	(Dr. Niino, Dr. Oka, Yokohama)
Epac1-camps-JNC in pcDNA3	(this work)

2.1.4 Enzymes

Pfu DNA Polymerase (2-3 U/µL)	(Promega)
Go *Taq* DNA Polymerase (5 U/µL)	(Promega)
Restriction enzymes for molecular cloning	(New England Biolabs GmbH)
T4 DNA ligase 400,000 U/mL	(New England Biolabs GmbH)
Proteinase K	(Applichem)
Liberase DH (purified Collagenase I and II)	(Roche)
Trypsin, ready-to-use 2.5 % trypsin solution	(Invitrogen)

2.1.5 Antibodies

Primary antibodies:

anti-RYR2 mouse monoclonal antibody	(Affinity BioReagents, #MA3-916)
anti-GAPDH mouse monoclonal antibody	(Bio Trend)
anti-Phospho-PLN (Ser16) rabbit polyclonal antibody	(Badrilla)
anti-PLN A1 mouse monoclonal antibody	(Badrilla)
anti-α-Tubulin mouse monoclonal antibody	(Sigma)
anti-Phospho-VASP (Ser239) rabbit poyclonal antibody	(Cell Signaling)
anti-NO-GCα1 rabbit polyclonal antibody	(Prof. Andreas Friebe, Würzburg)
anti-NO-GCβ1 rabbit polyclonal antibody	(Prof. Andreas Friebe, Würzburg)
anti-GC-B guinea pig polyclonal antibody	(Prof. Hannes Schmidt, Berlin)

Secondary antibodies:

goat anti-mouse HRP conjugated antibody	(BioRad)
goat anti-rabbit HRP conjugated antibody	(BioRad)
goat anti-guinea pig HRP conjugated antibody	(Jackson Laboratories)
goat anti-mouse Cy3 conjugated antibody	(Life Technologies)

2.1.6 Chemicals

Acrylamide (Rotiphoreses Gel 30)	(ROTH)
Agarose	(peqlab)
Ammonium persulfate (APS)	(Sigma)
Ampicillin	(Applichem)
ANP (mouse, rabbit, rat)	(Bachem)
Angiotensin II	(Bachem)
A71915 (mouse, rabbit, rat)	(Bachem)
BAY 58-2667	(Adipoen International)
BAY 60-7550	(Cayman)
BNP	(Bachem)
Bovine serum albumin (BSA)	(Sigma)
2,3-butanedione monoxime (BDM)	(Sigma)
Bromphenol blue	(AppliChem)
BRL 37344	(Sigma)
8-Br-2´-*O*-Me-cAMP-AM	(BioLog Life Science Inst.)

8-Br-2´-*O*-Me-cGMP	(BioLog Life Science Inst.)
$CaCl_2$	(Merck Millipore)
CGP-20712A	(Sigma)
cGMP	(Sigma)
Cilostamide	(Sigma)
CNP (human, porcine)	(Merck Millipore)
Complete protease inhibitor cocktail tablets	(Roche)
Diethylamine NONOate (DEA/NO)	(Sigma)
Dimethylsulfoxide (DMSO)	(AppliChem)
Ethylene glycol tetraacetic acid (EGTA)	(AppliChem)
Ethylenediaminetetraacetic acid (EDTA)	(AppliChem)
Ethidium bromide solution	(ROTH)
Forane (Isoflurane)	(Abbott)
Forskolin	(Sigma)
Glycerol	(Sigma)
Glycine	(Sigma)
Goat serum	(Thermo Scientific)
Heparin	(Ratiopharm)
1H-[1,2,4]oxadiazolo-[4, 3-a]quinoxalin-1-one (ODQ)	(Merck Millipore)
4-(2-hydroxyethyl)-1-piperazineethanesulfonic acid (HEPES)	(Sigma)
ICI 118,551	(Sigma)
Isoproterenol (ISO)	(Sigma)
3-Isobutyl-1-methylxanthine (IBMX)	(Sigma)
Kanamycin	(Applichem)
KCl	(Merck Millipore)
$KHCO_3$	(Sigma)
KH_2PO_4	(Merck Millipore)
MDL-12,330A	(Sigma)
2-Mercaptoethanol	(Sigma)
8-methoxymethyl-3-isobutyl-1-methylxanthine (8-MMX)	(Sigma)
Melatonin	(Sigma)
Methanol	(ROTH)
$MgCl_2$	(Sigma)
$MgSO_4x7H_2O$	(Sigma)
milk powder	(ROTH)
100 mM dATP, dCTP, dGTP, dTTP	(Promega)

NaCl	(Merck Millipore)
NaOH	(ROTH)
$Na_2HPO_4x2H_2O$	(Merck Millipore)
$NaHCO_3$	(Sigma)
N,N-bis-(2-hydroxyethyl)-2-aminoethanesulfonic acid (BES)	(AppliChem)
N,N,N',N'-Tetramethylenediamine (TEMED)	(Sigma)
Novaminsulfon Ratiopharm 500 mg/mL	(Ratiopharm)
Paraformaldehyde (PFA)	(Sigma)
Phenol-red	(Sigma)
PhosphoSTOP phosphatase inhibitor cocktail tablets	(Roche)
Polyethyleneglycol 3.000 monondisperse solution	(Fluka)
Ponceau S	(Sigma)
PROLI NONOate (PROLI-NO)	(Cayman)
Rolipram	(Sigma)
Sildenafil citrate	(Sigma)
S-Nitroso-N-acetyl-DL-penicillamine (SNAP)	(Sigma)
Sodium nitroprusside dihydrate (SNP)	(Sigma)
Sodium azide	(Sigma)
20 % Sodium dodecyl sulfate solution (20 % SDS)	(Fluka)
SQ 22,536	(Sigma)
Tadalafil	(Altana)
Taurine	(Sigma)
Tris(hydroxymethyl)-aminomethan (Tris)	(ROTH)
10 % Triton X-100 solution, peroxide-free	(AppliChem)
Tween20	(Sigma)

2.1.7 Materials for cell culture

Minimum Essential Medium (MEM)	(Invitrogen)
Dulbecco´s Modified Eagle Medium (DMEM)	(Biochrom)
Opti-MEM, Reduced Serum Medium, no phenol red	(Invitrogen)
DMEM/F12, GlutaMax	(Gibco)
Medium 199	(Sigma)
Phosphate Buffer Saline Dulbecco´s (PBS)	(Biochrom)
Fetal Bovine Serum, FBS Superior (FBS)	(Biochrom)
Penicillin / Streptomycin (10.000 U/mL / 10.000 µg/mL)	(Biochrom)
Insulin-Tranferrin-Selenium-Sodium Pyruvate supplement	(Invitrogen)

Trypsin / EDTA Solution (0.05 %, 0.02 %)	(Biochrom)
L-Glutamine, 200 mM	(Biochrom)

2.1.8 Kits and others

BCA Protein Assay Kit	(Thermo Scientific)
[^{3}H]-cGMP	(American Radiolabeled Chemicals Inc)
Crotalus atrox snake venom	(Sigma)
Direct PCR-Tail	(peqLab)
Enhanced chemiluminescence reagent	(Thermo Scientific)
iScript cDNA Synthesis Kit	(Bio-Rad)
LB–agar powder	(Applichem)
LB medium powder	(Applichem)
Protein ladder (Protein marker V)	(peqLab)
1 kb DNA-ladder	(New England Biolabs)
100 bp DNA-ladder	(New England Biolabs)
5x loading dye (for agarose gel electrophoresis)	(Applichem)
Lipofectamine 2000 Transfection Reagent	(Invitrogen)
Laminin	(Sigma)
Qiagen Plasmid Mini Kit	(Qiagen)
Qiagen Plasmid Midi Kit	(Qiagen)
QIAquick Gel Extraction Kit	(Qiagen)
RNeasy Fibrous Tissue Kit + QIAshredder	(Qiagen)
Restriction enzymes	(New England Biolabs)
Roticlear	(ROTH)
10xTAE buffer	(Applichem)
Vectashield Mounting Medium	(Vector Laboratories)
Wheat Germ Agglutinin (WGA)	(Sigma)

All oligonucleotides were purchased from Eurofins MWG Operon and diluted to 100 µmol/L in H_2O.

2.2 Methods

2.2.1 Genetic engineering

Molecular cloning was performed to produce and modify recombinant DNA encoding for FRET-based biosensors. Constructs were stored in plasmid form or linearized for the generation of transgenic mice.

2.2.1.1 Polymerase chain reaction

The Polymerase Chain Reaction (PCR)[202] is used to amplify DNA. A typical PCR program contains three major steps: First, denaturation of the double-stranded template at 94°C, followed by a decrease in temperature to allow oligonucleotide annealing to the single-stranded DNA, and finally elongation by DNA polymerase at 72°C. These three steps are repeated 28-35 times for sequence amplification. In this work, PCR reaction was performed to amplify cDNA fragments for molecular cloning steps, mouse genotyping and adenovirus vector generation. For clonings, the PCR reaction mix contained 10 µL of 10x *Pfu* reaction buffer, 1 U *Pfu* polymerase, 2 µL of 10 mmol/L desoxyribonucleotide triphosphates mix (dNTPs), 2.5 µL forward primer dilution (final conc. 25 µmol/L), 2.5 µL reverse primer dilution (final conc. 25 µmol/L), 100–300 ng cDNA template and H_2O up to a volume of 100 µL and was run on a thermocycler (Labcycler, Sensoquest, Göttingen). Annealing temperature (T) was adapted to the melting temperature (T_m) of the oligonucleotides (5°C below the lowest primer´s T_m) and the elongation time (t) was dependent on the length of the desired PCR product (*Pfu* polymerase replicates 1kbp in 2 min).

PRC program: (94°C – 5 min, 30x(94°C – 30 s, T°C – 30 s, 72°C - t), 72°C – 7 min, 4°C - ∞)

2.2.1.2 Agarose gel electrophoresis

DNA fragments of varying lengths are separated by agarose gel electrophoresis, where an electric field is applied and negatively charged DNA molecules migrate to the anode according to their size. Control-digested plamid probes and mouse genotyping PCR results were routinely run on 1 % agarose gels at 100 V. For gel preparation 2 g agarose were dispersed in 200 mL TAE buffer, heated in a microwave oven to melt particles, was poured into a cast and supplemented with ethidium bromide for DNA staining. Samples were mixed with 5x loading dye and and loaded onto the gel; a DNA ladder served as a standard and was run in parallel. Images were aquired using a documentation system (Multi Image Light Cabinet Transilluminator, Alpha Innotech Corporation) and printed. In addition, gel

electrophoresis was performed to isolate DNA fragments, later needed for ligation reactions during molecular cloning. The DNA was visualized under a UV transilluminator at 312 nm, and a slice of agarose gel that contained the DNA fragment of interest was excised with a scalpel. DNA was extracted and purified using QIAquick Gel Extraction Kit, according to the manufacturer's protocol and eluted in 30-50 µL H_2O.

2.2.1.3 Restriction digestion of plasmid DNA

Type II restriction endonucleases recognize a specific nucleotide sequence and cut the double-stranded DNA within this sequence to generate blunt or overhanging ends.[203] Restriction digestion was performed for DNA analysis or to create a DNA fragment for further use. To conduct a diagnostic digest, 500 ng template (or 8 µL from a mini-preparation) were supplemented with 1.5 µL New England Biolabs buffer (NEBuffer), 0.5 µL of each restriction enzyme, 0.15 µL BSA if recommended by the manufacturer, and H_2O up to a volume of 15 µL. The digest was incubated at 37°C for 1 hour. In case of a double digest, the buffer was determined according to the NEBuffer performance chart for restriction endonucleases. For cloning, larger amounts of plasmid DNA are necessary. Therefore 6–8 µg of vector plasmid or template DNA were mixed with 5 µL NEBuffer, 2.5 µL of each restriction enzyme, 0.5 µL BSA if recommended by the manufacturer, and H_2O up to a volume of 50 µL. Preparative digests were incubated at 37°C for 4 hours, DNA was isolated by gel electrophoresis, extracted and eluted in 30 µL H_2O (vector fragment) or 50 µL H_2O (insert). The DNA fragments of interest were used for subsequent ligation reactions.

2.2.1.4 Ligation reaction

Ligation reaction is performed to insert a DNA fragment into a vector plasmid. Therefore both fragments were digested with the same enzymes to produce compatible ends that can be covalently connected by T4-DNA ligase. The ligation reaction was performed overnight at 14°C, and the reaction mix contained 1 µL vector (1 µg), 11.5 µL insert / or digested PCR product, 1.5 µL of 10x ligase reaction buffer, and 1 µL T4 DNA ligase. To optimize ligation efficiency, different vector-to-insert ratios were run in parallel.

2.2.1.5 Transformation of competent E. coli

Ligation products were introduced into competent *E. coli* bacteria for the purpose of amplification using chemical transformation with 5x KCM buffer containing 500 mmol/L KCl, 150 mmol/L $CaCl_2$, and 250 mmol/L $MgCl_2$. 65 µL H_2O and 20 µL of 5x KCM buffer were mixed with 15 µL of the ligation product and incubated on ice for 5 minutes. In parallel,

100 µL competent bacteria were thawed on ice and added to the ligation mixture followed by incubation on ice for 20 minutes and a further 10 minutes at room temperature before 1 mL Luria-Bertani (LB) medium (without antibiotics) was added. Cells were incubated at 37°C with 600 rpm for 45 min, pelletized, and plated on selective LB-agar plates. Recombinant bacteria were grown overnight at 37°C, and single colonies became visible the next day.

- **Luria-Bertani (LB) medium** containing 0.5 % yeast extract, 1 % tryptone and 1 % NaCl: 25 g LB medium powder were dissolved in 1 L H_2O, autoclaved, and stored at 4°C.
- **Selective LB-agar plates** containing 1.5 % agar in LB medium: 25 g LB–agar powder in 500 mL H_2O, autoclaved, cooled down to 55°C, supplemented with antibiotics, and poured into petri dishes.

2.2.1.6 Plasmid purification

Following transformation, 5-10 colonies were picked, and each clone was grown in 5 mL selective LB medium overnight at 37°C under shaking. Plasmid DNA was isolated and subjected to restriction analysis to identify recombinant colonies that carried the ligated plasmid. To quickly isolate small amounts of plasmid DNA, a modified protocol of the Qiagen Plasmid Mini Kit was used, which is based on alkaline lysis of the *E.coli* bacteria and precipitation of plasmid DNA in 2-propanol. The protocol lacks plasmid purification via anion-exchange chromatoraphy to skip centrifugation steps. Thus, 2 mL of the overnight culture were pelletized and resuspended in 300 µL P1 buffer (50 mmol/L Tris, 10 mmol/L EDTA, 100 µg/mL RNase, pH 8.0). Bacteria were lysed in 300 µL lysis buffer P2 (200 mmol/L NaOH, 1 % sodium dodecyl sulfate) and the solution was neutralized by adding 300 µL neutralization buffer P3 (3 mol/L potassium acetate, pH 5.5). The cell suspension was centrifuged at 13.000 rpm for 3 min and 800 µL supernatant were mixed with 700 µL 2-propanol to precipitate DNA. The pellet was dried for 10 min and resuspended in H_2O, 8 µL probes were used for restriction analysis. Positive colonies were further grown for increased-scale and high-quality plasmid preparations. To do this, 50 mL selective LB medium were inoculated with 50 µL of the positive starter colony and grown under vigourous shaking at 37°C overnight. Bacteria were harvested at 5.000 rpm for 5 min at 4°C and used for Qiagen plasmid midi-preparation according to the manufacturer's protocol (Qiagen Plasmid Midi kit), which includes plasmid purification by anion-exchange chromatography. DNA was dissolved in H_2O, and DNA concentration was determined using a UV/Vis spectrophotometer (Nano Drop 2.000, Thermo Scientific).

2.2.1.7 Measurements of DNA concentrations

Concentration of DNA samples was measured with a UV/Vis spectrophotometer (Nano Drop 2.000, Thermo Scientific) according to the Lambert-Beer Law. DNA was measured at 260 nm optical absorption, a value of 1 represents 50 µg/mL for dsDNA. Water was used as blank reference, sample purity ratio of A_{260}/A_{280} was calculated by the software to check for protein impurities and values of 1.8–2.2 were accepted.

2.2.2. Generation of transgenic mice

2.2.2.1 Generation of transgenic mice by pronuclear-microinjection

Transgenic mice were generated by the pronuclear-microinjection method, where donor zygotes from preovulated female mice are injected with a DNA construct that randomly integrates into the mouse genome. The embryo is subsequently transferred into pseudo-pregnant recipient mice, and the offspring to the foster mothers is genotyped since only 10-20 % of the pups have integrated the transgene.[204, 205] Prior to DNA injection and mouse breeding, the plasmid encoding the sensor construct was linearized and purified to remove vector backbone DNA and ions that might damage the embryo and cause poor integration efficiency of the fragment. 50 µg sensor plasmid was digested overnight at 37°C using 10 µL restriction enzyme, 20 µL reaction buffer, supplemented with BSA if recommended by the manufacturer in a reaction volume of 200 µL. The total digest was run on a 1 % agarose gel in TE buffer (10 mmol/L Tris, 0.1 mmol/L EDTA, pH 7.4, sterile filtered) to separate the fragment of interest, which was extracted and purified with QIAquick gel extraction kit. The DNA was eluted in 100 µL TE buffer, filtered via a 0.2 µm filter under sterile conditions, and dialyzed for 3 hours to remove impurities and ethidium bromide. Dialysis was repeated three more times against fresh TE buffer to further purify the DNA fragment. For pronuclear injection, DNA amounts of at least 200 µL with a concentration of 30 ng/µL were provided to the transgenic core unit of the Max-Planck Institute for Experimental Medicine in Göttingen, which performed pronuclear-microinjection and mouse breeding.

2.2.2.2 PCR-based mouse genotyping

Since Epac1-camps-JNC and red cGES-DE mouse lines were maintained as hemizygotes, all offspring was subjected to PCR-based genotyping to distinguish between transgenic and wild-type mice. Mouse tail biopsies were digested overnight in 200 µL lysis buffer (Direct PCR tail solution containing 0.5 mg/mL Proteinase K) at 55°C under vigorous shaking. On the next day, Proteinase K was inactivated at 85°C for 45 minutes, and the probes were

cooled down to 4°C. Undigested tissue and hair were sedimented, and 0.5 µL of the supernatant served as template for PCR amplification. The mastermix contained 4 µL of 5x Go Taq reaction buffer, 0.5 µL deoxynucleotide triphosphates (10 mmol/L dNTPs, each), 0.05 µL of forward and reverse primer each, 0.2 µL *Taq* polymerase (Go Taq 5 U/µL) and 14.7 µL H_2O per mouse tail probe. A positive control (1 ng plasmid encoding the sensor) and negative control (H_2O) were amplified in parallel using the same mastermix and PCR protocol. Following PCR reaction, probes were mixed with 5x loading dye and run on a 1 % agarose gel.

Primer sequences:

red cGES-DE5 forward	5´ TGACAGACAGATCCCTCCTAT 3´
red cGES-DE5 reverse	5´ GGATGCTCAGGTAGTGGTT 3´
Epac1-camps-JNC forward	5´ TGACAGACAGATCCCTCCTAT 3´
Epac1-camps-JNC reverse	5´ CATGGCGGACTTGAAGAAGT 3´

Program red GES-DE5 mice (~ 690 bp fragment):

(94°C – 5 min, 35x(94°C – 30 s, 56°C – 30 s, 72°C – 80 s), 72°C – 7 min, 4°C - ∞)

Program Epac1-camps-JNC mice (~ 340 bp fragment):

(94°C – 5 min, 35x(94°C – 30 s, 62°C – 30 s, 72°C – 50 s), 72°C – 7 min, 4°C - ∞)

2.2.2.3 Mouse breeding

Transgenic and wildtype FVB/NRj mice, from Janvier Labs, Saint Berthevin, France were accommodated in the animal facility of the University Medical Center Göttingen and Max Planck Institute for Experimental Medicine, Göttingen. Mice were sacrificed to perform heart and cardiomyocyte isolation for experiments at the age of 2-16 months. The mouse lines were managed online using Pyrat and Tbase software, while technicians of the animal facilities took care of the mice. All animal work was performed according to institutional and governmental guidelines.

2.2.2.4 Cardiomyocyte isolation

To perform FRET measurements in single cells, cardiomyocytes from hearts of transgenic mice were isolated by the Langendorff method, which is based on retrograde perfusion of the heart through the aorta with enzyme solution.[206] First, a heart perfusion system was assembled, which requires a peristaltic pump (for perfusion speed of 3 mL/min), a water bath

(the temperature of the solutions perfusing the heart should be 37°C for optimal tissue digestion), a canule for hanging the heart (21 G canule), and plastic tubing (Fig. 8A). Furthermore, a stereomicroscope was used to mount the heart onto the canule.

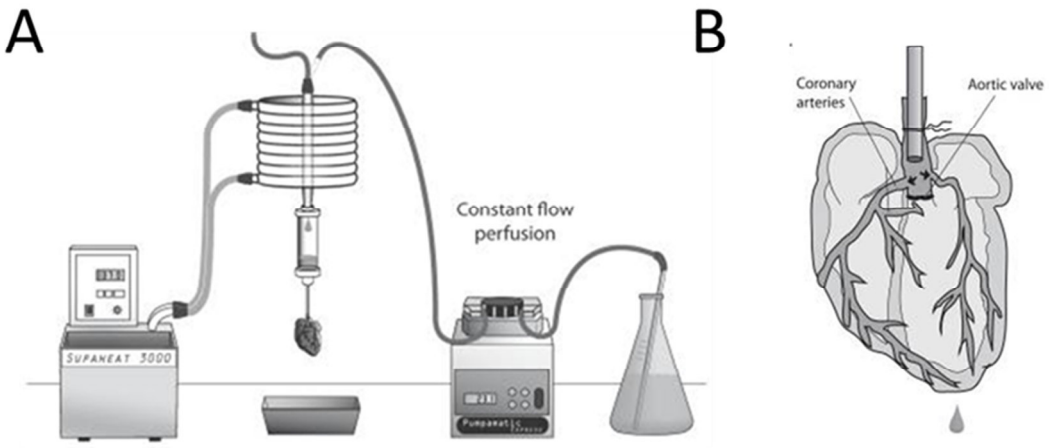

Figure 8. Isolation of adult ventricular cardiomyocytes from mouse hearts by the Langendorff method. (A) Heart perfusion system containing a peristaltic pump, a canule for "hanging" the heart, a tubing system to allow perfusion of the heart, and a heating system. **(B)** The heart is removed and mounted on a canule to allow retrograde perfusion with enzymes via the coronary arteries, figures modified from Louch *et al*. [206]

Before starting the isolation process, the water bath was heated up and the tubing system was rinsed with perfusion buffer. In addition to the perfusion buffer, two stopping buffers (stopping buffer 1 and 2) and a digestion buffer were prepared in advance. The Liberase concentration of the digestion buffer is critical and needs to be adjusted, one was working with concentrations of 0.021-0.042 mg/mL, depending on the size of the mouse and Liberase batch quality. Trypsin concentration was kept constant at 0.025 %, both enzymes were added shortly before starting the isolation and 2.5 mL of digestion buffer were transferred into a beaker. The mouse was heparinized, anesthetized and sacrificed by cervical dislocation, the heart was removed and mounted via the aorta onto the canule, fastened (2 thread loops around the canule) and perfused (Fig. 8B). After 3 min, the perfusion buffer was changed to a digestion buffer and perfused until the buffer was used up. The heart was demounted and transferred into the beaker with the 2.5 ml digestion buffer inside. The atria were removed, and the heart was mechanically crushed for 30 seconds using small scissors. To inhibit the enzymatic digestion, 2.5 mL stopping buffer 1 were added. To further dissociate the remaining pieces of tissue by shearing force, the suspension was pulled up and down using a 1 mL insulin syringe without a needle for 3 min. The suspension was filtered through a 150 µm cell-culture mesh and the cells were sedimented at room temperature. The cell pellet was resuspended in stopping buffer 2. Calcium concentration

was increased to 1 mmol/L by stepwise addition of calcium solutions according to a recalcification protocol. The following solutions were added, in between each step, a break of 4 minutes was taken: 50 µL of 10 mmol/L calcium chloride solution twice, 100 µL of 10 mmol/L calcium chloride solution, 30 and 50 µL of 100 mmol/L calcium chloride solution. Following recalcification, cells were incubated at 37° for 15 min. A small pellet was visible, and most of the supernatant was removed; about 1 mL was left in the falcon covering the cell pellet. Cells were resuspended in the remaining supernatant, and 50 µL cell suspension was seeded on laminin-coated coverslips. Next, cells were left to settle down and adhere to the laminin-coated coverslips for at least 45 minutes, before cell culture medium was added. Cells were cultured at 37°C and 5 % CO_2. More detailed protocols have been published recently ([207, 208] AfCS Procedure protocol PP00000125, available online http://www.signaling-gateway.org/data/cgi-bin/ProtocolFile.cgi?pid=PP00000125). For FRET measurements of cGMP, cardiomyocytes were incubated in medium for at least 3 hours, before starting FRET experiments.

- **Perfusion buffer** in mmol/L: 113 NaCl, 4.7 KCl, 0.6 KH_2PO_4, 0.6 $Na_2HPO_4x2H_2O$, 1.2 $MgSO_4x7H_2O$, 12 $NaHCO_3$, 10 $KHCO_3$, 10 HEPES, 30 taurine, 10 2,3-butanedione-monoxime, 5.5 glucose, 0.03 phenol red, pH 7.4 in H_2O.
- **Liberase DH solution** (4.2 mg/mL): 50 mg of Liberase DH were dissolved in 12 mL of sterile water, reconstituted on ice for 20 min and stored in 150 µL aliquots at -20°C.
- **Digestion buffer**: 30 mL of the perfusion buffer were supplemented with 12.5 µmol/L $CaCl_2$, 150-450 µL of Liberase solution, and 300 µL of 2.5 % trypsin solution. Enzymes were added straight before use.
- **Stopping buffer 1:** 2.5 mL perfusion buffer supplemented with 50 µmol/L $CaCl_2$ and 1 % bovine serum albumin (BSA).
- **Stopping buffer 2**: 10 mL perfusion buffer supplemented with 37.5 µmol/L $CaCl_2$ and 0.5 % bovin serum albumin (BSA).
- **Culture medium**: Minimum essential medium (MEM) supplemented with 0.1 % BSA , 2 mM L-glutamine, 10 mM BDM, antibiotics (100 U/mL Penicillin, 100 µg/mL Streptomycin) and insulin-transferrin-selenium supplement.

2.2.3 Cell culture and transfection techniques

2.2.3.1 Transfection of HEK 293 cells

Most work was done in primary mouse cardiomyoctes, but also cultured Human Embryonic Kidney 293 (HEK 293) cells were used, which can easily be transfected with FRET biosensors. HEK 293 cells were grown in culture medium (Dulbecco´s MEM medium with

4.5 g/L glucose containing 10 % Fetal Bovine Serum (FBS), 2 mmol/L L-glutamine, 100 U/mL penicillin, and 100 µg/mL streptomycin) at 37°C and 5 % CO_2. Cells were passaged at 70–90 % confluency. To do this, cells were washed once with phosphate buffered saline (PBS), detached by trypsinization, and split in a ratio of 1:10 in medium. For transient transfection with FRET biosensors, cells were seeded onto autoclaved glass coverslips (24 mm, Menzel, Thermo Scientific) and grown in multiwell plates. In general, 6-well plates were used (CytoOne, 6–well plate, USA scientific) containing one coverslip per well covered with 2 mL culture medium; cell density on the day of transfection with calcium phosphate precipitation method was ~60 %. A transfection mix sufficient for one 6-well plate was prepared, containing 10 µg sensor plasmid DNA, 50 µL of 4.5 mol/L $CaCl_2$ solution, 440 µL H_2O, supplemented with 500 µL of 2x BBS buffer. The reaction mix was incubated for 10 min at room temperature and dispensed to equal parts onto the cells; imaging experiments were performed after 24 hours. Transfections using $CaCl_2$ solutions are based on the formation of calcium phosphate crystals, which bind to the DNA and enter the cell by a mechanism which is not completely understood (probably associated with micropinocytosis). As an alternative method, Lipofectamine 2000 was used, a cationic lipid-mediated transfection reagent which allows higher transfection efficiency and quality. A protocol was performed that is sufficient for the transfection of a 6-well multi plate with a transfection efficiency of 75-95 %. The transfection mix contained 300 µL Opti-MEM, 2 µg plasmid DNA and 7 µL Lipofectamine 2000 reagent. The mix was incubated for 20 min to allow formation of a DNA-cationic-lipid complex, which interacts with the negatively charged cell membrane via its cationic surface, to allow DNA introduction by endocytosis. On the day of transfection, cell density was ~70 % and the culture medium was changed to serum-reduced Opti-MEM before the transfection mix was added to the cells. After 2-3 hours, the Opti-MEM was replaced by culture medium, and cells were subjected to FRET measurements after 24 hours.

- **2xBBS buffer** containing 1.5 mmol/L Na_2HPO_4, 280 mmol/L NaCl and 50 mmol/L N,N-bis-(2-hydroxyethyl)-2-aminoethanesulfonic acid (BES).

2.2.3.2 Transfection of neonatal rat cardiomyocytes

Neonatal rat cardiomyocytes were isolated from Wistar rats by Karina Zimmermann (AG Nikolaev, Cardiology) as described previously.[209] Cells were plated onto coverslips and grown in culture medium (DMEM/F12 containing GlutaMax, supplemented with 1 % penicillin/streptomycin and 10 % FBS). The following day, cells were washed twice and the medium was changed to a serum-free culture medium (DMEM + M119 in a ratio of 1:4, each supplemented with 1 % penicillin/streptomycin and 1 % L-glutamin). On day 3, cells were

transfected with sensor plasmids using Lipofectamine 2000 according to the manufacturer`s protocol and subjected to FRET experiments after 24 hours.

2.2.3.3 Adenoviral transduction of adult rat cardiomyocytes

The transfection techniques described above do not work for adult cardiac myocytes.[206] Instead, viral-based transduction methods allows gene transfer not only in neonatal but also adult rat cardiomyocytes.[210] Adenoviruses encoding Epac1-camps-JNC and red cGES-DE5 were generated by Karina Zimmermann (AG Nikolaev, Cardiology). Adult rat cardiomyocytes were isolated from male Wistar rats by Tobias Goldak (AG Nikolaev, Cardiology) as described previously,[211] seeded on laminin-coated coverslips and cultured in Medium 199 supplemented with 5 mmol/L taurine, 5 mmol/L carnitine, 5 mmol/L creatine, penicillin/streptomycin and L-glutamine supplement. Myocytes were infected at multiplicity of infection (MOI) of 100 to 300 with adenovirus encoding FRET biosensors. The medium was renewed after 12 hours and FRET experiments were performed after 48 hours.

2.2.4 Characterization of the transgenic mouse lines

2.2.4.1 Histological analysis

The hearts of 3 and 6 months old mice were perfused with PBS, fixed in Roti Histofix (containing 4% formaldehyde in PBS) overnight at 4°C, paraffin-embedded, and sectioned using Leica RM 2165 microtome (Leica Biosystems). For hematoxylin-eosin staining, tissue slides were deparaffinized and rehydrated by performing 9 washing steps (2x xylene for 20 min, 100 % ethanol, 90 % ethanol, 80 % ethanol, 65 % ethanol, 50 % ethanol, 25 % ethanol, tap water; incubation for 5 min each). Heart sections were stained three times with hematoxylin and twice with eosin for 2 min each at the Department of Pathology, University of Göttingen, Medical Center. Images of stained cross-sections were acquired on a Stemi 2000-C microscope binocular equipped with Axio Cam ICc1 and AxioVision software (Carl Zeiss MicroImaging, Jena, Germany). In addition, membrane stainings were carried out using wheat germ agglutinin (WGA) lectin for analysis of cell diameter. Cross-sections were incubated with WGA (75 µg/mL) in the dark for 30 min, washed three times with PBS and mounted in Vectashield Mounting Medium. Images were acquired using Zeiss Axiovert 200 inverted fluorescence microscope equipped with AxioCam and appropriate filters. One hundred cells from 5 sections per heart were analyzed by using ImageJ program (National Institutes of Health, Maryland, USA). Karina Zimmermann (AG Nikolaev, Cardiology) was involved in the histology work.

2.2.4.2 Morphometric analysis

Morphometric analysis of wildtype and transgenic hearts was performed at the age of 3 and 6 months. Tibia length was measured using a sliding caliper, the heart weight was determined with an analytical balance (BP300S, Sartorius, Göttingen, Germany).

2.2.4.3 Echocardiography

Analysis of *in vivo* heart function was performed by Kirsten Koschel and Julia Steinbrecher (AG Lehnart, Cardiology, UMG Göttingen) using transthoracic echocardiography (Visual Sonics Vevo 2100, Toronto, Canada).

2.2.5 Transverse aortic constriction surgery

Red cGES-DE5 mice were subjected to transverse aortic constriction surgery (TAC)[212] to study cGMP dynamics in an animal model of cardiac hypertrophy. Female transgenic mice (9-13 weeks of age) were split into TAC and SHAM group. The SHAM mice underwent the same surgical procedure without aortic constriction. Mice were anesthetized using 1.5-2 % isofluorane in pure O_2; a surgical incision was made to uncover the aortic arch under a binocular macroscope using microsurgical technique. The constriction was performed between the first and second trunk of the aortic arch using a 6-0 polyviolene suture and a 26-gauge to perform banding with a defined constriction. The mice were under analgesic therapy 3 days before the surgery and for 1 week following operation. Three days post-surgery, the pressure gradient was measured by transthoracic echocardiography. The TAC and SHAM surgery was carried out by Julia Steinbrecher (AG Lehnart, Cardiology UMG Göttingen).

2.2.6 Working heart experiments

Isolated hearts were perfused via the pulmonary vein and left atrium with Krebs-Henseleit buffer (KH buffer) in an anterograde mode. Venous return (preload) and aortic pressure (afterload) were adjusted to 5 mL/min and 50 mmHg, respectively.[29, 213] Following 20 min perfusion with KH buffer, agonists or vehicle were perfused for 10 min via the coronary arteries. The heart was removed and left ventricles were shock frozen in liquid nitrogen. Probes were split for radioimmunoassay measurements and immunoblot analysis. Working heart preparations were carried out by Katharina Völker and Birgit Gassner (AG Kuhn, Department of Physiology Würzburg)

- **KH buffer** contained in mmol/L: 118 NaCl, 4.7 KCl, 1.2 $MgSO_4$, 1.2 $CaCl_2$, 1.2 KH_2PO_4, 25 $NaHCO_3$, and 11 glucose. The buffer was oxygenated by gasing the solution with 95 % O_2 and 5 % CO_2.

2.2.7 Biochemical techniques

2.2.7.1 Cell and tissue lysis

Cardiac myocytes were freshly isolated, sedimented in stopping buffer 2 (lacking BSA) and shock frozen in liquid nitrogen. Cultured HEK 293 cells or neonatal rat cardiac myoctes were washed once with ice cold PBS and harvested with a cell scraper. Cells were centrifuged and shock frozen using liquid nitrogen. Cell pellets were resuspended in homogenization buffer and incubated on ice for 15 min, followed by centrifugation for 5 min at 8.000 rpm and 4°C. Finally, the supernatant (lysate) was transferred to a new eppendorf cup and stored at -80°C, protein concentrations were determined by Bicinchoninic Acid Assay (BCA assay).

- **Homogenization buffer** in mmol/L: 150 NaCl, 1 EGTA, 2 $CaCl_2$, 300 sucrose, 10 HEPES, 1 % Triton-X, pH 7.4 in H_2O, supplemented with phosphatase and protease inhibitor cocktail (1 tablet each per 10 mL homogenization buffer).

For tissue lysis, the heart of a mouse was quickly removed, perfused with ice cold PBS, the atria were removed and the ventricles were homogenized with an ultra turrax device (MICCRA D-1 Homogenizer, ART, Müllheim) in 500 µL homogenization buffer lacking Triton X detergent to avoid foam formation. After homogenization, the suspension was supplemented with 1 % Triton X and incubated on ice for 10 min, inverted every 2 min, followed by centrifugation for 5 min at 8.000 rpm and 4°C. The supernatant was transferred to a new eppendorf cup and stored at -80°C. Protein concentration was determined by BCA assay.

2.2.7.2 Quantification of proteins with bicinchoninic acid assay

The amount of proteins after cell or tissue lysis was quantified with the Bicinchoninic Acid Assay (BCA), where Cu^{2+} is reduced to Cu^{1+} by protein bonds. Cu^{1+} and bicinchoninic acid form a purple-colored complex that can be detected at 562 nm. [214] Lysates and blank were diluted 1:10 with H_2O before 200 µL assay reagent (BCA Protein Assay Kit, Thermo Scientific) was added to 25 µL sample or blank dilution and incubated at 37°C for 30 minutes. Samples and blank were run in duplicate in 96-well format on a multi plate reader (µQuant microplate spectrophotometer, BIO-TEK, Bad Friedrichshall). The BSA standard curve was

used to determine the sample concentrations by plotting absorbance against the concentration.

2.2.7.3 SDS-polyacrylamide gel electrophoresis

Proteins were separated by sodium dodecyl sulfate polyacrylamide gel electrophoresis (SDS-PAGE) according to their size. Samples were supplemented with 5x SDS loading buffer, filled up to a total volume of 30 µL with homogenization buffer and incubated at 95°C for 5 min for protein denaturation. Gels were prepared in advance, samples and protein ladder were run at constant 100 V for about 1.5 hours in SDS running buffer using Mini Protean Tetra electrophoresis system from BioRad. The stacking gel was discarded and the separation gel subjected to immunoblot analysis.

- **Stacking gel** (recipe sufficient for 2 gels): 500 µL Rotiphorese 30, 940 µL of 4x Tris/SDS pH 6.8 (500 mmol/L Tris, 0.4 % SDS, pH 6.8), 2.31 mL H_2O, 18.8 µL of 10 % ammonium persulfate (APS), 7.5 µL N,N,N',N'-Tetramethylenediamine (TEMED). The last component was TEMED.
- **10 % separating gel** (recipe sufficient for 2 gels): 8 mL Rotiphorese 30, 6 mL of 4x Tris/SDS pH 8.8 (1.5 mol/L Tris, 0.4 % SDS, pH 8.8), 10 mL H_2O, 96 µL of 10 % ammonium persulfate (APS), 36 µL N,N,N',N'-Tetramethylenediamine (TEMED). The last component was TEMED.
- **5x SDS loading buffer** containing 200 mmol/L Tris 200, 6 % SDS, 15 % glycerol, 0.3 % bromphenol blue, 10 % 2-mercaptoethanol in H_2O, pH 6.7.
- **SDS-PAGE running buffer** containing 25 mmol/L Tris, 190 mmol/L glycine, 1 % SDS in H_2O, pH 8.3.

2.2.7.4 Immunoblot analysis

After separation, the proteins were transferred from the gel onto the blotting membrane and detected by immunostaining. First, the blotting sandwich was assembled, plugged into Mini Trans-Blot Transfer Cell from Bio-Rad, filled up with ice cold transfer buffer containing 32 mmol/L Tris, 192 mmol/L glycine, 4 % methanol, and blotted for 2 hours by applying an electric field of 100 V. After the transfer, proteins were attached to the nitrocellulose membrane (Protran, Whatman), incubated in Ponceau S solution for 5 min and washed with water until clear bands were visible. The membrane was cut so that one probe could be screened for different proteins. To prevent unspecific binding, the probes were incubated in blocking solution (milk or BSA in TBS-Tween20, containing 0.1 % Tween20 in TBS buffer) for 1 hour at room temperature, before incubation with primary antibody was done overnight in

the same blocking buffer at 4°C. The membrane was washed three times with TBS-Tween20 and incubated with horseradish peroxidase (HRP)-coupled secondary antibody for 1 hour at room temperature. After 3 further washing steps, the membrane was incubated in enhanced chemiluminescence reagent (ECL, Thermo Scientific), a substrate of HRP activity, leading to a luminescent reaction. Images of various acquisition times (1 s-10 min) were acquired with a film processor (SRX 101A Konica, USA). Films (Fuji Medical X-Ray Films, Fujifilm) were scanned and subjected to densiometric analysis of the protein bands using Image J. To reprobe a protein on the same western blot, stripping with 200 mmol/L NaOH for 8 min was performed to remove primary and secondary antibodies from the membrane.

Blotting sandwich: (–) sponge / 2 filter papers / gel / membrane / 2 filter papers /sponge (+)

2.2.7.5 Phosphodiesterase hydrolytic activity assay

PDE hydrolytic activity from lysates of cardiomyoctes was measured with an *in vitro* assay according to Thompson and Appleman as previously described.[201, 215, 216] Single cardiomyocytes were isolated, pelletized, and resuspended in washing buffer (40 mmol/L Tris, pH 8.0); cell lysis was performed in 500 µL homogenization buffer (recipe see 2.2.7.1) and protein concentration was determined by BCA assay. 75 µg protein of each sample were filled up with homogenization buffer to 200 µL in the presence of the selective PDE blockers: 10 µmol/L 8-MMX (PDE1), 100 nmol/L BAY 60-7550 (PDE2), 10 µmol/L cilostamide (PDE3), 100 nmol/L tadalafil (PDE5), and broad-spectrum blocker 100 µmol/L IBMX. The samples were kept at 4°C for 5 min to get effective PDE inhibition. Next, 200 µL of reaction buffer containing 10 mmol/L $MgCl_2$, 10 mmol/L 2-mercaptoethanol, 2 µmol/L cGMP, 1.5 mg/mL BSA, and 0.1 µCi [^{3}H]-cGMP were added to start hydrolysis of [^{3}H]-cGMP at 33°C. The reaction was finished after 10 min by addition of 200 µL stop solution (15 mmol/L EDTA, pH 8.0) and inactivation at 95°C for 1 minute. Samples were centrifuged twice, and supernatant was incubated with 50 µg of *Crotalus atrox* snake venom at 33°C for 20 min, to hydrolyze 5`phosphate bond of cGMP. Anion exchange chromatography was performed to separate uncharged guanosine (3´-and 5´-phosphate bond of cGMP was hydrolyzed due to PDE- and snake venom hydrolytic activity) from guanosine 3´-monophosphate, which was not degraded by PDE activity and still carried negative charge. The column contained AG1-X8 resin (BioRad) to bind guanosine 3´-monophosphate while PDE-hydrolyzed [^{3}H]-GMP was collected and quantified with a scintillation counter (MicroBeta^2, Perkin Elmer). The effect of the selective PDE blockers was normalized to broad-spectrum PDE inhibitor IBMX to quantify the percentage each PDE family provides to total cGMP hydrolysis.

- **Homogenization buffer** (for PDE activity assay): 10 mmol/L $MgCl_2$, 40 mmol/L Tris, 1 % Triton-X, pH 8, supplemented with phosphatase and protease inhibitors. One tablet phosphatase and protease inhibitor cocktail each was added per 10 mL homogenization buffer.
- ***Crotalus atrox* snake venom**: *Crotalus atrox* snake venom 1 mg/mL. 20 mg of Crotalus atrox snake venom were diluted in 20 mL H_2O.

2.2.7.6 Radioimmunoassay

Cardiomyocytes were isolated and incubated in tyrode solution,[29] containing 500 µmol/L IBMX, for 15 min. Stimulations with various agonists of guanylyl cyclase activity were performed for 10 min, followed by cell lysis using ice cold 70 % ethanol. For stimulations carried out in perfused working heart preparations, frozen left ventricular tissue was homogenized and processed analogously to single cardiomyocytes (cGMP extraction with 70 % ethanol). Lysates were centrifuged at 3,000 x g at 4°C, and the supernatants were dried using a speed vacuum concentrator, resuspended in 50 mmol/L sodium acetate buffer, acetylated, and subjected to radioimmunoassay (RIA). For the determination of protein content, cell pellets of the ethanol extracts were used.[29, 217] RIAs were performed by Birgit Gassner (AG Kuhn, Department of Physiology, University of Würzburg).

2.2.7.7 Immunofluorescence studies

Immunostaining of RyR2 was performed to co-localize Epac1-camps-JNC with the RyR2. Single sensor expressing cardiomyocytes were seeded on laminin-coated coverslips, washed once in pre-warmed PBS and fixed in 4 % paraformaldehyde (PFA) solution for 10 min to immobilize RYR2 antigens, while subcellular structures were retained. Embedded cells were incubated with blocking solution (20 % goat serum and 0.15 % Triton X in PBS) for 20 min to permeabilize the cells for antibody penetration and to block unspecific binding. Cells were washed once with PBS and incubated with primary mouse antibody against RYR2 (1:500) for 2 hours, followed by washing step with PBS and treatment with secondary anti-mouse Cy3 conjugated antibody for 30 min. All blocking and incubation steps were performed in a humidified chamber at room temperature.

- **4 % paraformaldehyde solution** (PFA): 0.4 g PFA was dissolved in 8 ml sterile PBS and 5 µL of 1 mol/L NaOH and heated up to 70°C in a closed up tube. The solution appeared clear, was cooled down to room temperature and 10 mL sterile PBS were added, filtered via a 0.2 µm sterile filter and stored at - 20°C.

- **Antibody dilutions for immunochemistry:** Antibodies were diluted in PBS, containing 1 % goat serum and 0.15 % Triton X.

2.2.8 FRET-based measurements of cAMP and cGMP

Typical systems for FRET-based imaging contain a source of light to excite donor fluorescent intensity, a beam splitter to divide emission light into two independent channels, and a camera to detect donor and acceptor channel intensities simultaneously (Fig. 9).

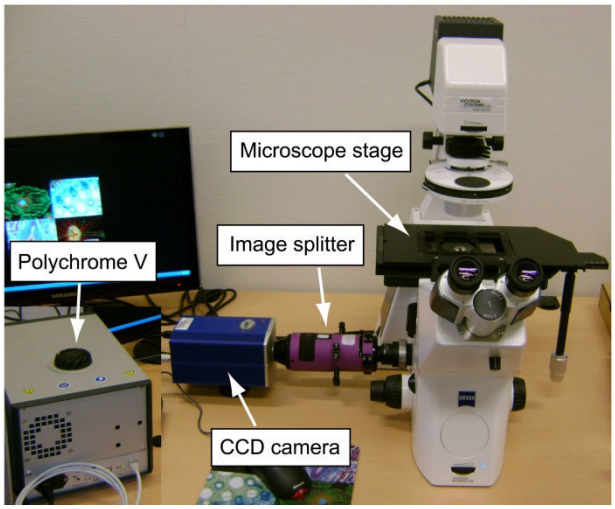

Figure 9. FRET imaging setup containing a microscope stage (Zeiss Axiovert 200) equipped with a source of light (Polychrom V), an image splitter (Quad View beam splitter) to detect donor and acceptor intensities simultaneously, and a charge coupled device (CCD) camera. Picture was taken from Börner *et al.*[191], but shows the setup in Göttingen, which was used for cGMP measurements.

The FRET data were acquired using two different imaging setups. For most experiments, a monochromator-based light source was used (Polychrome V containing a 150 W xenon lamp, TILL photonics, Gräfelfing, Germany), so any wavelength between 320 nm and 680 nm could be chosen for donor excitation, which made the system suitable for cGMP measurements with excitation of T-Sapphire at 405 nm, as well as for cAMP measurement using 436 nm for CFP. The imaging setup was based on a standard inverted microscope (Zeiss Axiovert 200), equipped with an EC Plan-Neofluar 63x/1.25 oil-immersion objective (Zeiss, Jena, Germany) and a wheel to switch between filter cubes. For cGMP measurements a filter cube equipped with a BP 405/20 excitation filter and a DCLP455 dichroic mirror was used. For cAMP imaging one switched to a BP 436/20 excitation filter containing the same dichroic mirror (AHF Analysentechnik, Tübingen, Germany). Emission light was split into donor and acceptor channel using the Photometrics Quad View beam splitter (Photometrics), which implies three dichroic mirrors 500-, 535- and 565dcxr, and four emission filters BP487/25, BP515/30, BP550/40 and BP590/40, for cyan (CFP), green

(T-Sapphire), yellow (YFP) and red (Dimer2), respectively. Single channel intensities were collected with a charge coupled device (CCD) camera (CoolSNAP HQ, Roper scientific) and monitored online in real-time using VisiView software (TILL photonics).

cAMP measurements at RYRs were exclusively performed on an imaging setup, which was based on a Nikon inverted microscope (Nikon Ti-U stage). CFP was excited with a single-wavelength light-emitting diode (CoolLED *p*E-100, 440 nm), which was controlled using Arduino digital-to-analogue input-output board (Arduino Duemilanove). The filter cube contained ET436/30M excitation filter and a DCLP455 dichroic mirror (CFP/YFP filter set, Chroma technology, emission filter was removed), emission light was split by DV2 beam splitter (DualView, Photometrics), which contained 05-EM filter set (includes 505dcxr dichroic mirror, ET480/30M, ET535/40M emission filters) to collect cyan and yellow emission intensities at 480 nm and 535 nm using ORCA-03G CCD camera (Hamamatsu Photonics). Micro-Manager 1.4.5 software was used to control the system and to perform time-lapse image acquisition.

For FRET-based measurements, cells were seeded onto coverslips (for adult cardiomyocytes the coverslips were coated with laminin) and cultured at 37°C and 5 % CO_2 in medium. To perform imaging experiments, cells were mounted onto the microscope, medium was replaced by FRET buffer and changes in cyclic nucleotide dynamics were monitored upon application of drugs at room temperature or 37°C. Donor and acceptor images were acquired simultaneously every 5 seconds.

- **FRET buffer for cardiomyocytes** containing 144 mmol/L NaCl, 5.4 mmol/L KCl, 1 mmol/L $MgCl_2$, 1 mmol/L $CaCl_2$, and 10 mmol/L HEPES.

- For HEK 293 cells a **FRET buffer with higher Ca^{2+}** concentration was used, containing 144 mmol/L NaCl, 5.4 mmol/L KCl, 1 mmol/L $MgCl_2$, 2 mmol/L $CaCl_2$, and 10 mmol/L HEPES.

During the imaging experiment a stack of donor and acceptor images is build up. At the end of the experiment one can open these two stacks to draw a region of interest and transfer the single intensity values to Microsoft Excel software. The raw intensity data need further correction since emission spectra of donor and acceptor fluorescent proteins overlap (bleedthrough), cross-excitation of acceptor fluorescent protein and photobleaching may occur. However correction of cross-excitation was not performed, neither was the background substraction performed.

Bleedthrough correction was performed to calculate the corrected single channel intensities. To achieve this, T-Sapphire protein was expressed in HEK 293 cells alone, to measure fluorescent intensity in T-Sapphire and Dimer 2 emission channels upon T-Sapphire excitation. In this case, the ratio of T-Sapphire/Dimer 2 intensity represents the bleedthrough coefficient which was 0.94 for T-Sapphire spillover into the Dimer 2 channel. For cAMP imaging, a coefficient of 0.9 and 1 (representing 90 % and 100 % channel cross-talk) was determined using single CFP protein. Bleedthrough corrected FRET ratio traces were calculated as follows:

For cGMP measurements: FRET ratio = (RFP-0.94xGFP) / GFP

For cAMP measurements: FRET ratio = (YFP-0.9xCFP) / CFP

FRET ratio =(YFP-1xCFP) / CFP (depending on the imaging setup)

For simplicity, T-Sapphire was termed as GFP and Dimer2 as RFP. The ratiometric traces were transferred to GraphPad Prism 4 or Origin Pro 8 software, normalized to baseline, and corrected for photobleaching if necessary.[191] FRET responses were quantified and statistics performed using Origin 8 software.

2.2.9 Confocal microscopy

Confocal images were acquired using Zeiss LSM 710 laser scanning confocal microscope (Carl Zeiss MicroImaging, Jena, Germany) with a Plan-Apochromat x63/1.40 oil-immersion objective, and analyzed using ZEN 2010 software (Zeiss). Excitation and detection settings for simple confocal images and immunofluorescence studies were as follows:

T-Sapphire (405 nm diode laser excitation, detection 490-520 nm)

Dimer2 (561 nm diode laser excitation, detection 580-630 nm)

YFP (488 nm argon ion laser excitation, detection 498-555 nm)

Cy3 (561 nm diode laser excitation, detection 569-641 nm)

2.2.10 Statistics

Data were analyzed with Origin Pro 8 software and shown as means ± SE. In case of FRET experiments in neonatal or adult cardiomyocytes, the number of single cells (n) and isolations (N) was written above the graphs as n/N. To test for normal distribution, the Kolmorogov-Smirnov test was applied. Data, which were normally distributed were compared using 2-way ANOVA followed by Bonferoni post-test for multi-group comparisons, or 1-way ANOVA for two-group comparison. If not normally distributed non parametric tests (Kruskall-Wallis followed by Dunns test or Mann-Whitney) were applied.[208] Differences were considered significant at $p<0.05$.

3. Results

3.1 Real time visualization of cAMP dynamics in the vicinity of the RyR2 using Epac1-camps-JNC transgenic mice

3.1.1 Design of the Epac1-camps-JNC construct for the generation of transgenic mice

For FRET-based measurements of cAMP dynamics at the RyR2, the cytosolic Epac1-camps was fused with junctin protein to create a targeted cAMP biosensor that can monitor local cAMP dynamics at the RyR2 signaling complex (Fig. 10A). The first version of the Epac1-camps-JNC sensor construct was available, containing Epac1-camps[189, 193] genetically fused with junctin encoding sequence in pcDNA3-based vector (provided by Dr. Nikolaev). The construct was modified for the generation of transgenic mice expressing Epac1-camps-JNC in the myocardium. First, the linker region was reduced to 19 base pairs using the *Kpn*I restriction sites since the original sequence, connecting the promoter with the biosensor encoding sequence, was too long and thus prevented transgenic sensor expression. Furthermore, YFP was replaced with EYFP cDNA, for increased brightness of FRET acceptor protein, and the modified sensor sequence was cloned into the pB-αMHC vector[188] between *Kpn*I and *Xho*I restriction sites to permit cardiomyocyte-specific sensor expression. The insert containing the αMHC promoter, the encoding sequence, and polyadenylation signal was excised with *Not*I, gel-purified and used for pronuclear injection to create transgenic mice (Fig. 10B). Prior to this, one had to test the functionality of the cAMP sensor in living cells. Therefore, the sequence encoding the sensor protein was subcloned into a pcDNA3-based vector using *Kpn*I and *EcoR*V restriction sites. This vector contains the cytomegalovirus enhancer-promoter to drive sensor expression in mammalian cells and allows transient transfection of HEK 293 cells with the Epac1-camps-JNC biosensor for FRET experiments. For imaging experiments, cells were maintained in a bath of saline buffer and treated with isoproterenol to increase cAMP concentrations, changes in cAMP concentrations were monitored by epifluorescence FRET microscopy. ISO-induced cAMP production led to a strong decrease in FRET ratio trace and concomitant opposing effects in single YFP and CFP intensity channels, indicating that the sensor was able to monitor changes in cAMP content in living cells (Fig. 10C, D).

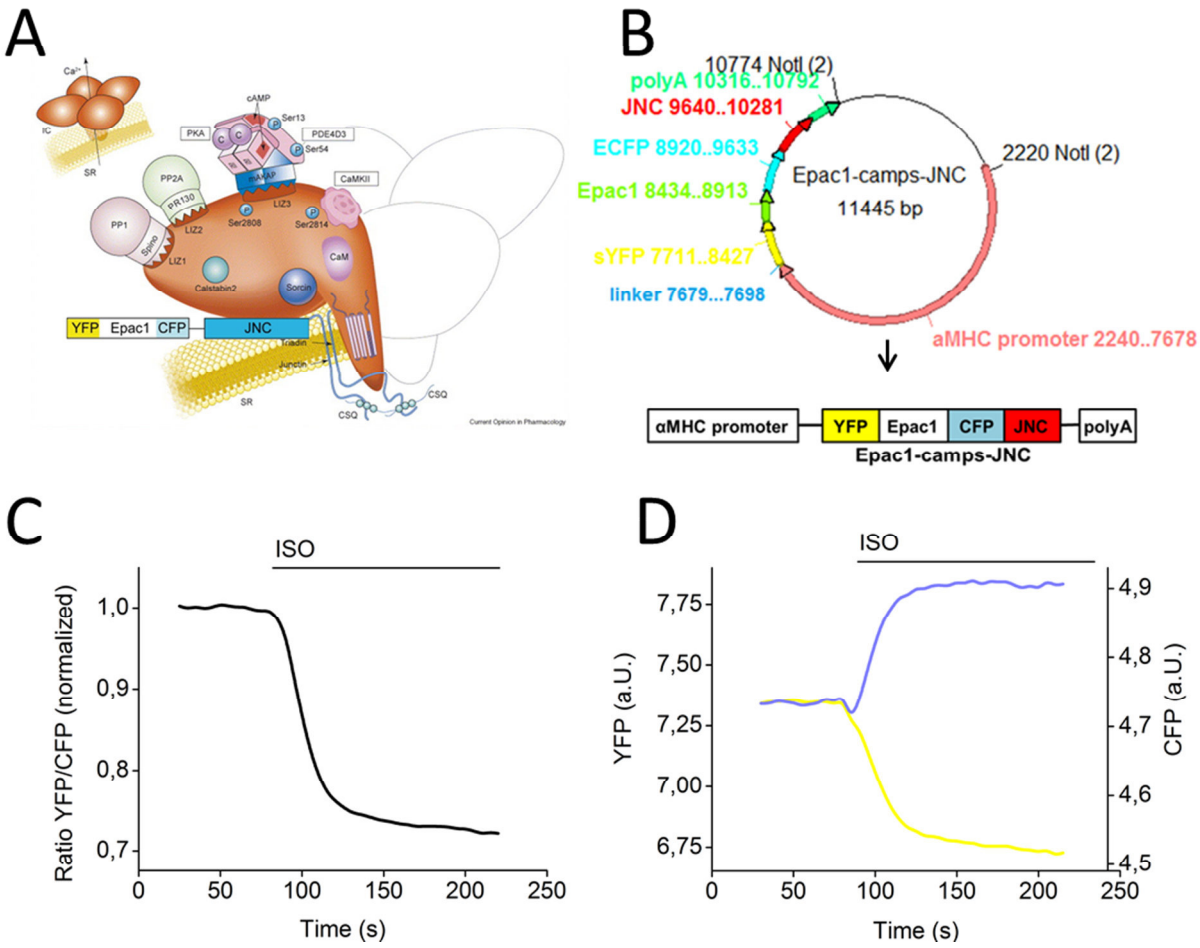

Figure 10. Design of Epac1-camps-JNC construct for pronuclear-microinjection; imaging of cAMP dynamics in HEK 293 cells using Epac1-camps-JNC. (A) Cartoon showing the RyR2 signaling complex and the Epac1-camps-JNC targeted to the RYR2 complex. Modified from Lehnart *et al.*[45] **(B)** pB-αMHC vector containing the Epac1-camps-JNC encoding sequence. *NotI* was used to linearize the plasmid for pronuclear injections. **(C)** Representative FRET ratio trace recorded in HEK 293 cells carrying Epac1-camps-JNC. Isoproterenol (ISO)-induced increase in cAMP led to a decrease in FRET ratio, ISO 100 nmol/L was applied. **(D)** Single YFP and CFP intensity recordings of the same cell. cAMP caused an increase in CFP intensity (donor) and a decrease in YFP (FRET acceptor) intensity. For simplicity ECFP and EYFP are designated as CFP and YFP, respectively.

3.1.2 Generation and characterization of Epac1-camps-JNC transgenic mice

The generation of transgenic mice was performed using the pronuclear-microinjection method. Two rounds of injections gave rise to 10 unique PCR-positive founder lines, which were screened for sensor expression using fluorescence microscopy in isolated cardiomyocytes. The offspring of founder mice showed high levels of sensor expression, which was sufficient for FRET experiments. Analysis of single cardiomyocytes did not reveal any significant differences in fluorescent signal among the founder lines. In contrast, one noticed a high diversity in the number of cells that express the sensor, ranging from 5–90 % of total cardiomyoctes, which usually depends on the time point of transgene integration. One founder line (with ~70 % of total ventricular cardiomyocytes expressing the sensor) was established as the working line for experiments.

The mice bred normally, appeared healthy and showed no abnormal behavior. Morphometric analysis, histology and analysis of cardiac function by echocardiography was performed to monitor any influence that sensor overexpression might have on the heart. Morphometric analysis of male hearts at 6 months of age did not reveal any differences between wildtype and transgenic hearts (Fig. 11A, B). There were also no changes in heart to body weight ratios at the age of 3 months detectable (5.0 ± 0.1 and 4.8 ± 0.1 for wildtype and transgenic mice, respectively, n=13-14), and in heart weight to tibia length ratios for 3 month old male mice (71.0 ± 2.0 and 69.1 ± 2.4 for wildtype and transgenic mice, respectively, n=13 each). Hematoxylin-eosin stainings of heart cross sections also showed no differences at 3 months of age (Fig. 11C).

Staining of glycoproteins on the surface of individual myocytes was performed with wheat germ agglutinin to determine cell size and diameter, which were not changed in transgenic cells (Fig. 11D). Finally, *in vivo* performance of Epac1-camps-JNC mice at the age of 6 months was assessed by transthoracic echocardiography (Table 3). Left ventricular end-systolic and end-diastolic dimensions and functional parameters such as fractional shortening or ejection fraction were not altered, but one observed a slight but significant increase in ventricular wall thickness of transgenic hearts compared to wildtype (anterior wall thickness 0.80 ± 0.01 mm and 0.86 ± 0.02 mm for wildtype and transgenic mice, n=10-12). Increased wall thickness with no changes in functional parameters like ejection fraction indicate that overexpression of the transgene might have caused a mild hypertrophy without any impairment of heart function.

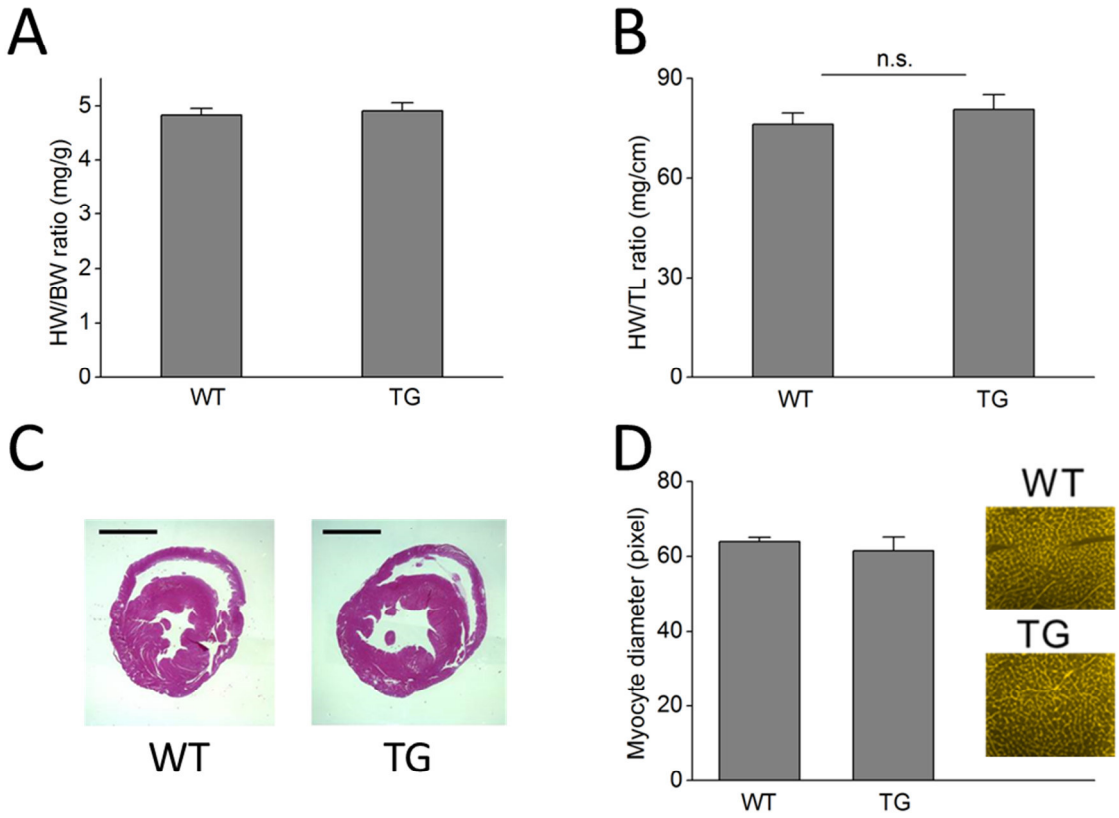

Figure 11. Characterization of Epac1-camps-JNC transgenic mice. (A) Heart to body weight ratios and **(B)** heart weight to tibia length ratios at the age of 6 months were not significantly increased. Data are means ± SE, n=13-14 each. **(C)** Representative cross-sections of transgenic and wildtype hearts at the age of 3 months stained with hematoxylin-eosin were lacking any apparent pathological findings, scale bar, 2 mm. **(D)** There was no significant difference in cardiomyocyte diameter between wildtype and transgenic cardiomyocytes at 6 months of age. Cell membranes were stained with wheat germ agglutinin, shown are data from 6 wildtype and 4 transgenic hearts with 100 cells counted for each heart, means ± SE. None of the parameters was significantly different between the groups at $p<0.05$.

Parameter	Wildtype animals	Transgenic animals
LV-ESD (mm)	3.35 ± 0.1	3.26 ± 0.12
LV-EDD (mm)	4.53 ± 0.06	4.42 ± 0.09
FS (%)	26.2 ± 1.68	26.4 ± 1.8
EF (%)	49.8 ± 2.2	48.0 ± 2.2
Cardiac output (mL/min)	24.9 ± 2.1	21.8 ± 1.3
Stroke volume (µl)	53.4 ± 2.9	46.4 ± 2.4
PWTD (mm)*	0.80 ± 0.01	0.85 ± 0.02
AWTD (mm)*	0.80 ± 0.01	0.86 ± 0.02
Heart rate (bpm)	459 ± 20	470 ± 17

Table 3. Characterization of Epac1-camps-JNC mice using transthoracic echocardiography. *In vivo* performance of the heart was assessed in transgenic and wildtype mice at the age of 6 months. This is shown as means ± SE, n= 10-12 mice per group. LV-ESD, left ventricular end-systolic dimension; LV-EDD, left ventricular end-diastolic dimension; FS, fractional shortening; EF, ejection fraction; PWTD, posterior wall thickness in diastole; AWTD, anterior wall thickness in diastole; bpm, beats per minute. Significant differences ($p<0.05$) are indicated with asterisks.

3.1.3 Characterization of the Epac1-camps-JNC biosensor in cardiomyocytes

Following characterization of the mouse line, one had to analyze subcellular localization of the cAMP indicator in single cardiomyocytes. Fluorescent microscopy of freshly isolated Epac1-camps-JNC cardiomyocytes was performed and revealed strong YFP signals, which were organized in fine parallel striations with hardly any cytosolic background signal (Fig. 12A, right). This was in clear contrast to cardiomyocytes from Epac1-camps mice,[192] which emitted fluorescent light throughout the whole cell, lacking any hot spots of increased intensity levels (Fig 12A, left). These findings obviously demonstrate that the Epac1-camps is homogenously distributed in the cytosol, while the Epac1-camps-JNC probe cannot diffuse freely, but is targeted to a subcellular compartment. To analyze the association of Epac1-camps-JNC with the RyR2 compartment, immunostainings of RyR2 in cardiomyocytes, carrying the Epac1-camps-JNC, were performed to co-localize sensor molecules with the RyR2. Confocal images demonstrated that YFP intensity, representing the sensor probe, completely overlapped with the RyR2 (Fig. 12C), showing that the sensor localization corresponds to that of the RyR2.

In a next step, one had to confirm that the fusion of Epac1-camps with junctin protein did not greatly alter the affinity of the biosensors for cAMP, since it was intended to compare cytosolic cAMP dynamics with the RyR2 compartment. Dose-response curves were

measured using 8-Br-2´-O-Me-cAMP-AM,[191] a cell-permeable cAMP analogue which has the same affinity to Epac as cAMP and is routinely used to calibrate biosensors in cardiomyocytes (Fig. 12B). Both sensor probes showed similar affinities for cAMP (EC_{50} is the cAMP concentration where a half-maximal FRET response was observed; for Epac1-camps-JNC and Epac1- camps the EC_{50} values were 1.15 ± 0.14 µM and 1.25 ± 0.44 µM, means ± SE, n= 5-9, from one mouse each). In cardiomyocytes, cytosolic cAMP levels have been amounted to ~ 1 µmol/L,[191] which means that the sensor is already partially activated at basal state; furthermore, there might be differences in basal cAMP concentrations between cytosol and RyR2 microdomain. Hence it might be helpful to decrease intracellular cAMP to minimal levels, before performing dose-response titrations. Unfortunately, inhibitors of adenylyl cyclase such as MDL-12,330A caused significant cell damage and were not applicable in cardiomyocytes, in my hands. For these reasons, sensor affinity values were determined in HEK 293 cells that have low basal cAMP (EC_{50} value for Epac1-camps was 0.95 ± 0,14 µM[191] and 1.11 ± 0.24 µM, n=12 cells for Epac1-camps-JNC). Both sensors showed a suitable signal-to-noise ratio, while the Epac1-camps had a higher dynamic range (max. FRET responses to isoproterenol 100 nmol/L + IBMX 100µmol/L in cardiomyocytes from Epac1-camps mice was 24.2 ± 0.6 % (n=42 from 4 mice) and 13.1 ± 0.6 % (n=34 from 8 mice) in cardiomyocytes from Epac-1-camps-JNC mice).

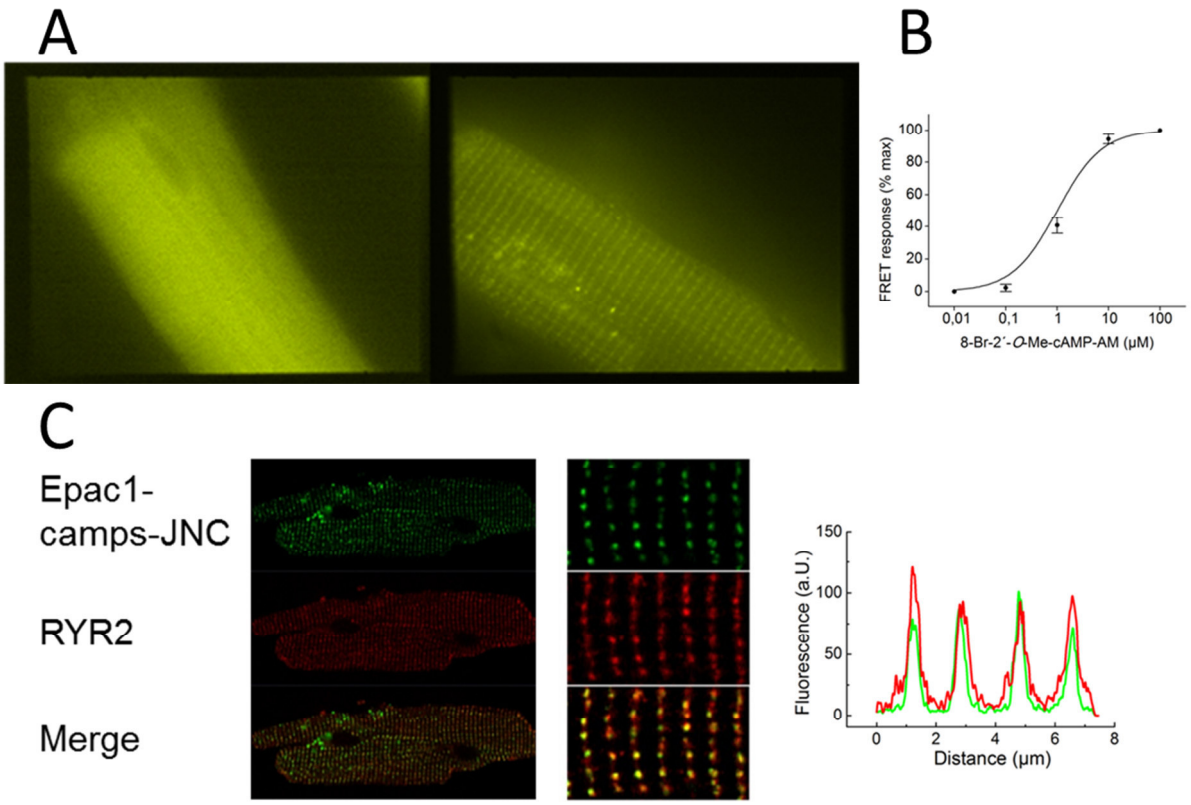

Figure 12. Localization of the Epac1-camps-JNC in single adult cardiomyocytes and sensor affinity (A) Images of YFP intensity revealed a targeted subcellular localization of Epac1-camps-JNC (left), while the cytosolic Epac1-camps (right) is homogenously distributed throughout the whole cell. **(B)** Cardiomyocytes from Epac1-camps-JNC mice were treated with increasing amounts of 8-Br-2´-*O*-Me-cAMP-AM, FRET responses are expressed as percent of maximal change (100 % is the response induced by 8-Br-2´-*O*-Me-cAMP-AM 100 µmol/L) and were plotted against the log (8-Br-2´-*O*-Me-cAMP-AM) to fit a concentration-response dependency curve. Figure was calculated from 5 cells out of 1 isolation **(C)** Cardiomyocytes isolated from Epac1-camps-JNC were stained with primary antibody recognizing RyR2 and visualized by confocal microscopy using Cy3-labeled secondary antibody. Sensor probe was monitored by YFP intensity. Images of sensor probe (green) and RyR2 (red) were superimposed; yellow color indicates regions of overlapping intensities (left, middle). The merge demonstrates that the biosensor co-localizes with the RyR2 (right).

3.1.4 FRET-based measurements of cAMP in cardiomyocytes isolated from Epac1-camps and Epac1-camps-JNC transgenic mice

3.1.4.1 β-adrenergic receptor-mediated cAMP signaling

The β-adrenergic receptor system is the predominant regulator of heart function. It does so by mediating the effects of endogenous catecholamines.[11] β_1- and β_2-adrenergic receptor subtypes both increase cAMP by activation of adenylyl cylases via G_s-proteins.[218] To analyze which receptor subtype modulates cAMP levels in the RyR2 microdomain, FRET-based measurements of cAMP upon selective stimulation of β_1-and β_2-AR activity were performed in cardiomyocytes isolated from Epac1-camps-JNC and Epac1-camps mice.

To activate only one receptor subtype, the non-selective β-adrenergic agonist isoproterenol (ISO) was applied in the presence of the β_1-or β_2-selective inhibitors CGP-20712A and ICI 118,551 respectively. It is not possible to accurately compare absolute FRET response detected in the cytosol with those in the RyR2 compartment since the data were acquired using two biosensors with slightly different characteristics, as described in *3.1.3*. Consequently, absolute FRET responses were expressed as the proportion of the maximal Forskolin 10 µmol/L + IBMX 100 µmol/L response to allow a comparison of cytosolic and RyR2-localised cAMP fluctuations. Forskolin and IBMX strongly induce cAMP production via activation of adenylyl cyclases and non-selective inhibition of PDE-mediated cAMP degradation, respectively. The β_1-AR evoked strong increases in cAMP, which were detectable in the cytosol and RyR2 compartment (Fig. 13A, C). In contrast, stimulation of the β_2-AR caused only small signals, which were not present in every cell (Fig. 13B, D). There were no significant differences in cAMP formation in the entire cytosol versus RyR2 compartment detectable. However, compared with the whole cytosol, β_2-AR-induced cAMP signals at RyR2 were slightly reduced and hardly detectable (Fig. 13E).

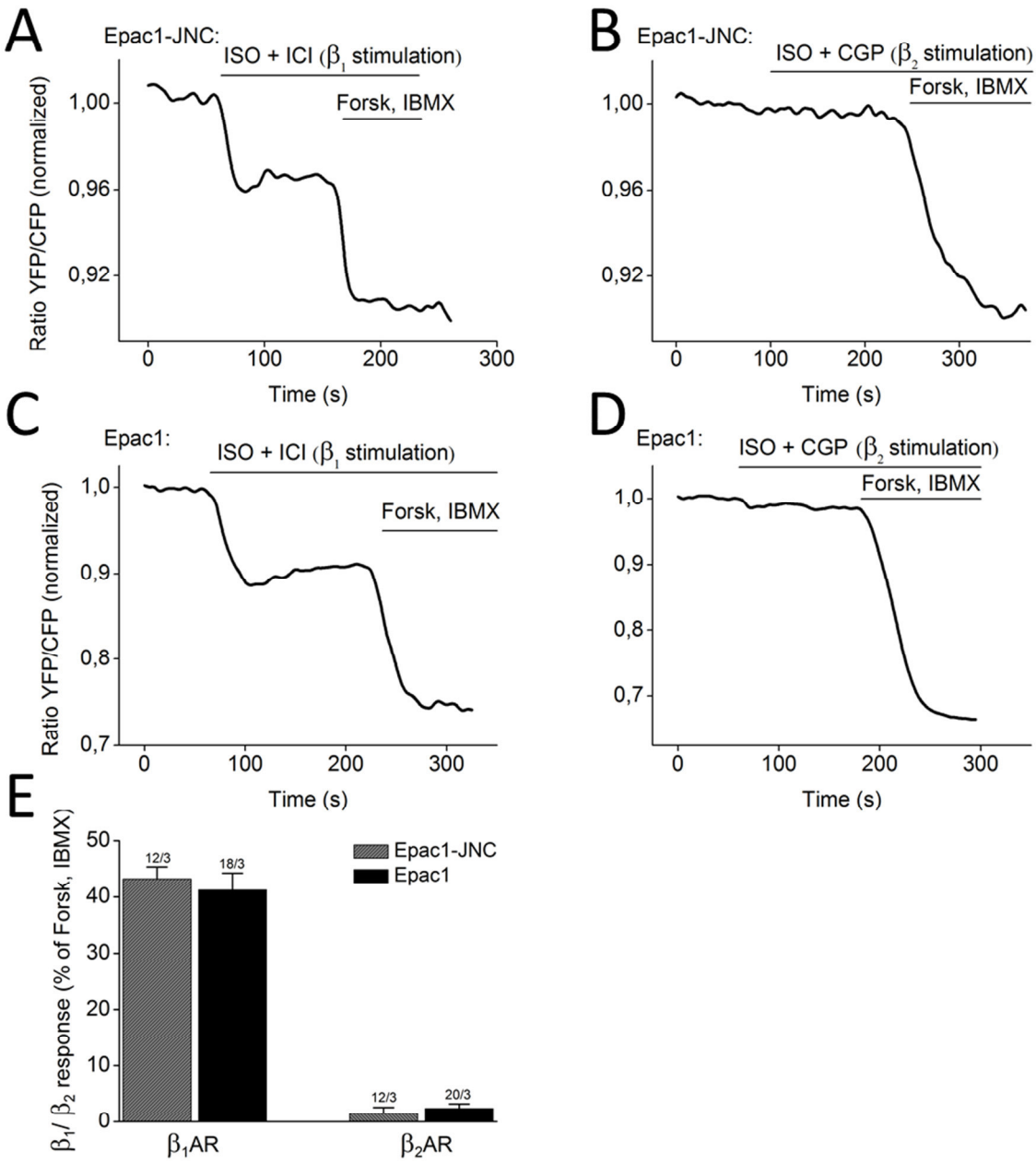

Figure 13. β-AR-induced cAMP dynamics in the cytosol and RyR2 compartment. Single cardiomyocytes isolated from Epac1-camps-JNC **(A, B)** and Epac1-camps **(C, D)** mice were subjected to FRET experiments. Cells were pretreated with ICI 118,551 50 nmol/L to antagonize β_2 AR activity and CGP-20712A 100 nmol/L to block β_1 ARs followed by application of ISO 100 nmol/L to activate the unaffected receptor subtype. A decrease in the FRET ratio curve corresponds with an increase in cAMP. **(A, C)** After selective stimulation of β_1ARs or **(B, D)** β_2ARs, Forskolin (Forsk.) 10 µmol/L plus IBMX 100 µmol/L were applied on top to activate cAMP production. FRET responses were related to the maximum response (Forsk + IBMX) to compare bulk cytosolic cAMP levels with the RyR2 compartment. **(E)** Quantification of FRET responses shown in A to D, means ± SE. The numbers of mice and cells per condition are shown above the bars (as n cells/N mice), there were no significant differences between cytosol and RyR2 compartment, at $p<0.05$.

3.1.4.2 cAMP degradation by PDE hydrolytic activity at basal state

cAMP production is counterbalanced by hydrolytic activity of PDEs, which can shape a cAMP signal after β-adrenergic stimulation but also regulate basal cAMP concentrations. To monitor the contribution of various PDE isoforms to cAMP degradation, cardiomyocytes were treated with selective PDE inhibitors of all major cAMP-PDE isoforms expressed in the murine heart, namely PDE1, 2, 3 and 4.[118] Cells were challenged with 8-methoxymethyl-3-isobutyl-1-methylxanthine 10 µmol/L to block PDE1, BAY 60-7550 100 nmol/L to inhibit PDE2, cilostamide 10 µmol/L to antagonize PDE3, rolipram 10 µmol/L for PDE4 inhibition, and IBMX 100 µmol/L to induce unselective PDE inhibition. Increases in cAMP accumulation upon PDE inhibition were expressed as the proportion of the response to ISO 100 nmol/L.

Compared to other cell types, cardiomyocytes have relatively high basal cAMP levels, even in the absence of stimulatory catecholamines.[191] PDE3 activity was found to be the main regulator of those basal cAMP levels, while PDE4 alone was less active, and inhibition of PDE1 and 2 had no effect (Fig. 14A, C). Interestingly, IBMX alone led to strong increases in basal cAMP (Fig. 14B, C), which exceeded a simple additive effect of PDE3 and 4 hydrolytic activity. It seems like both isoforms regulate basal cAMP levels in a concerted manner, while one PDE can replace the function of the other, in case of selective inhibition.

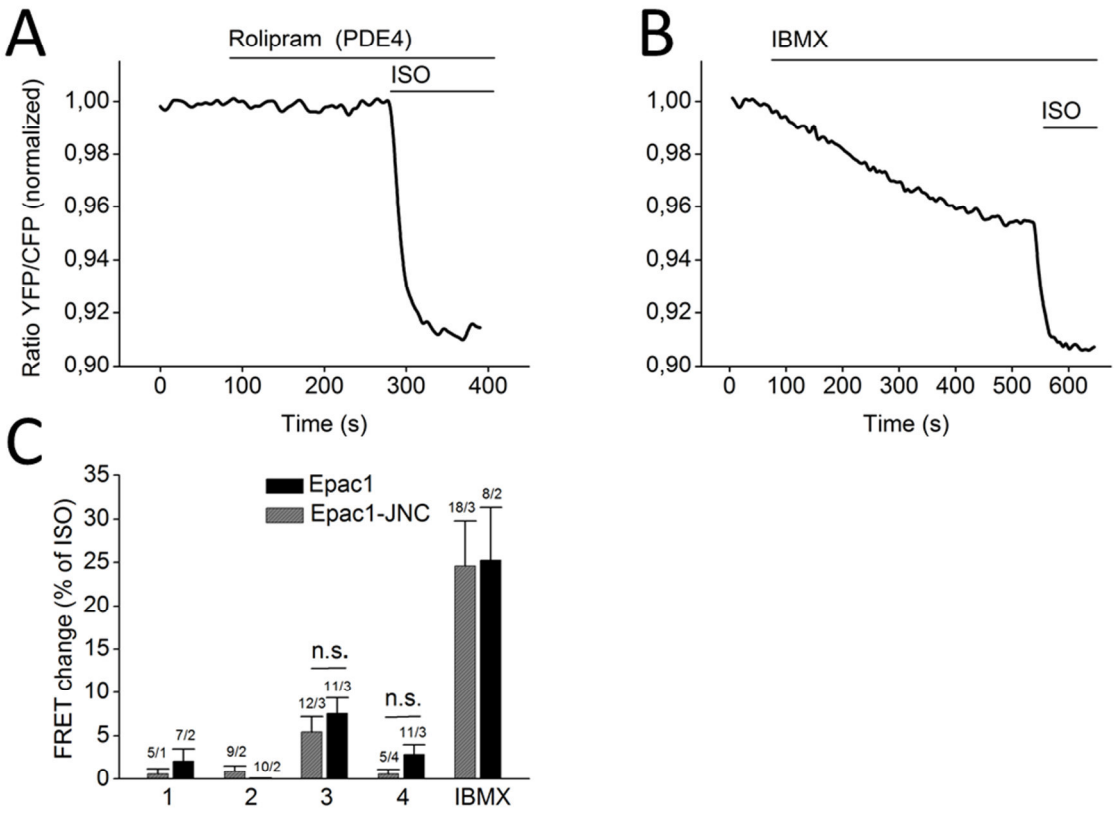

Figure 14. FRET-based measurements of basal cAMP-PDE activity. **(A)** Inhibition of PDE4 with Rolipram 10 µmol/L did not increase basal cAMP levels, **(B)** while non-selective PDE inhibition with IBMX 100 µmol/L raised basal cAMP levels; subsequent addition of ISO further increased cAMP levels. Both ratio traces were recorded in cardiomyocytes isolated from Epac1-camps-JNC mice. Selective PDE inhibitors were added to isolated cardiomyoctes, 8-MMX 10 µmol/L for PDE1, BAY 100 nmol/L for PDE2, cilostamide 10 µmmol/L for PDE3, Rolipram 10 µmol/L for PDE4 and IBMX 100 µmol/L for non-selective PDE inhibition. Subsequently, isoproterenol (ISO) was applied. **(C)** Quantification of FRET responses, shown are means ± SE, as n cells from N mice, written above the bar graphs. Cilostamide showed the strongest effects, while the other showed only negligible effects. FRET experiments were performed in cardiomyocytes from Epac1-camps and Epac1-camps-JNC. There were no significant differences between cytosol and RyR2 compartment detectable ($p<0.05$).

3.1.4.3 cAMP degradation by PDE hydrolytic activity after β-adrenergic stimulation

There were no significant differences between PDE profiles in the cytosol and RyR2 compartment at unstimulated state detectable, so one had to analyze PDE activity after prestimulation with ISO 100 nmol/L. β-adrenergic receptor-mediated cAMP is mainly restricted by PDE4 hydrolytic activity (Fig. 15B). Since stimulation with ISO 100 nmol/L led to a massive increase in cAMP *per se*, addition of the PDE4 inhibitor rolipram on top further strongly raised cAMP concentration to levels that were high enough to saturate the FRET sensors. To measure in the dynamic range of the FRET sensors, PDE4 inhibition was performed upon stimulation with ISO 5 nmol/L, which evoked smaller increases in cAMP than ISO 100 nM, allowing visualization of the complete FRET response to rolipram (233 ± 33 % of ISO measured in Epac1-camps; 251 ± 28 measured in Epac1-camps-JNC, n=8-9 cells from 2 mice each, no significant difference between cytosol and RyR2 compartment). In addition, it was observed that PDE3 is less active than PDE4 after β-AR stimulation, while PDE1 and 2 play only minor roles in murine heart (Fig 15A, B).

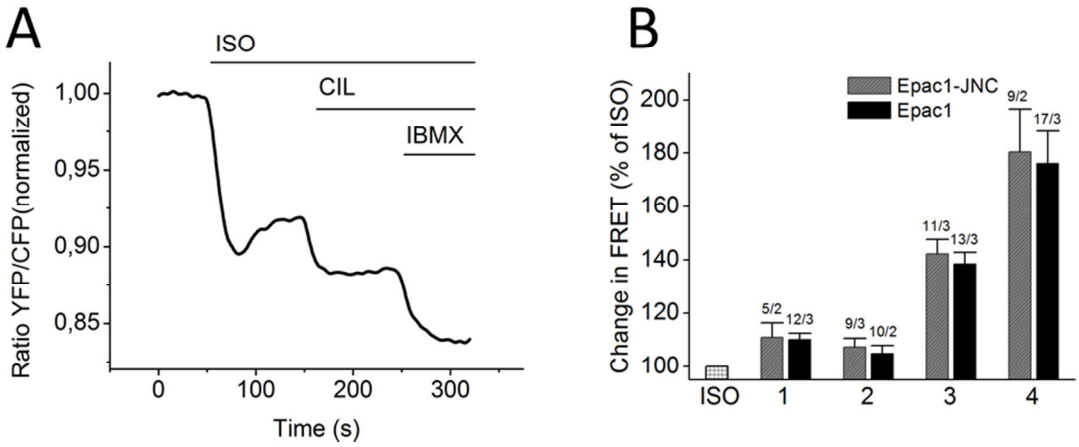

Figure 15. cAMP-PDE activity after β-adrenergic stimulation. (A) Cardiomyocyte expressing the Epac1-camps-JNC was stimuled with isoproterenol (ISO) 100 nmol/L, followed by cilostamide (CIL) 10 µmol/L to block PDE3 and IBMX 100 µmol/L to fully block all PDEs. Representative FRET ratio trace is shown. **(B)** Quantification of FRET responses. The effects of PDE blockers were related to the ISO response to compare cytosol (Epac1) with the RyR2 compartment (Epac1-camps-JNC), there were no significant differences between cytosol and RyR2 compartment detectable. Quantification of FRET responses, shown are means ± SE, as n cells from N mice, written above the bar graphs.

3.2 Real time visualization of cGMP dynamics in adult cardiomyocytes using red cGES-DE5 transgenic mice

3.2.1 Generation and characterization of red cGES-DE5 transgenic mice

Transgenic mice with cardiomyocyte-specific expression of red cGES-DE5 biosensor were created by random transgenesis using α-myosin heavy chain (αMHC) promoter fragment. Red cGES-DE5 encoding pcDNA3.1 plasmid[198] was kindly provided by Dr. Niino and Dr. Oka, cut with *Kpn*I and *Xho*I restriction enzymes and pasted into pB-αMHC vector.[188] The fragment containing αMHC promoter, red cGES-DE5 sensor-encoding sequence, and polyadenylation signal, was excised with *Spe*I, purified and used for pronuclear injections of one-cell FVB/NRj mouse embryos (Fig. 16A). The cGMP indicator is based on a cGMP binding domain from PDE5 and flanked by green (T-Sapphire) and red (Dimer2) fluorescent proteins. The construct used for pronuclear-microinjection was generated by Dr. Nikolaev.

One round of microinjections led to two founder lines that carried the transgene. Single cardiomyocytes isolated from these mice showed strong fluorescent intensity in T-Sapphire and Dimer2 channels, which was high enough for prospective FRET experiments. Different regions of the cell were emitting fluorescent light with similar intensities, indicating a homogenous cytosolic sensor distribution in living cardiomyocytes. This was in clear contrast to cardiomyocytes from wildtype mice, which failed to show fluorescent signals (Fig. 16B). Both mouse lines showed equal levels of biosensor expression with 95-100 % of total ventricular cardiomyocytes carrying the sensor. The mice appeared healthy, without any abnormalities in behavior and bred normally. One founder line was selected for future experiments.

In order to detect any influence that sensor expression might have on the heart, morphometric, histological and echocardiographic analysis were performed. Morphometric analysis of hearts from transgenic and wildtype mice at the age of 6 months did not reveal any significant increase in heart weight (Fig. 16C, D). Also, heart weight to body weight ratios were monitored in mice at 3 months of age, and no differences were observed between wildtype and transgenic mice (4.9 ± 0.1 for wildtype and also transgenic mice, n=12-14). The same was true for the heart weight to tibia length ratios (68.6 ± 2.4 and 68.1 ± 1.2 for wildtype and transgenic mice, respectively, n=12-14). Stainings of transgenic heart cross sections with hematoxylin-eosin were without pathological findings (Fig. 16E) and the diameter of single cardiomyocytes were not altered between wildtype and transgenic groups (Fig. 16F). Finally, transthoracic echocardiography was performed to evaluate heart morphology and function *in vivo* (Table 4). There were no significant differences in

echocardiographic parameters observed between wildtype and transgenic mice at the age of 6 months. These findings demonstrate that expression of red cGES-DE5 had no toxic or negative effects.

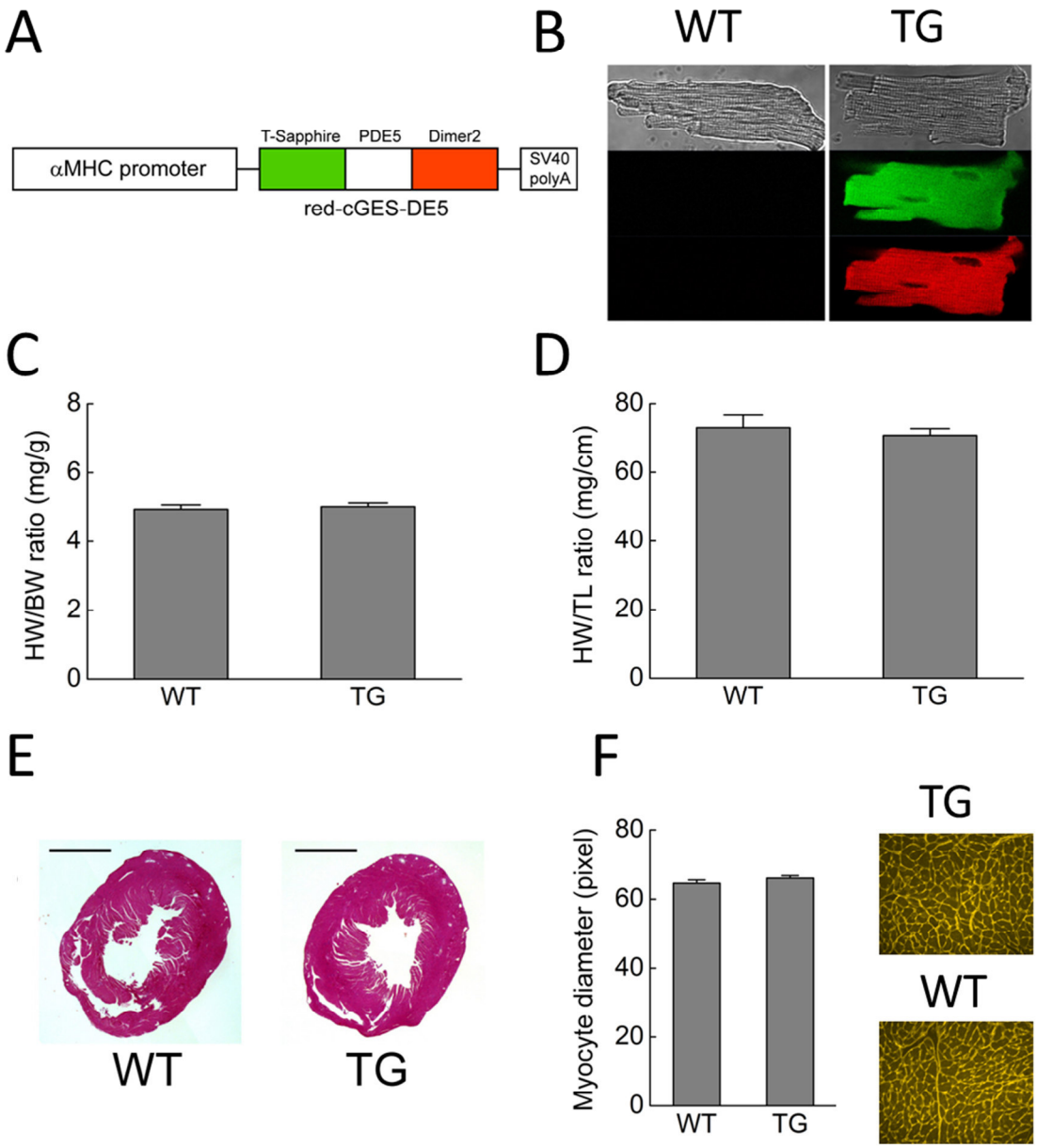

Figure 16. Generation and characterization of red cGES-DE5 transgenic mice. (A) The sensor construct is driven by the αMHC promoter, causing cardiomyocyte-specific expression of the red cGES-DE5 biosensor, which contains T-Sapphire and Dimer2 fluorescent proteins as a FRET pair. The cGMP binding domain was derived from PDE5. Schematic structure of the construct used to generate transgenic mice is shown. **(B)** Single isolated cardiomyocytes from red cGES-DE5 transgenic mice revealed high levels of sensor expression in T-Sapphire (green) and Dimer2 (red) intensity channels, such signals were not detectable in cardiomyocytes isolated from wildtype littermates. Confocal images are shown. **(C)** Analysis of heart weight to body weight ratios **(D)** and heart weight to tibia length ratios performed at the age of 6 months did not reveal a significant difference between wildtype and transgenic mice. Shown are means ± SE, n= 11-22, each. **(E)** Representative cross sections of hematoxylin-eosin-stained wildtype and transgenic hearts appeared normal; scale bar 2 mm. **(F)** There were no significant differences between wildtype and transgenic myocyte diameter, assessed in wheat germ agglutinin-stained heart cross sections. Shown are means ± SE**,** from 3 wildtype and 5 transgenic hearts; 100 cells from 5 sections per heart were analyzed.

Parameter	Wildtype animals	Transgenic animals
LV-ESD (mm)	3.00 ± 0.11	3.01 ± 0.08
LV-EDD (mm)	4.20 ± 0.06	4.21 ± 0.04
FS (%)	28.8 ± 2.1	28.5 ± 1.6
EF (%)	50.1 ± 3.1	52.1 ± 2.2
PWTD (mm)	0.76 ± 0.04	0.74 ± 0.01
PWTS (mm)	1.09 ± 0.03	1.12 ± 0.03
Cardiac output (mL/min)	20.0 ± 1.3	19.2 ± 1.3
Stroke volume (µl)	42.9 ± 2.2	44.5 ± 1.3
Heart rate (bpm)	465± 15	428 ± 20

Table 4. Characterization of red cGES-DE mice using transthoracic echocardiography. *In vivo* performance of the heart was assessed in transgenic and wildtype mice at the age of 6 months. This is shown as means ± SE, n= 8-12 mice per group. LV-ESD, left ventricular end-systolic dimension; LV-EDD, left ventricular end-diastolic dimension; FS, fractional shortening; EF, ejection fraction; PWTD, posterior wall thickness in diastole; PWTS, posterior wall thickness in systole; bpm, beats per minute. None of the parameters was significantly different between the groups at $p<0.05$.

3.2.2. Analysis of cGMP synthesis

3.2.2.1 Analysis of cGMP synthesis in single adult cardiomyocytes

Cardiomyocytes were freshly isolated from transgenic mice and subjected to FRET imaging experiments, which allow real time visualization of cGMP dynamics in living single adult cardiomyocytes. cGMP analogues[219] such as 8-Br-2´-*O*-Me-cGMP or 8-pCPT-cGMP failed to evoke signals, most likely due to insufficient cell membrane permeability in cardiomyocytes. Techniques that permeabilize the membrane, as demonstrated with β-escin in vascular smooth muscle cells,[194, 220] to allow calibration of red cGES-DE5 for cGMP in living cardiomyocytes, are not tolerated by this cell type. Therefore, it was not possible to calibrate the sensor directly in living cells. Nevertheless, the sensor showed high cGMP affinity (EC_{50} = 40 nmol/L) and selectivity for cGMP over cAMP (>1000 fold) *in vitro*.[198]

CNP-mediated stimulation of membrane-associated GC-B led to a strong increase in cGMP production, which could be monitored by a decrease in ratiometric FRET trace and concomitant changes in single FRET donor (T-Sapphire) and acceptor (Dimer2) intensities, which ran in opposing directions (Fig. 17A). At the level of single molecules, cGMP binds to the cyclic nucleotide binding domain, leading to a conformational change that causes an increase in the distance between donor and acceptor fluorescent proteins, inducing a decrease in FRET efficiency (Fig. 17B, C).

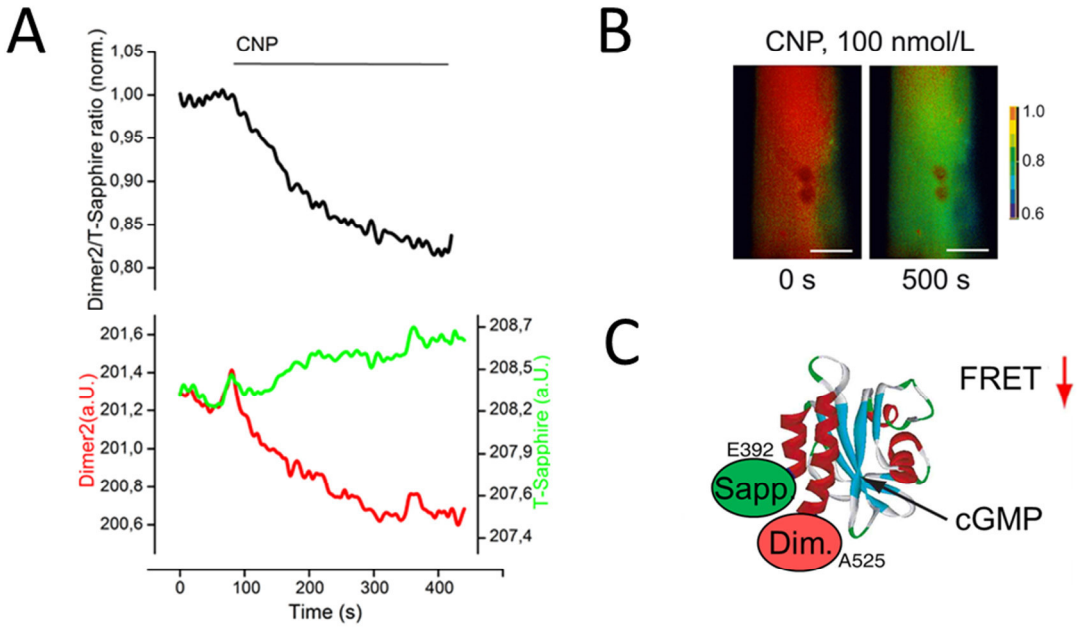

Figure 17. Visualization of cGMP dynamics in single living cardiomyocytes. (A) Stimulation of a single isolated cardiomyocyte with CNP 100 nmol/L caused an increase in intracellular cGMP, which was monitored by a decrease in acceptor (Dimer2) / donor (T-Sapphire) ratio trace. Representative ratiometric FRET trace is shown, corrected for bleedthrough of T-Sapphire into Dimer2 channel and normalized to baseline. The associated raw single channel (Dimer2 and T-Sapphire) intensities are shown below. **(B)** Ratio image of a cardiomyocyte before and after stimulation with CNP, background fluorescence was substracted, scale bar 20 µm. **(C)** The model of the sensor is based on a cGMP binding domain and red (Dimer2) and green (T-Sapphire) fluorescent proteins as FRET pair. An increase in cGMP is reflected by a decrease in FRET.

To assess GC activity, cardiomyocytes were treated with the natriuretic peptide hormones CNP and ANP to specifically stimulate membrane bound GC-B and GC-A, respectively. NO donors were used to activate NO-GC, which is mainly located in the cytosol. Stimulation of GC-B with CNP generated strong increases in cGMP, which could be further raised by subsequent inhibition of cGMP degradation with IBMX (Fig. 18A). Hence, the cGMP sensor is suitable to monitor GC-B activity since it is able to visualize the entire dynamic range of CNP-evoked cGMP concentrations (Fig. 18D).

In contrast to strong responses upon GC-B stimulation, ANP and BNP, the ligands of GC-A, failed to evoke robust signals. ANP showed only small responses (Fig. 18B), which were present in ~ 25 % of the cells. Furthemore, BNP 100 nmol/L did not increase cytosolic cGMP levels (0.24 ± 0.17, n=11 cells from 3 mice). Since PDE hydrolytic activity might maintain low cGMP levels even in the presence of a GC-A agonist, stimulation with natriuretic peptides was followed by application of IBMX to overcome possible barriers of cGMP detection. Nevertheless, IBMX on top of ANP failed to unmask potential GC-A-mediated signals, since FRET responses to ANP in presence of IBMX (3.86 ± 0.51, n=9 cells from 3 mice) did not differ from IBMX applied alone (4.1 ± 0.76, n=11 cells from 3 mice). Therefore, signals in

response to IBMX point to a source of basal cGMP production, which was negatively regulated by PDE hydrolyzing activity, but was not affected by activation of GC-A.

Finally, cardiomyocytes were challenged with the NO donor S-Nitroso-N-Acetyl-D,L-Penicillamine (SNAP) to investigate cGMP pools that were generated by NO-GC activity (Fig. 18C). Interestingly, SNAP failed to evoke FRET signals (Fig. 18E). To confirm the FRET data, analysis of natriuretic peptide- and NO-donor-mediated cGMP production was performed in lysates of isolated wildtype cardiomyoctes using radioimmunoassay technique, performed by Birgit Gassner (AG Kuhn, Würzburg, Department of Physiology). The results revealed strong cGMP production after CNP, while ANP induced a small increase in cGMP levels and SNAP failed to raise cGMP (Fig. 18F).

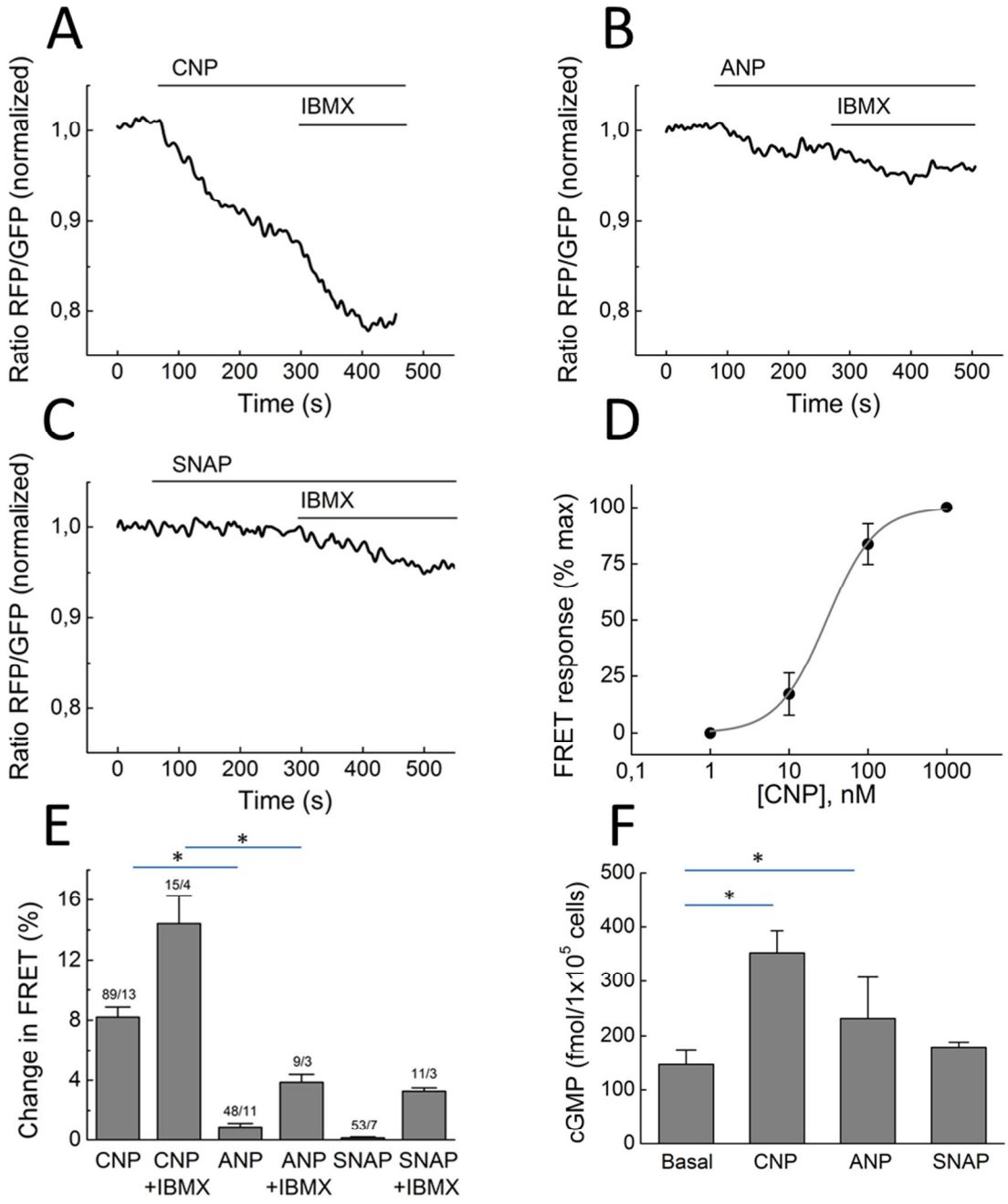

Figure 18. Measurements of cGMP synthesis in single adult cardiomyocytes. (A-C) Isolated cardiac myocytes were challenged with CNP 100 nmol/L, ANP 100 nmol/L or SNAP 100 µmol/L to stimulate GC-B, GC-A or NO-GC activity, respectively, and subsequently treated with IBMX 100 µmol/L to block cGMP hydrolysis by PDEs. Shown are representative FRET ratio traces, a decrease in Dimer2/T-Sapphire FRET ratio trace (termed Ratio RFP/GFP for simplicity) describes an increase in cGMP. **(D)** Dose titration curve for CNP, (n=8 cells from 3 mice). **(E)** Quantification of FRET responses from A-C, shown are means ± SE, as n cells from N mice written above the bars. **(F)** radioimmunoassay (cGMP-RIA) measurements of guanylyl cyclase activity were performed in lysates of isolated cardiomyocytes. Cells were pretreated with IBMX 100 µmol/L and challenged with CNP, ANP, or SNAP for 10 min. Shown are means ± SE, from 3-4 mice per condition. Significant differences ($p<0.05$) are indicated with asterisks.

The absence of an effect of SNAP was unexpected, so other NO donors were tested that display faster kinetics of NO release than SNAP, such as Diethylamine NONOate (DEA/NO) 1 µmol/L, PROLI-NONOate (PROLI-NO) 1 µmol/L, and sodium nitroprusside (SNP) 50 µmol/L. However, these compounds (Fig. 19A-C), as well as stimulation of the β_3-adrenergic receptor with ISO 100 nmol/L in the presence of β_1 / β_2-AR blockade with CGP-20712A 100 nmol/L and ICI 118,551 50 nmol/L (data not shown), failed to evoke signals. It has been demonstrated that NO-GC can be oxidized by ROS, leading to enzyme which is insensitive to stimulation with NO.[90, 91, 221] In addition, it is possible that the cell isolation process might induce oxidant stress, and provide an explanation for absent NO donor effects. To exclude this, myocyte isolation and imaging experiments were performed in the presence of the ROS scavenger melatonin.[222, 223] However, melatonin did not uncover DEA/NO-mediated effects, and BAY 58-2667 1 µmol/L, which has been described to activate oxidized NO-GC in an NO-independent manner,[91, 224] also failed to evoke signals.

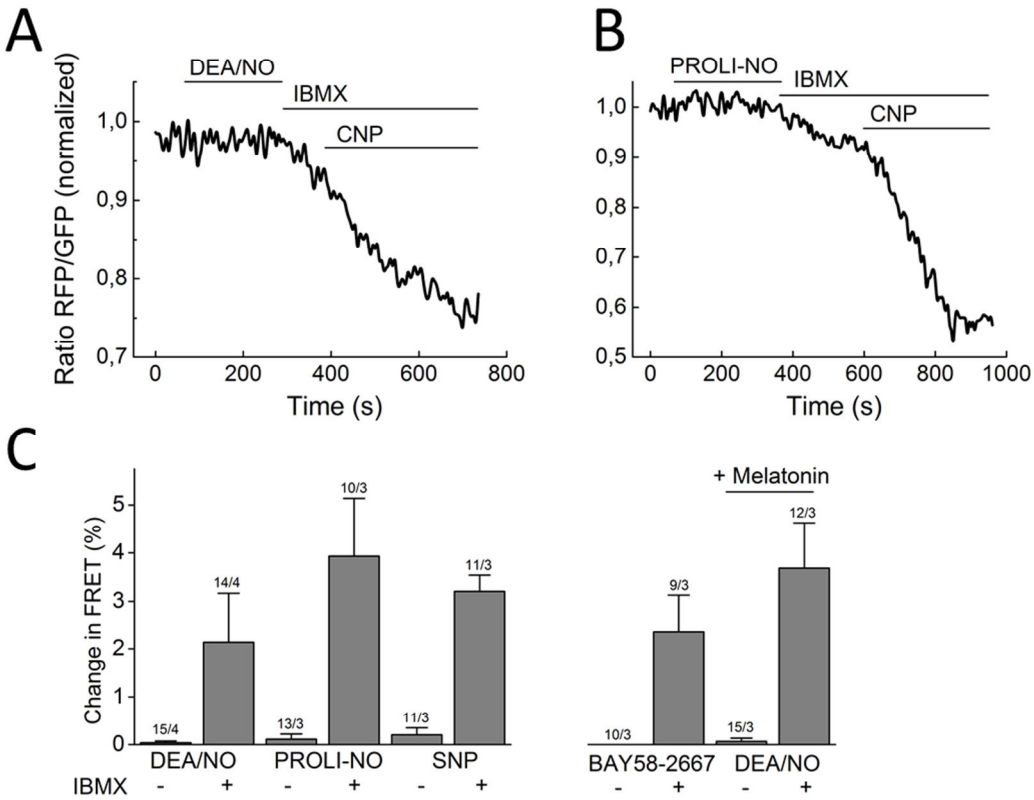

Figure 19. Analysis of NO-GC activity. Cardiomyocytes were stimulated with compounds that release NO or can directly activate NO-GC, followed by IBMX 100 µmol/L. CNP 1 µmol/L served as a positive control. In line with the SNAP-applications (Fig. 18C, E), other NO-donors such as **(A)** DEA/NO 1 µmol/L or **(B)** PROLI-NO 1 µmol/L failed to evoke FRET signals. **(C)** Quantification of FRET responses of A-B. In addition, sodium nitroprusside (SNP) 50 µmol/L, and the NO-GC activator BAY 58-2667 (Cinaciguat) 1 µmol/L showed comparable results using the same live-cell imaging protocol. Shown are means ± SE, as n cells from N mice, written above the bars. Finally, cell isolation and experiments were carried out in the presence of the ROS scavenger melatonin 100 µmol/L to prevent potential oxidation and inactivation of NO-GC, no effect on DEA/NO was detectable.

3.2.2.2 Analysis of cGMP synthesis and cGKI activity in a model of isolated working hearts

Given the fact that signaling properties in isolated cardiomyocytes might differ from cells located in intact heart tissue, stimulations of guanylyl cyclases were performed in isolated, perfused working heart preparations.[29, 115] Left ventricular tissue from hearts that were treated with ANP, CNP, SNAP or vehicle was subjected to cGMP-RIA and immunoblot analysis of cGKI activity. Working heart preparations and cGMP-RIA experiments were carried out by Katharina Völker and Birgit Gassner (AG Kuhn, Department of Physiology, Würzburg). As is the case in isolated cardiomyoctes, CNP induced the strongest increases in cGMP, while ANP failed to raise cGMP content (Fig. 20A). Surprisingly, SNAP evoked a small, but significant effect, which is most likely due to SNAP-induced cyclase activity from cardiac fibroblasts or vascular smooth muscle cells. Finally, strong CNP-induced increases in cGMP levels were associated with phospholamban (PLB) phosphorylation, which is a well-established substrate of cGKI, while SNAP and ANP had no effect on PLB phosphorylation (Fig. 20B). In conclusion, strong responses to CNP and absent effect of NO-donor, both detected with the FRET sensor in single isolated cardiomyocytes, were no artifacts due to the isolation process or cell culture procedure but also present in cardiomyocytes from working heart preparations.

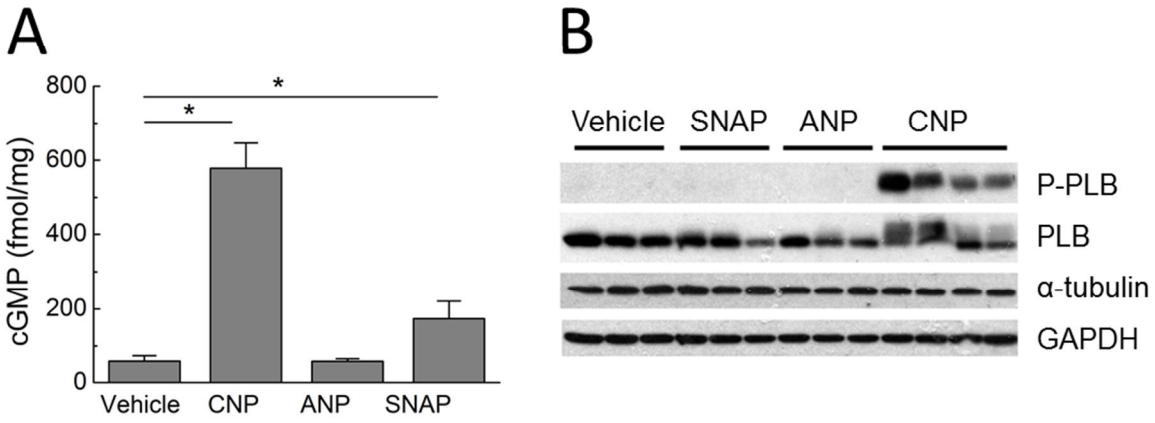

Figure 20. Analysis of cGMP synthesis and cGKI activity in isolated, perfused working heart preparations. (A) Living wildtype hearts were removed and perfused for 10 min with PBS vehicle, CNP 100 nmol/L, ANP 100 nmol/L, or SNAP 100 µmol/L through the pulmonary vein. After perfusion, left ventricular tissue was split for cGMP-RIA and immunoblot analysis. Total cGMP content in the left ventricle was assessed by cGMP-RIA. Shown are means ± SE, from 4-5 hearts each. **(B)** In addition, tissue samples were subjected to immunoblot analysis of cGKI activity. Probes stimulated with CNP showed high levels of phospholamban phosphorylation (P-PLB), while tissue treated with vehicle, SNAP and ANP did not reveal P-PLB. GAPDH, α-tubulin and total phospholamban (PLB) were used as loading controls. Significant differences ($p<0.05$) are indicated with asterisks.

3.2.3 Analysis of basal cGMP formation

3.2.3.1 Analysis of basal NO-GC and GC-A activity

SNAP and other drugs that were reported to stimulate NO-GC activity did not increase cGMP levels in adult cardiomyocytes, but inhibition of NO-GC with 1H-[1,2,4]oxadiazolo-[4,3-a]quinoxalin-1-one (ODQ) 50 µmol/L led to an increase in FRET ratio, which represents a decrease in cGMP concentrations (Fig. 21A). The findings that ODQ evoked a decrease in cGMP levels, while inhibition of cGMP hydrolysis caused an opposing effect, namely an increase in cGMP (Fig. 21B), supports the thesis that basal cGMP production must occur and is counterbalanced by PDE hydrolytic activity. However, basal cGMP levels could be amounted to ~10 nmol/L using dose response titration *in vitro*[198] and maximal FRET responses. The method for the calculation of intracellular cyclic nucleotide concentrations using FRET-based biosensors was described previously in detail by Börner and colleagues.[191] In addition, cardiomyocytes preincubated with ODQ showed significantly decreased responses to IBMX. In contrast, GC-A inhibition with A71915 did not decrease basal cGMP levels, while basal GC-B activity could not be tested since the only well-established and specific GC-B inhibitor HS-142-1, was not available[225]. These findings suggest that basal cGMP levels are most likely produced by NO-GC.

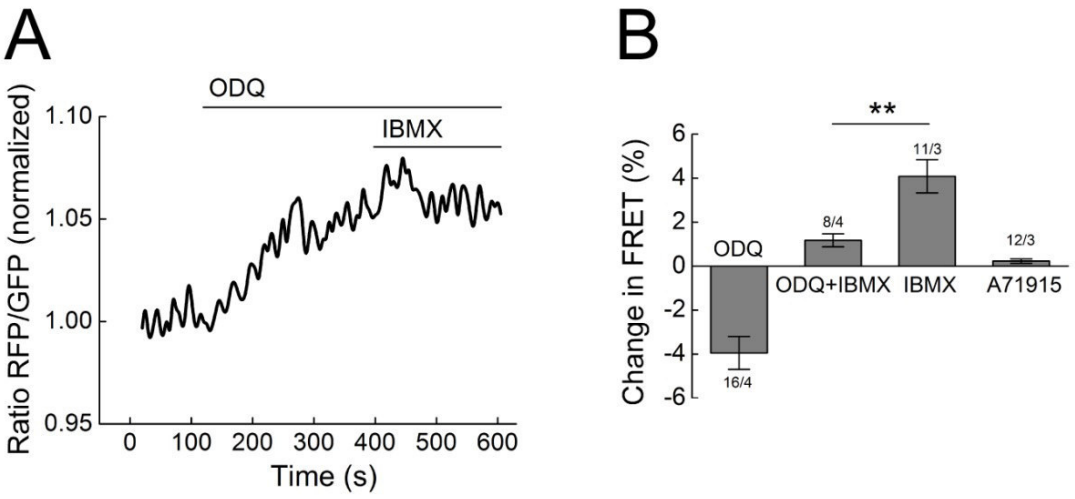

Figure 21. Basal cGMP production is regulated by NO-GC activity. (A) Inhibition of NO-GC with ODQ 50 µmol/L induced a decrease in basal cGMP levels, which is represented by an increase in ratiometric FRET trace. Subsequent inhibition of PDE hydrolytic activity with IBMX 100 µmol/L evoked responses that showed a reduction in the amplitude compared with IBMX-induced response in the absence of ODQ. **(B)** To facilitate the comparison, the response to IBMX alone from Fig. 23E is shown. The GC-A inhibitor A71915 failed to decrease basal cGMP levels. Shown are means ± SE. The numbers of single cells and mice are shown above the bars (as n cells/N mice). Differences are statistically significant at $p<0.01$.

3.2.3.2 Basal cGMP levels are regulated by β_3-adrenergic receptors

Red cGES-DE5 mice were crossbred with β_3-AR-TG and β_3-AR-KO mice to elucidate the involvement of the β_3-adrenergic receptor in the regulation of basal cGMP levels. As mentioned above, stimulation of the β_3-AR failed to evoke signals, but the ODQ-induced responses were significantly stronger in β_3-AR-TG compared to wildtype littermates; β_3-AR-KO revealed smaller ODQ effects (Fig. 22). In conclusion, the β_3-adrenoceptor is involved in basal NO-GC-mediated cGMP production since the β_3-AR-TG mice had increased basal cGMP levels, while the β_3-AR-KO mice showed decreased cGMP levels.

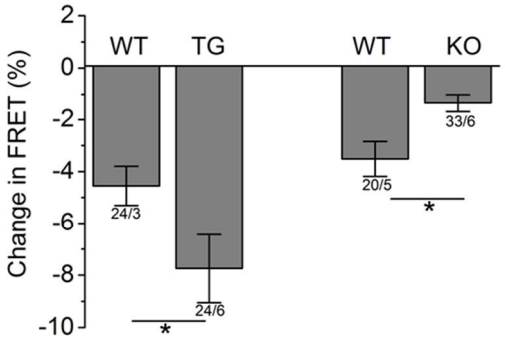

Figure 22. The β_3-AR participates in the regulation of basal cGMP levels. Red cGES-DE5 mice were mated with β_3-AR**-**TG mice to generate double-transgenic mice (redcGES-DE5$^{+/0}$; β_3AR$^{+/0}$, redcGES-DE5$^{+/0}$; β_3-AR$^{wt/wt}$). β_3-AR**-**TG mice are on C57/Bl6 background, while the red cGES-DE5 are FVB/NRj mice. To exclude differences among the mouse strains, control mice were generated by crossbreeding wildtype littermates of β_3-AR**-**TG with red cGES-DE5 mice. β_3-AR**-**KO mice, which were on FVB/NRj background, were also mated with red cGES-DE5 mice to generate double-transgenic mice (redcGES-DE5$^{+/0}$; β_3-AR$^{-/-}$). ODQ 50 µmol/L was applied. Shown are means ± SE. The numbers of single cells and mice are shown above the bars (as n cells/N mice). Differences are statistically significant at $p<0.01$.

3.2.4 Analysis of cGMP degradation by PDE hydrolytic activity

3.2.4.1 FRET-based measurements of basal cGMP-PDE hydrolytic activity

PDEs mediate cyclic nucleotide degradation, with four cGMP-PDE families (PDE1, 2, 3 and 5) expressed in the murine heart. To investigate which PDE families are involved in the regulation of basal cGMP, single cardiomyocytes were treated with family-specific PDE inhibitors. 8-MMX 10 µmol/L was used to inhibit PDE1, the selective inhibitors BAY 60-7550 100 nmol/L, cilostamide 10 µmol/L, and tadalafil 100 nmol/L were used to block PDE2, PDE3 and PDE5, respectively. IBMX 100 µmol/L was applied on top of selective blockers as a positive control to inhibit total cGMP hydrolysis. Inhibition of PDE1 and PDE5 could not raise cytosolic cGMP, the effects elicited by BAY 60-7550 (PDE2) were very weak and close to noise levels (Fig. 23A, B, D). Surprisingly, robust FRET responses upon PDE3 inhibition with

cilostamide were detected, which increased cGMP levels to the same extent as IBMX (Fig. 23C, E). Thus, PDE3 accounted for ~100 % of total cGMP hydrolyzing activity and was the major cGMP-PDE controlling the basal cGMP hydrolysis.

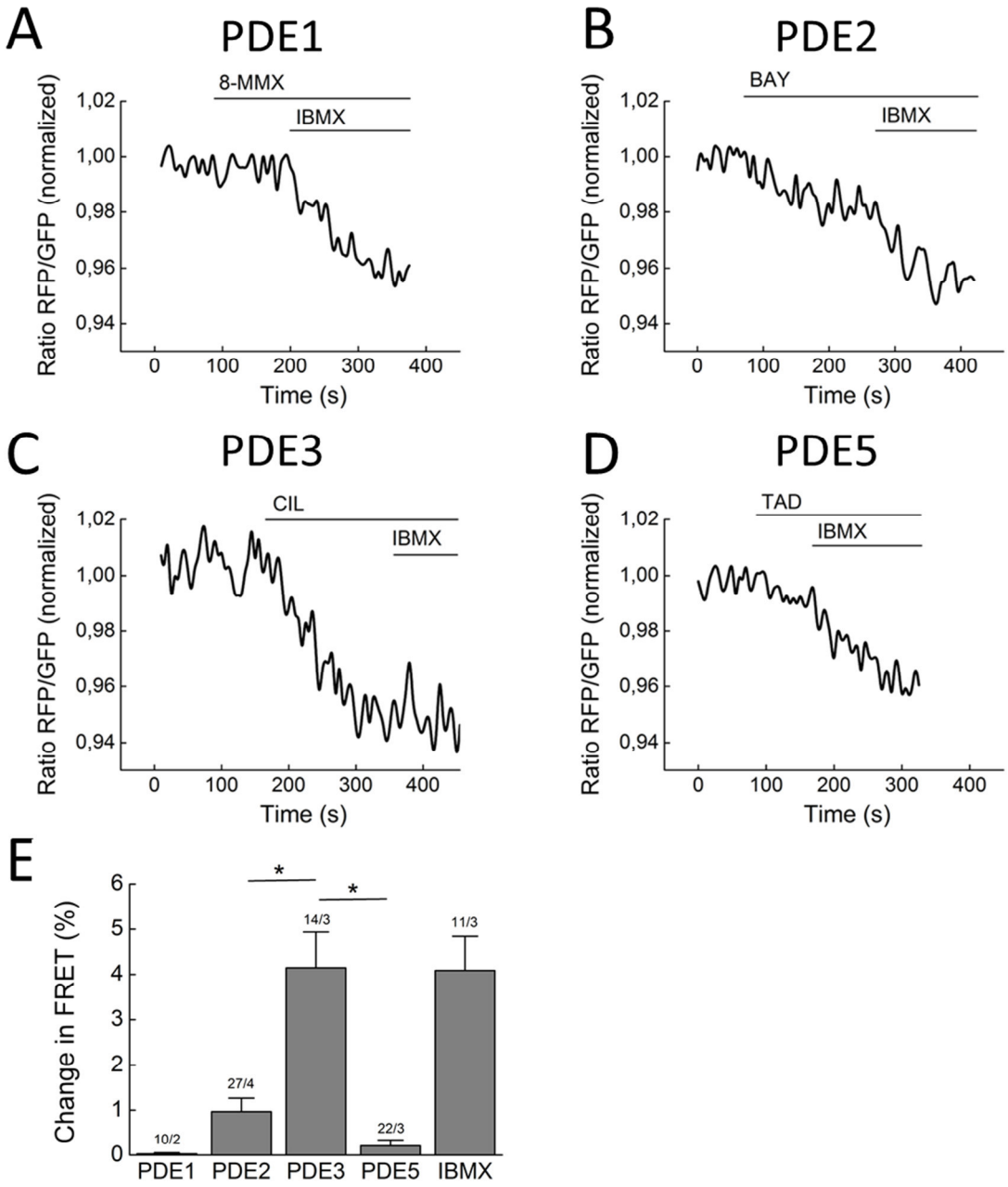

Figure 23. FRET-based measurements of basal cGMP-PDE activity. (A) Selective PDE inhibitors were added to isolated cardiomyocytes, 8-methoxymethyl-3-isobutyl-1-methylxanthine 10 µmol/L (8-MMX) to inhibit PDE1, **(B)** BAY 60-7550 100 nM (BAY) for PDE2, **(C)** cilostamide 10 µmol/L (CIL) to block PDE3 **(D)** and tadalafi 100 nmol/L (TAD) to inhibit PDE5. After selective PDE-inhibition, cells were challenged with IBMX 100 µmol/L as a positive control. Cilostamide showed the strongest effects. **(E)** Quantification of FRET responses from A-D; shown are means ± SE as n cells from N mice written above the bars. Significant differences ($p<0.05$) are indicated with asterisks.

3.2.4.2 FRET-based measurements of cGMP-PDE hydrolytic activity in the presence of cGMP and cAMP agonists

Next, the effects of selective PDE blockers in the presence of agents that raise cGMP or cAMP levels were investigated. It was felt that this might better reflect physiological conditions and those studies permit a comparison of PDE profiles recorded at basal and stimulated state. Cardiomyocytes were prestimulated for 5 minutes with the cGMP-elevating ligands CNP, ANP or SNAP and subsequently challenged with PDE blockers (Fig. 24A-C). In the presence of cGMP agonists, the PDE profiles did not differ from those recorded under resting conditions (Fig. 23E). Cilostamide-sensitive PDE3 remained the major regulator of cGMP hydrolysis, while inhibition of the other PDE families failed to induce clear FRET signals.

Since pretreatment with cGMP ligands did not cause any changes in PDE activity profile, PDE hydrolytic activity was reanalyzed in the presence of ISO 0.1 nmol/L, to mimic moderate catecholamine-induced cAMP levels present in a healthy heart. Within a context of elevated cAMP, it is worth mentioning that PDE3 is designated as the cGMP inhibited PDE since it has dual activity and cAMP can act as a competitive substrate to cGMP turnover.[118] To test whether PDE3 effect is still detectable when cAMP levels are increased, cells were prestimulated with ISO 0.1 nmol/L before PDE inhibitors were applied (Fig. 24D). Cilostamide-induced effects were reduced to half the amount of those detected in the absence of ISO (FRET response to cilostamide in the absence and presence of ISO, respectively, 4.1 ± 0.8 vs 1.9 ± 0.4, see Fig. 23E and 24D). Hence, it became possible to observe a clear decrease in cGMP hydrolytic activity of PDE3 when a competitive substrate was present. Nevertheless, PDE3 effects were still stronger than those of the other PDE inhibitors.

Finally, cardiomyoctes were pretreated with BNP and angiotensin II to simulate a neurohormonal activation status that occurs in patients with heart failure, where both peptides are strongly upregulated.[152, 226] Again, the PDE profile looked similar to those recorded in the absence of BNP and Angiotensin II, confirming the predominant role of PDE3 in cGMP hydrolysis (Fig. 24E).

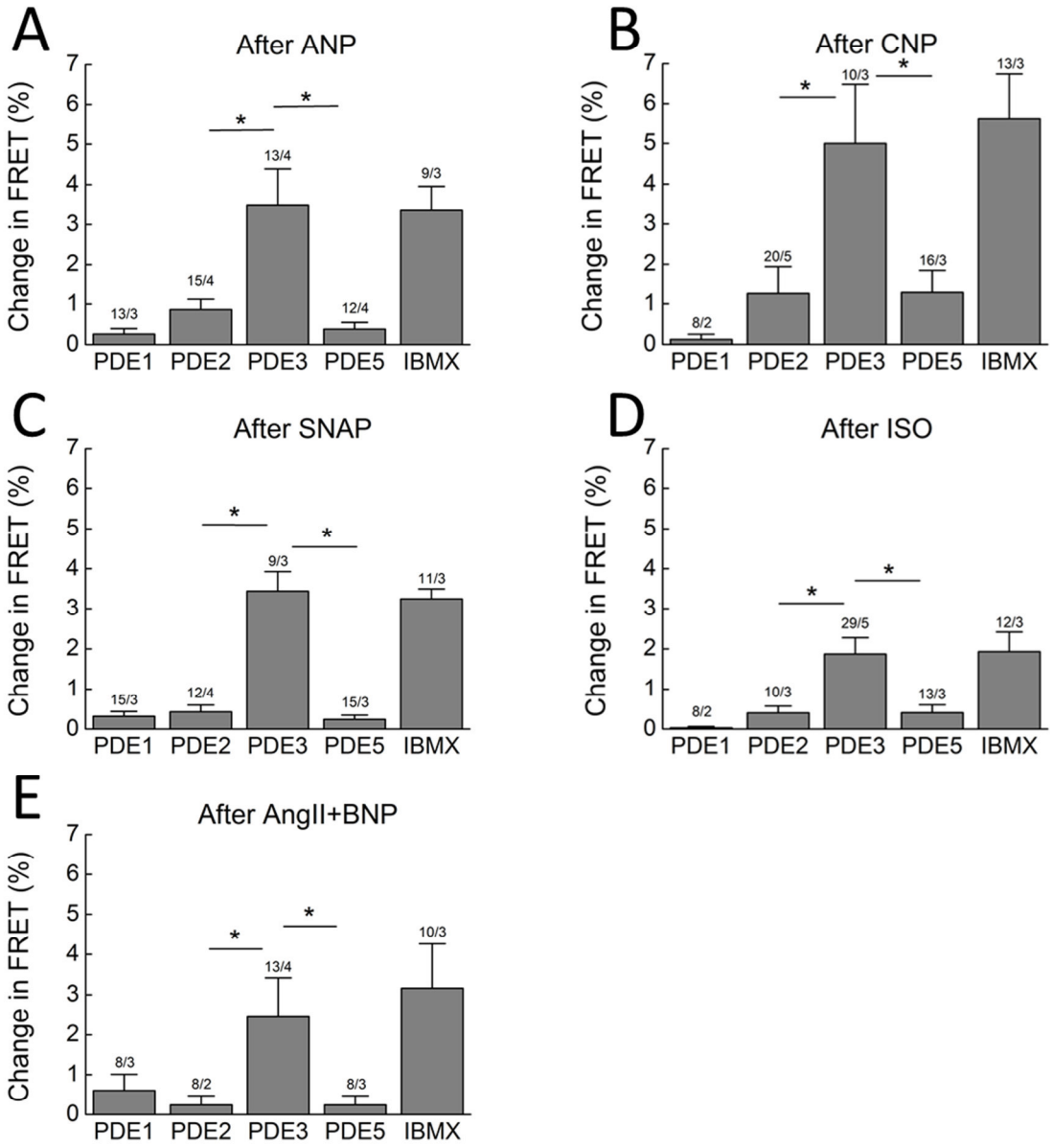

Figure 24. FRET-based measurements of cGMP-PDE activity at prestimulated states. Single isolated cardiomyocytes were prestimulated for 5 minutes with the cGMP-stimulating agents **(A)** ANP 100 nmol/L, **(B)** CNP 100 nmoL/L, **(C)** or SNAP 100 µmol/L and treated with selective PDE inhibitors, as described in Fig. 23. There were no differences among the PDE profiles, and PDE3 remained the major cGMP-PDE. **(D)** Cells were pretreated with isoproterenol 0.1 nmol/L to raise cytosolic cAMP levels, which served as a competitive substrate. cGMP hydrolytic activity of PDE3 was decreased. **(E)** Preincubation with angiotensin II (AngII) 100 nmol/L and BNP 100 nmol/L served as a model for heart failure. Shown are means ± SE, as n cells from N mice, written above the bars; significant differences ($p<0.05$) are indicated with asterisks.

3.2.4.3 Measurements of cGMP-PDE hydrolytic activity using an in vitro assay

In order to verify the FRET data on cGMP-PDEs, a classical *in vitro* assay was performed according to Thompson and Appleman. PDE hydrolytic activity was measured in lysates of cardiomyoctes isolated from transgenic and wildtype mice at cGMP 1 µmol/L.[49, 215] The assay revealed a dominant role of PDE2 and PDE5, while inhibition of PDE3 showed only minor effects (Fig. 25). These findings were contradictive to the FRET data, which showed PDE3 as the major cGMP-PDE.

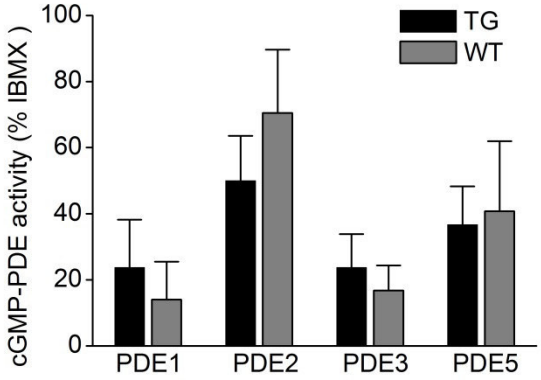

Figure 25. Measurements of PDE hydrolytic activity with a biochemical *in vitro* assay according to Thompson and Appleman. PDE activity was assayed in lysates of cardiomycytes isolated from wildtype and transgenic mice at 1 µmol/L cGMP. The effect of the selective PDE blockers was normalized to IBMX to quantify the percentage each PDE family provides to total cGMP hydrolysis. PDE2 and PDE5 were strongly involved in cGMP hydrolysis. Shown are means ± SE, from 3-4 mice per condition.

3.2.5 FRET measurements of cGMP in a model of moderate pressure-overload induced hypertrophy

To combine the live cell imaging approach with an experimental model of cardiovascular disease, transgenic mice underwent transverse aortic constriction (TAC) surgery to induce cardiac hypertrophy and remodeling. Mice were split into TAC operated group and control animals, which underwent the same operation procedure without aortic constriction (SHAM), to compare cGMP signaling in diseased versus healthy cardiomyocytes. Echocardiography at 8 weeks post TAC/SHAM operation demonstrated significant increases in heart weight to body weight ratios, wall thickness, and left ventricular end-systolic dimensions, with small but not significant reductions in functional parameters such as ejection fraction and fractional shortening, indicating a mild and compensated model of cardiac hypertrophy (Table 5).

Parameter	SHAM animals	TAC animals
Pressure gradient (mmHg)	4.7 ± 0.5	84.8 ± 4.7*
HW/BW ratio (mg/g)	4.34 ± 0.27	6.58 ± 0.44*
AWTD (mm)	0.74 ± 0.04	1.11 ± 0.05*
PWTD (mm)	0.73 ± 0.04	1.10 ± 0.05*
LV-ESD (mm)	2.85 ± 0.10	3.24 ± 0.12*
LV-EDD (mm)	3.91 ± 0.08	4.24 ± 0.03*
FS (%)	27.22 ± 1.68	23.7 ± 2.34
FAS (%)	44.65 ± 1.49	41.27± 3.08
EF (%)	50.91 ± 1.43	47.26 ±2.40
Heart rate (bpm)	443 ± 20	483 ± 24

Table 5. Characterization of transgenic mice after TAC and SHAM surgery using transthoracic echocardiography. Transgenic mice at the age of 9-13 weeks underwent transverse aortic constriction (TAC) or control (SHAM) operation. Shown are means ± SE, n= 6 mice per group, significant differences ($p<0.05$) are indicated with asterisks. HW/BW ratio, heart weight body weight ratio; AWTD, anterior wall thickness in diastole; PWTD, posterior wall thickness in diastole LV-ESD, left ventricular end-systolic dimension; LV-EDD, left ventricular end-diastolic dimension; FS, fractional shortening; FAS, fractional area shortening; EF, ejection fraction.

Since only a limited number of operated mice was available, it was decided to focus on GC-B-induced cGMP signaling, basal NO-GC activity and PDEs. A strong contribution of cilostamide-sensitve PDE3 to total cGMP-PDE hydrolytic activity could be observed (Fig. 26). Furthermore, small FRET responses upon PDE5 inhibition with tadalafil in TAC cells, which were absent in control cardiomyocytes (SHAM), were detected, indicating an upregulation of PDE5 activity during cardiac hypertrophy. Finally, there was no difference in GC-B activity between TAC and SHAM cells (Fig. 26).

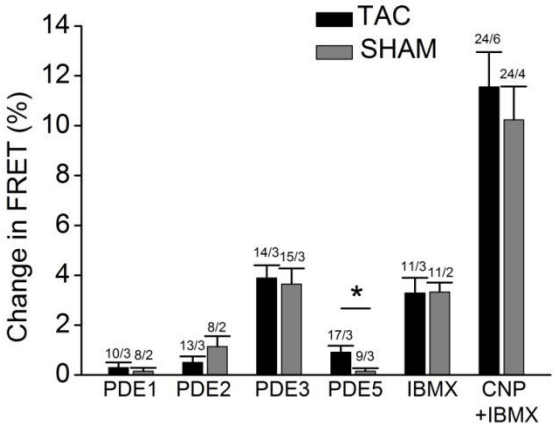

Figure 26. cGMP dynamics in a model of cardiac hypertrophy. Mice were subjected to transverse aortic constriction (TAC) surgery to induce hypertrophy, SHAM-operated mice served as controls. Myocytes isolated from TAC and SHAM mice were subjected to FRET experiments. 8-MMX 10 µmol/L was used to block PDE1, BAY 60-7550 100 nmol/L (BAY) for PDE2, cilostamide 10 µmol/L for PDE3, tadalafil 100 nmol/L (TAD) for PDE5 and IBMX 100 µmol/L (nonselective). CNP 100 nmol/L was added on top of IBMX 100 µM. An upregulation of PDE5 hydrolytic activity in the TAC model was observed. Shown are means ± SE, as n cells from N mice, written above the bars, significant differences ($p<0.05$) are indicated with asterisks.

3.2.6 Analysis of cGMP/cAMP crosstalk in adult mouse cardiomyocytes

Analysis of cGMP dynamics in cardiomyocytes from red cGES-DE5 mice revealed a major role of PDE3 in cGMP breakdown. There is considerable evidence suggesting an interplay between cAMP and cGMP signaling,[141, 227] mediated via PDE3 activity and it is worth to emphasize again that PDE3 is known as the “cGMP inhibited PDE”, since cGMP can act as an inhibitor to cAMP catabolism.[118] It was investigated whether cGMP might influence β-adrenoceptor-mediated cAMP signals through inhibition of PDE3. To study cyclic nucleotide crosstalk, FRET measurements of cAMP dynamics were performed in adult cardiomyocytes isolated from Epac1-camps mice,[192] which express the FRET-based biosensor for cAMP, Epac1-camps.[189, 193]

Cardiomyoctes were stimulated with ISO 100 nmol/L to raise cAMP concentrations by activation of β-adrenergic receptors; a decrease in FRET ratio trace indicates an increase in intracellular cAMP. Next, cAMP dynamics were monitored upon application of various agonists of guanylyl cyclase activity to assess which cGMP signaling cascade affects cAMP concentrations. Application of CNP to stimulate GC-B further increased cytosolic cAMP levels (Fig. 27A), which could be quantified as ~ 50 % of maximal PDE inhibition with cilostamide 10 µmol/L (Fig. 27E, F). Activation of GC-A trough ANP also increased cAMP generation (Fig. 27B), but the signals detected were significantly smaller than those evoked by CNP (Fig. 27F). Stimulation of NO-GC with SNAP could not increase cAMP levels. In the presence of the PDE3 inhibitor cilostamide, the effects of CNP and ANP on β-adrenergic

receptor-induced cAMP levels were not detectable (Fig. 27C, D), demonstrating that PDE3 regulates GC-A and GC-B-mediated cGMP/cAMP crosstalk after β-adrenergic stimulation.

In addition to PDE3-mediated cAMP/cGMP interplay, PDE2 has been shown to be involved in crosstalk of those cyclic nucleotides.[35, 141] cGMP stimulates PDE2 hydrolytic activity and thereby leads to a decrease in cAMP levels. Thus, activated cAMP catabolism of PDE2 might mask or even prevent a PDE3-mediated increase in cAMP. To test this hypothesis, cells were prestimulated with the PDE2 inhibitor BAY 60-7550 to evaluate if this might further increase CNP-induced cAMP generation. There was no additive effect on cAMP concentrations elicited by CNP (115.9 ± 4.4 % of ISO, n=9 cells from 3 mice) in the presence of BAY 60-7550 compared to cardiomyocytes that were solely stimulated with ISO and CNP (118.1 ± 2.8 % of ISO, n=28 cells from 6 mice, Fig. 27F). This confirmed that PDE3 conveys CNP-mediated cAMP/cGMP crosstalk after β-adrenergic stimulation, while PDE2 is not involved in the regulation of this specific cAMP/cGMP interaction.

Strong effects of CNP on cAMP generation were measured after β-adrenergic stimulation, while CNP alone in the absence of ISO failed to induce cAMP generation (0.38 ± 0.38 % of ISO, n=13 cells from 2 mice, ISO application followed CNP and served as positive control). This was expected, since cilostamide can only evoke strong signals after prestimulation with ISO (Fig. 27E). Hardly any signals were detectable at basal state (ISO + CIL 139 ± 4 % of ISO versus CIL basal 8 ± 2 % of ISO, n=11-13 cells from 3 mice each).

Finally, in contrast to natriuretic peptides, SNAP alone could not induce an increase in cAMP, but in the presence of PDE5 inhibition using tadalafil (TAD), small increases in cytosolic cAMP could be observed (Fig. 27F), while ANP and CNP-induced cAMP could not be further increased by TAD. In summary, stimulation of GC-B by CNP evokes a strong increase in cytosolic cGMP that can directly inhibit PDE3 hydrolytic activity and thus increase cAMP levels in the cytosolic department after β-adrenergic stimulation (Fig. 28).

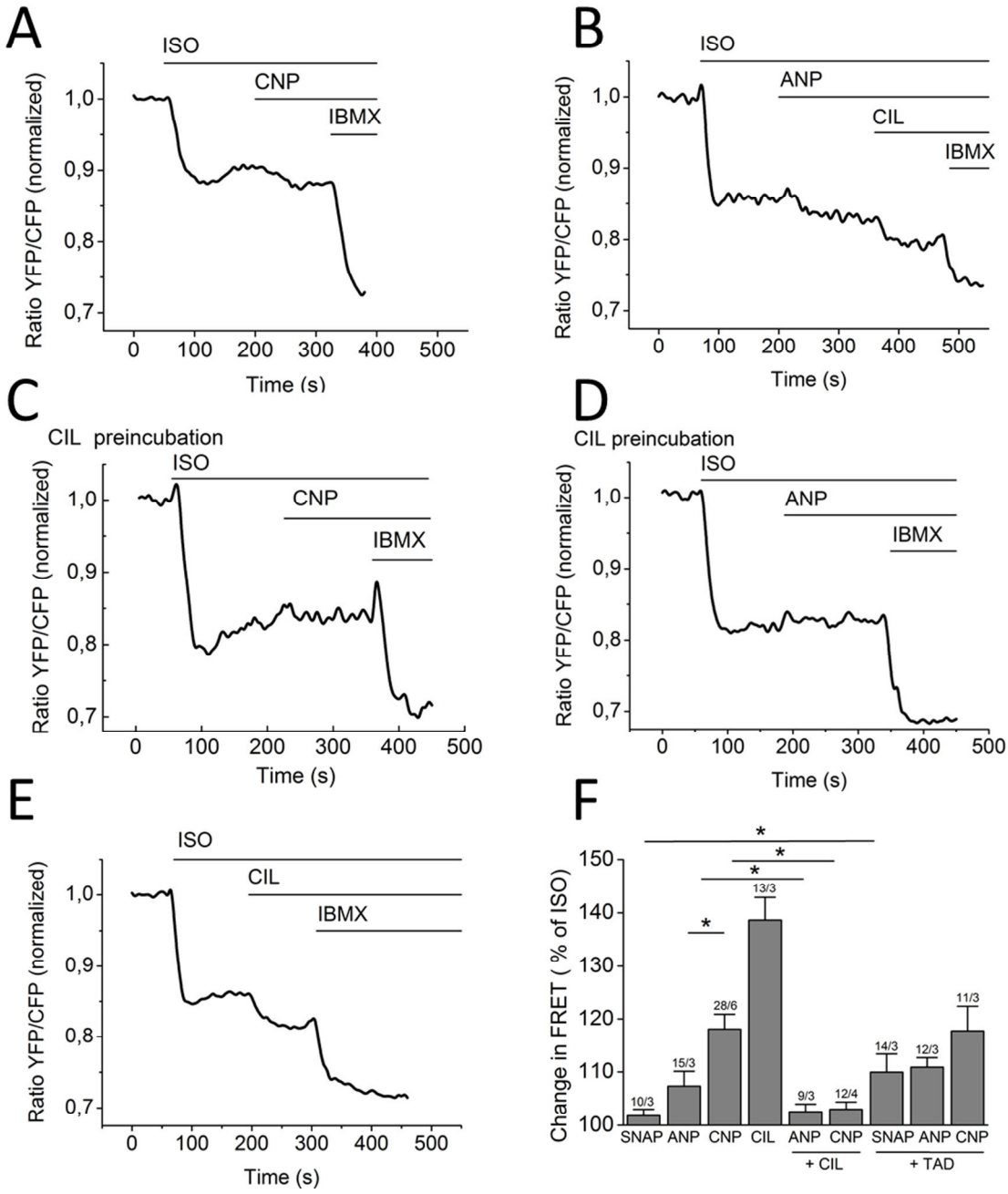

Figure 27. FRET measurements of cGMP/cAMP crosstalk. Imaging of cAMP dynamics using cardiomyocytes from Epac1-camps transgenic mice. A decrease in YFP/CFP ratio corresponds to an increase in cAMP. **(A)** CNP 100 nmol/L **(B)** and ANP 100 nmol/L further increased cAMP after β-adrenergic stimulation with isoproterenol 100 nmol/L (ISO). **(C, D)** Natriuretic peptide-induced cAMP generation was due to inhibition of PDE3, since preincubation with cilostamide 10 µmol/L (CIL) for 3 min blocked CNP and ANP effects. **(E)** Cilostamide on top of ISO served as a positive control. Final application of IBMX 100 µmol/L **(A-E)** led to a strong signal, indicating that effects evoked by CNP, ANP and CIL were in the dynamic range of the sensor. **(F)** Quantification of FRET responses from A-E, shown are means ± SE, as n cells from N mice, written above the bars, significant differences ($p<0.05$) are indicated with asterisks. Inhibition of PDE5 with tadalafil 100 nmo/L (TAD) induced small increases in cAMP upon SNAP application. PDE 5 did not affect ANP-and CNP-induced cAMP generation. Quantification of FRET responses is also shown in **(F)**.

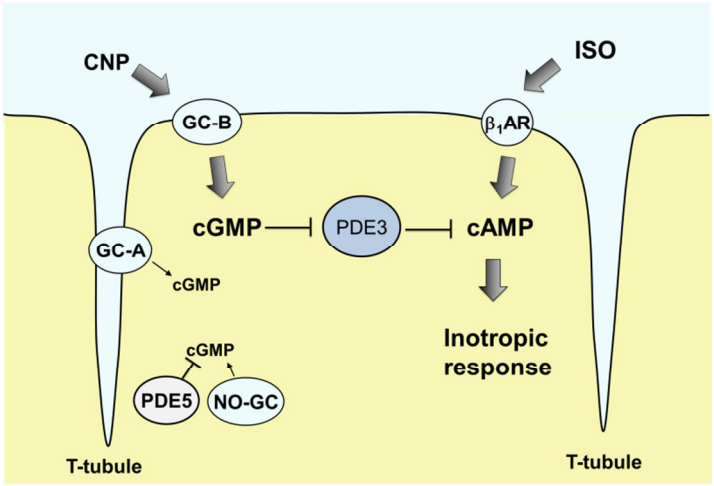

Figure 28. Schematic diagram showing cGMP/cAMP interplay mediated by PDE3. Stimulation of GC-B with CNP leads to a robust increase in cytosolic cGMP levels. This pool of cGMP is a competitive substrate to cAMP hydrolysis of PDE3 and can be described as a PDE3 inhibitor. Thus, GC-B-induced cGMP blocks PDE3 activity and raises cAMP levels after β-adrenergic activation. GC-A can also induce cGMP levels that modify PDE3 activity. NO-GC-mediated cGMP is tightly controlled by PDE5 hydrolytic activity.

3.2.7 Measurements of cGMP synthesis in neonatal and adult rat cardiomyocytes

Neonatal rat cardiomyocytes were transfected with red cGES-DE5 encoding sensor plasmid and subjected to FRET measurements. Stimulation of GC-A and GC-B activity with natriuretic peptides resulted in small increases in cGMP upon ANP and strong CNP-evoked signals, which were quite similar to those detected in adult mouse cardiomyocytes (Fig. 29A). Interestingly, clear responses to NO-GC stimulation were detected with SNAP 100 µmol/L in neonatal rat cells, as reported by others.[141, 148] These SNAP responses were absent in adult cardiomyocytes (Fig. 18E). Immunoblot analysis of NO-GC expression revealed a 2.9 ± 0.2-fold higher NO-GC protein levels in neonatal versus adult cardiomyocytes, which might explain the absent SNAP response in adult cardiomyocytes (Fig. 29B).

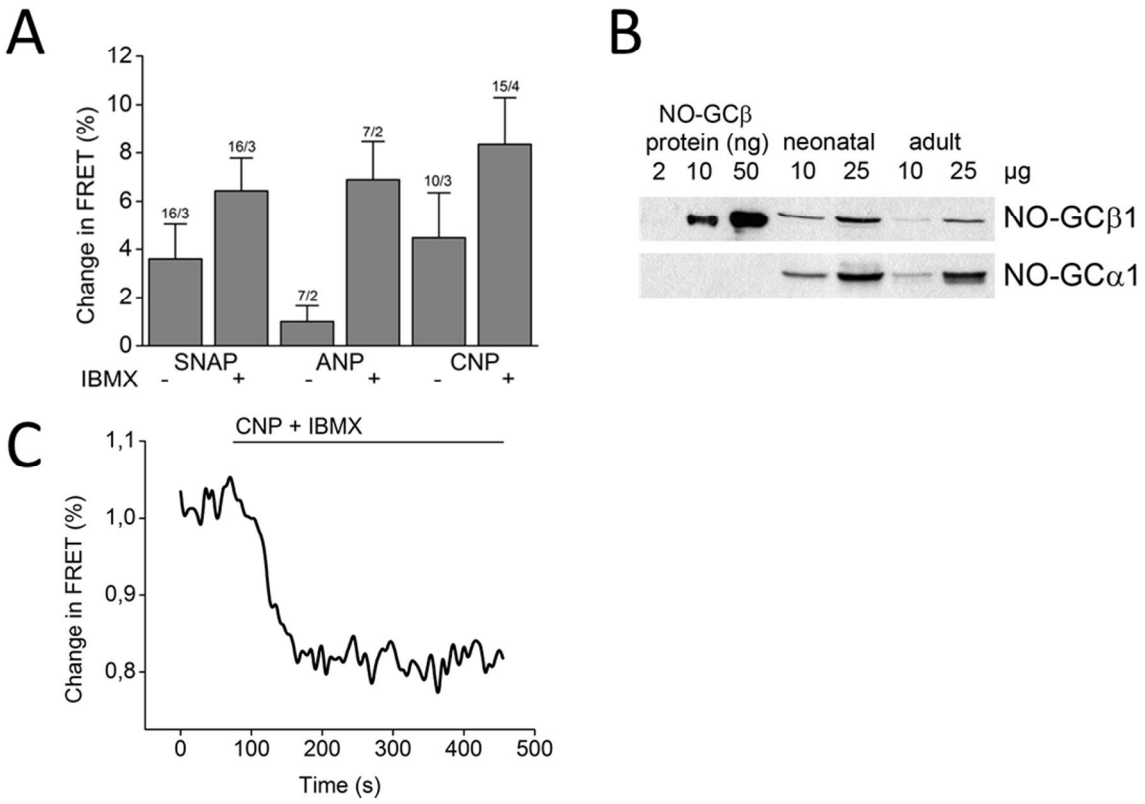

Figure. 29 FRET measurements of cGMP production in neonatal rat cardiomyocytes, NO-GC expression levels in neonatal versus adult cardiomyocytes, and CNP-induced increase in cGMP detected in adult rat cardiomyocytes. (A) Neonatal rat cardiomyocytes transiently transfected with red cGES-DE5 showed a robust FRET response to SNAP 100 µmol/L, which was not detectable in adult mouse cardiomyocytes (see Fig. 18E). Stimulation with ANP 100 nmol /L and CNP 100 nmol/L also increased cGMP synthesis, IBMX was added with a concentration of 100 µmol/L. Shown are the quantifications of FRET responses as means ± SE, as n cells from N isolations, written above the bars. **(B)** Immunoblot analysis of NO-GC expression in neonatal versus adult cardiomyocytes. Expression levels were compared with 2, 10 and 50 ng recombinant NO-GCβ protein. Neonatal rat cardiomyocytes (mouse hearts are too tiny for isolation protocol) express 2.9 ± 0.2-fold more NO-GC than adult mouse cardiomyocytes (mean ± SE). **(C)** Isolated adult rat cardiomyocytes were infected with adenovirus encoding red cGES-DE5 and subjected to FRET experiments. Representative recording is shown: CNP 1 µmol/L + IBMX 100 µmol/L caused a strong increase in cGMP.

Finally, adult rat cardiomyocytes were infected with red GES-DE5 adenovirus and revealed desirable FRET responses on stimulation with CNP, as observed in mice (Fig. 29C).

4 Discussion

4.1 Real time visualization of cAMP dynamics in the vicinity of the RyR2 using Epac1-camps-JNC transgenic mice

4.1.1 Generation and characterization of Epac1-camps-JNC transgenic mice

A new transgenic mouse model was generated to allow live cell imaging of cAMP dynamics in vicinity of the cardiac ryanodine receptor (RyR2). To do so, a targeted FRET-based biosensor was created by the fusion of cytosolic Epac1-camps with junctin molecule. It is established that junctin is associated with the RyR2, and direct binding interactions of both proteins were identified.[54, 228, 229] The RyR2, calsequestrin, triadin and junctin form a quaternary complex that facilitates Ca^{2+} release from the SR. A functional role of junctin in Ca^{2+} cycling was proposed.[229] However, cardiomyocyte-restricted sensor expression did not affect heart performance but caused a mild compensated hypertrophy revealed by significantly increased wall thickness (see Table 3). In a previous report, 10-fold overexpression of junctin, using the same promoter and mouse background, caused mild hypertrophy with slightly impaired relaxation, a 30 % reduction in the expression levels of the RyR2, and almost unaffected Ca^{2+} transients.[230] Yet a 30-fold overexpression caused a much more severe phenotype.[231] However, Ca^{2+} transients and expression levels of junctional proteins were not investigated in the Epac1-camps-JNC transgenic mice, since the decision was made to focus on the red cGES-DE5 mouse model. The fact that the Epac1-camps-JNC mice develop modest hypertrophy represents a certain limitation, since it was initially intended to study cAMP dynamics during cardiac hypertrophy after aortic banding, as this was done with the red cGES-DE5 mice. Here, one can consider the possibility to cross Epac1-camps-JNC mice into junctin null background using junctin knock-out mice.[232]

4.1.2 Characterization of the Epac1-camps-JNC biosensor in cardiomyocytes

The Epac1-camps-JNC represents a targeted version of the cytosolic FRET-based Epac1-camps to permit cAMP detection not virtually everywhere within the cell, but with a spatially highly defined resolution. Epifluorescence images of cardiomyocytes expressing Epac1-camps-JNC showed a striated localization of the biosensor, which was in clear contrast to cardiomyocytes from Epac1-camps mice emitting fluorescent light throughout the whole cell (see Fig. 12A). In addition, one could co-localize the Epac1-camps-JNC with the RyR2 in

cardiomyocytes, giving good evidence that the sensor is associated with the RyR2 (see Fig. 12B). Nonetheless, it is important to consider that co-localization and other methods for the analysis of protein interactions are of only limited value for this study, since they do not provide the essential information whether the sensor and the investigated cAMP microdomain actually overlap or not. Thus, association of the biosensor to the RyR2 does not imply that the sensor and, even more important, its cAMP binding domain sits in the right position, namely in the cAMP compartment that is supposed to regulate RyR2 function. Dose-response titrations in cardiomyocytes and HEK 293 cells confirmed that fusion of the Epac1-camps with junctin molecule did not alter its affinity for cAMP (see 3.1.3). This finding was highly relevant, since it was intended to compare cytosolic cAMP dynamics (recorded with the Epac1-camps) with the cAMP dynamics at the RyR2 (measurements carried out with the Epac1-camps-JNC). However, the Epac1-camps-JNC showed smaller signal changes compared with the Epac1-camps. This is illustrated by the fact that ISO + IBMX induced a 13 % change in FRET using Epac1-camps-JNC and a 24 % change in FRET was observed with the Epac1-camps (see 3.1.3). One can expect such a signal decrease since the Epac1-camps-JNC contains the junctin protein probably influencing the conformational movement upon cAMP binding. Thus, for the comparison of cAMP fluctuations in the cytsosol and the RyR2 associated compartment, one cannot consult absolute changes in FRET, but it is necessary to relate the data to physiological values (such as an ISO response, see Fig. 15). In conclusion, the *in vitro* characterization of Epac1-camps-JNC gave proof that the biosensor was promising for the visualization of local cAMP dynamics at RyR2 and that a comparison of cAMP dynamics recorded with its untargeted predecessor Epac1-camps is possible.

4.1.3 FRET-based measurements of cAMP synthesis

Classical signaling of β_1-and β_2-adrenergic receptors involves the formation of cAMP. It was demonstrated by Nikolaev *et al.* that the β_1-AR subtype shows a broad distribution on the membrane, while the β_2-AR is locally restricted in the T-tubular invaginations.[233] Furthermore, it was shown that the β_1 subtype induces a major increase in cAMP throughout the whole cell, wheras the β_2-initiated signals are spatially highly confined.[188] Indeed, robust increases in cAMP content were detected upon selective stimulation of β_1-ARs using both biosensors (see Fig. 13). In contrast, the β_2 signals were absent in almost all cardiomyocytes isolated from Epac1-camps-JNC, while very small β_2 responses were observed in the Epac1-camps mice. There were no significant differences between the RyR2 microdomain and the bulk cytosol. Yet, one might postulate that the β_2-signals do not reach the biosensor targeted to the RyR2, while there were very small responses detectable in ~50 % of cardiomyocytes carrying the cytosolic Epac1-camps. However, given the fact that two biosensors have

slightly different characteristics and the Epac1-camps-JNC shows significantly smaller changes in FRET signal and a decreased signal-to-noise ratio, these differences are most likely due to the variations in biosensor properties but do not reflect differences in physiology of cAMP signaling. A pair of biosensors with increased affinity for cAMP, for instance Epac2-camps-JNC and Epac2-camps might help resolve this issue.

4.1.4 FRET-based measurements of cAMP degradation

It was demonstrated that PDE4D3 and other key components of cAMP signaling (PKA and phosphatases) are associated with the RyR2 via mAKAP and form a cAMP microdomain that regulates the RyR2.[50, 51] Furthermore, it was postulated that cardiac remodeling, which occurs during heart failure, causes depletion of PDE4D3 form the microdomain leading to PKA-mediated hyperphosphorylation of the RyR2 at single serine 2808 and associated Ca^{2+} leak.[50] Finally one has to consider that global cAMP levels were amounted to ~10 µmol/L, whereas the affinity of PKA is in the range of 10 nmol/ –100 nmol/L *in vitro*. This would imply that PKA is ultimately fully active, even at basal and unstimulated state.[1] Thus, the major working hypothesis for this study was that local PDE4D3 activity shapes a pool of low cAMP concentrations at the cardiac RyR to protect the channel from excessive phosphorylation. In healthy hearts, β-adrenergic stimulation causes an increase in cAMP, strong enough to overcome the PDE4D3 barrier, to activate PKA for channel phosphorylation and Ca^{2+} gating to facilitate myocyte contraction. Quite similar, pathological remodeling causes PDE4D3 depletion, hyperphosphorylation and leaky RyRs (increased Ca^{2+} gating during diastole), which are associated with heart failure and arrhythmias.

In consequence, application of rolipram to selectively block PDE4 activity should mimic “depletion of PDE4D3” to cause cAMP diffusion into the RyR2 associated microdomain, where the Epac1-camps-JNC is supposed to reside and evoke a FRET signal. However, significant FRET responses upon rolipram were not detected (see Fig 14A). Analysis of basal cAMP hydrolysis revealed a major contribution of PDE3 to total cAMP hydrolysis, and to a very small extent PDE4 was also involved (at least detected with the Epac1-camps). Non-selective PDE inhibition with IBMX caused strong FRET signals in myocytes from Epac1-camps as well as Epac1-camps-JNC mice, indicating high basal cAMP levels, which had amounted to ~1 µmol/L previously.[191] The raise in cAMP upon IBMX significantly exceeded the effects of single inhibition of PDE3 and PDE4, thus one might propose that these PDEs from a “double layer” which controls cAMP levels and one PDE can replace the other (see Fig. 14).[234] Nevertheless, the Ca^{2+} leak hypothesis implies that chronic catecholaminergic overload causes hyperphosphorylation of the RyR2. Therefore, inhibition of PDEs was performed after beta adrenergic stimulation with isoproterenol 100 nmol/L. It was found that

PDE4 is the major regulator of cAMP amount after beta adrenergic stimulation and a smaller contribution of PDE3, as described by others.[142, 188, 235] Since inhibition of PDE4 caused increases in cAMP levels which were close to the sensor saturation, PDE4 inhibition was repeated after a smaller amount of ISO (5 nmol/L) to measure in the dynamic range of the FRET sensors. Finally, there was no significant difference in PDE4 activity detectable, when comparing RyR2 compartment and cytosol, as this was the case after isoproterenol 100 nmol/L (see Fig. 15).

4.1.5 Outlook

In conclusion, there were no differences in cAMP signaling detectable using cytosolic Epac1-camps and its targeted version Epac1-camps-JNC. The findings argue against a cAMP microdomain that is under control of PDE4 hydrolytic activity. A potential explanation is that the cAMP indicator, or at least its cAMP binding domain might be excluded from the microdomain and reflects changes in the bulk cytosol despite of cAMP dynamics of the so-called RyR2 compartment. One has to imagine that the RyR2 is a large protein, and the sensor is targeted to junctin molecule which is not associated to the N-terminal domain of the RyR2 where PDE4 should reside but is anchored in the SR membrane only in close proximity to the RyR2. Thus, it is most likely that the Epac1-camps-JNC is simply orientated in an unfavourable angle to the receptor and localized too far away from the microdomain formed by PDE4 activity. One could think of fusing Epac1-camps to another protein of the RyR2 signaling complex to test whether this sensor might be better located inside this microdomain.

4.2 Real time visualization of cGMP dynamics in adult cardiomyocytes using red cGES-DE5 transgenic mice

4.2.1 Generation and characterization of red cGES-DE5 transgenic mice

A new transgenic mouse model with cardiomyocyte-specific expression of the FRET-based cGMP biosensor red cGES-DE5[198] was generated to allow real time visualization of cGMP dynamics in adult cardiomyocytes.[208] Transgenic expression of the cGMP indicator did not influence morphology of cardiomyocytes and whole hearts, as demonstrated by histological and morphometric analysis (see Fig. 16). Neither was any impact on *in vivo* heart performance detectable using transthoracic echocardiography (see Table 4). The fact that the transgenic mice have healthy hearts provides the potential to combine the biosensor mouse model with various genetic and experimental models of cardiovascular disease to monitor cGMP under normal and modified conditions. Red cGES-DE5 mice were crossbred with β_3-AR-TG or β_3-AR-KO mice to generate double transgenic mice, which showed sensor expression and overexpression of the β_3-AR (red cGES-DE5$^{+/0}$; β_3-AR$^{+/0}$), or sensor expression and β_3-AR deficiency (red cGES-DE5$^{+/0}$; β_3-AR$^{-/-}$), to study β_3-AR-mediated cGMP signaling (see Fig. 22).[158] Finally transverse aortic constriction surgery was performed on red cGES-DE5 mice, to monitor signaling of cGMP in an experimental model of cardiac hypertrophy (see Fig. 26).[236, 237] As demonstrated by the double transgenic and TAC operated mice, the red cGES-DE5 transgenic mice can serve as a basis for further investigations, which might help identify new targets for the treatment of heart failure and other cardiovascular diseases.

An alternative to the transgenic mouse is adenovirus-mediated sensor expression in isolated cardiomyocytes.[206, 210] This technique is not dependent on the time-consuming generation of a new transgenic animal model, but has serious disadvantages compared with the sensor mice. Single cardiomyocytes are isolated from wildtype mice, infected with red cGES-DE5 encoding adenovirus and imaging experiments are performed after 48 hours of cell culture, which is required for biosensor expression. Culture of isolated cardiomyocytes leads to a decrease in cell quality and drastic changes in morphological structures[238] that are relevant in the regulation of compartmentalized signaling of cyclic nucleotides.[233] However, isolation and culture of cardiomyocytes have been challenging, especially of adult mouse myocytes.[206] The red cGES-DE5 mice provide the possibility to perform imaging experiments in freshly isolated cardiomyocytes showing high levels of cell quality, which is strongly necessary for imaging experiments in living cells. In contrast to adult mouse cardiomyocytes, it is much

simpler to handle neonatal and adult rat cardiomyocytes, which can be infected with adenovirus and kept in culture showing high cell quality (see Fig. 29).

Measurements of cGMP dynamics are highly demanding and little is known about the spatio-temporal organization of cGMP in cardiomyocytes, which is mainly due to limitations of imaging techniques. There were reports on cGMP measurements in neonatal rat cardiomyocytes using FRET-based live cell imaging.[35, 141, 148] It is worth mentioning that neonatal cardiomyocytes have strongly elevated cGMP levels compared to adult cells, and important morphological structures involved in cyclic nucleotide-mediated signaling, are absent (such as T-tubules)[239, 240] or not fully developed.[241] Therefore, neonatal cardiomyocytes might not properly reflect cGMP signaling in adult cells. Even more important, measurements of real time dynamics of cGMP in cultured rat adult cardiomyocytes have been performed using rat olfactory cyclic nucleotide gated (CNG) channels as reporters for cGMP.[49, 201] Since CNG channels are located at the plasma membrane, cGMP detection is limited to the subsarcolemmal compartment and recordings do not reflect overal changes in cGMP. Another drawback is very poor selectivity for cGMP over cAMP.[242] Recently, other cGMP-FRET mouse models were published, with ubiquitous and smooth muscle-specific expression of cGi500 probe.[220] These mice allow *in vivo* FRET measurements of cGMP in vascular, colon and bladder smooth muscle cells, while measurement in the heart were not reported. Due to its lower cGMP affinity (see Table 2), cGi500 can detect cGMP levels from approximately 100 nmol/L to 3 µmol/L,[180, 220] while cGMP levels in adult cardiomyocytes may be below the dynamic range of this sensor.[191] To my knowledge, red cGES-DE5 transgenic mice allowed the first FRET-based measurements of cGMP in adult mouse cardiomyocytes.

4.2.2 Analysis of cGMP synthesis

First, cGMP production was induced by treating cardiomyocytes with natriuretic peptides and NO donors to activate particulate (GC-A, GC-B) and soluble (NO-GC) guanylyl cyclases. Stimulation of GC-B with CNP resulted in strong increases in cytosolic cGMP, while the GC-A ligands ANP and BNP evoked only border line responses and SNAP failed to generate NO-GC-mediated cGMP (see Fig. 18). Similar results were obtained using RIA-based measurements of cGMP stimulations in wildtype cardiomyocytes, which confirms the FRET imaging of cGMP, but also suggests that the FRET-based cGMP reporter describes total changes in cGMP amount, that most likely occur in the entire cytosol.

One might conclude that stimulation of GC-B with CNP generates cGMP that can diffuse deep into the cell and leads to a remarkable increase in cytosolic cGMP. This cGMP pool

was associated with phosphorylation of phospholamban (PLB), a target of cGMP dependent kinase type I (cGKI) in a model of isolated working mouse hearts (see Fig. 20). Various studies have showed that CNP causes a robust increase in cGMP levels and cGKI-mediated phosphorylation of PLB[29, 115, 165, 243, 244] that influences heart function. Most authors described posititve lusitropic effects of CNP, while negative[29, 243-245] and positive[115, 246, 247] influence on contractility have been reported. Interestingly, CNP stimulations in working heart preparations induced stronger increases in cGMP amount compared with single cardiomyocytes (see Fig. 20A, 18F), most likely due to GC-B activity in cardiac fibroblast,[248] which were excluded in the single myocyte measurements. Yet, phosphorylation of PLB gave proof that the raise in cGMP was also mediated by GC-B activity in cardiomyocytes of working hearts, since fibroblasts lack the PLB protein (see Fig. 20B).

Even more important is the fact, that RIA-based measurements of cGMP stimulations in transgenic mice are required to directly compare cyclase activity in transgenic versus wiltype cells. Anyway, measurements of cGMP in FVB/NRj mice proved difficult to perform due to low cGMP levels and several attempts to detect cGMP amounts failed. A limited number of experiments performed by Birgit Gassner (AG Kuhn, Department of Physiology, Würzburg) revealed slightly stronger CNP-stimulated cGMP content in transgenic versus wildtype cardiomyocytes which was not statistically significant (352 ± 49 versus 586 ± 92 fmol/1x10^5cells, n= 3-4 hearts), therefore further experiments are needed. Due to the fact that several attempts to detect cGMP by RIA failed and C57/Bl6 mice show stronger increases in cGMP detected with RIA (Michaela Kuhn, personal communication), crossing red cGES-DE5 mice into C57/Bl6 background for further investigations was initiated. It is worth mentioning that potent CNP-evoked cGMP signals were observed in neonatal and adult rat cardiomyocytes infected with red cGES-DE5 sensor (see Fig. 29) further indicating a pronounced role of GC-B in cGMP production in rodent cardiac myocytes.

In contrast to strong cytosolic CNP-mediated cGMP, stimulation of GC-A with ANP and BNP evoked only minor effects. However, an absent effect of ANP, as the FRET and RIA measurements might suggest, is not postulated. One has to refer to the possibility that ANP-evoked cGMP pools might be localized close to the plasma membrane and do not reach the deeper parts of the cytosol.[35, 49, 141] This might also explain the very small effects of GC-A stimulation detected in C57/Bl6 mice,[29] and in isolated rat cardiomyocytes[244] (in both studies ANP << CNP), with no influence on contractility.[29] In addition, one could observe small effects on cAMP levels mediated by PDE3 inhibition after β-adrenergic stimulation, detected in Epac1-camps transgenic mice (see Fig. 27). Given the fact that cGMP signaling is compartmentalized,[49, 141, 148] and PDEs are crucially involved in the regulation of cAMP and cGMP microdomains,[249, 250] ANP-induced cGMP production might be strictly counterbalanced

by its degradation via PDEs. Still, subsequent PDE inhibition failed to unmask ANP-generated cGMP. Hence, one might suggest that other mechanisms, such as physical barriers[251] could be involved in the organization of cGMP compartments. A localized version of the red cGES-DE biosensor, targeted to the plasma membrane compartment might help resolve this issue. Finally, small responses to ANP were detected in neonatal rat cardiomyocytes (see Fig. 29), as described in the literature.[141]

The lack in FRET signals after treatment with SNAP was unexpected, since numerous studies found effects on cardiac functionality, although with contradictory outcomes.[68] There are several aspects that might help explain the divergent results. First NO acts through various pathways, it stimulates NO-CG and thus activates the cGMP/cGKI signaling, but also direct effects of NO on proteins via oxidative modification of thiol groups, termed S-nitrosylation, have been described;[252] those are independent of NO-GC and cGMP. Second myoglobin acts as a scavenger of NO and prevents NO to reach the target receptor.[25, 253] Anyway, red cGES-DE5 mice were created to monitor cGMP levels and not heart function. It is established that NO donors increase cGMP amount in the heart, including vascular smooth muscle cells, where classical NO/cGMP signaling occurs. In contrast, cGMP formation in cardiomyocytes remains less clear, with studies showing NO-donor-mediated increase in cGMP,[49, 69] as well as no effects on cGMP content.[254]

SNAP is well-established and is the most widely used NO donor, but it might act to slow for live cell imaging experiments since the half-life of SNAP is approximately 6 hours at 37°C.[255] Thus, other agents that spontaneously release NO (no prodrugs) were applied, such as sodium nitroprusside (SNP) 50 µmol/L, Diethylamine NONOate (DEA/NO) 1 µmol/L and PROLI-NONOate (PROLI-NO) 1 µmol/L, which have a different pharmacokinetic profile. For instance, DEA/NO and PROLI-NO release NO rapidly in a pH dependent manner, following first order process with a half-life of 2 min or 1.8 seconds at 37°C, respectively.[256-258] SNP agent was prepared freshly before added to the cells, where it releases NO when the drug gets in contact with the cell membrane, independently of enzymes. However this class of compounds that activate NO-GC via release of NO failed to evoke cGMP signals (see Fig. 19). Hence, stimulation of β_3-adrenergic receptors was tested to induce NO-GC activity, with ISO 100 nmol/L in the presence of selective β_1-and β_2-blockers.[35] Neither in wildtype, nor β_3-AR-overexpressing mice (red cGES-DE5$^{+/0}$; β_3-AR), robust increases of cGMP amount were detectable. Also, the NO-GC activator BAY 58-2667 (Cinaciguat), which activates even insensitive NO-GC,[91] failed to evoke signals.

As demonstrated, various drugs did not stimulate cGMP production via NO-GC in single isolated cardiomyocytes, but the isolation process itself might cause cell damage via

generation of ROS in the cardiomyocyte, which can oxidize NO-GC and cause insensitive enzyme. To exclude this possibility, cardiomyocyte isolation and imaging experiments were performed in the presence of the ROS scavenger melatonin,[222] which did not lead to measurable NO-donor effects.

Small increases of cGMP upon NO donor treatment have been reported in neonatal rat cardiomyocytes, as detected with FRET-based cGMP probes.[141, 148] Therefore, neonatal rat cardiomyocytes were transiently transfected with red cGES-DE5 biosensor to test, whether the cGMP indicator is able to detect cGMP pools that are associated with NO-GC activity or if the sensor might be excluded from the NO-GC compartment. Indeed, clear increases in cGMP upon stimulation with SNAP were observed (see Fig. 29), as described with the other FRET-based cGMP reporters. A possible explanation for SNAP signals detectable in neonatal, but absent in adult cells might be a ~3-fold higher expression of NO-GC in neonatal versus adult cardiomyocytes.

As for the neonatal cells, a small increase in cGMP amount was observed in left ventricular heart tissue that has been perfused with SNAP in a working heart preparation. The effect was rather small compared with the rise in cGMP generated by CNP (~3-fold versus ~12-fold increase in cGMP contents) and did not cause cGKI-mediated PLB phosphorylation (see Fig. 20). This raise in cGMP is most likely due to stimulation of NO-GC in smooth muscle cells, which showed strong increases in cGMP production upon application of NO-donors.[220] However, SNAP effect was absent in isolated cardiomyocytes also using RIA-based cGMP detection technique (see Fig. 18F). Last, the absence of PLB phosphorylation, which is expressed in myocytes but not in smooth muscle cells, supports the hypothesis that increases in cGMP content upon SNAP, observed in heart tissue, were generated via the classical NO/NO-GC/cGMP-pathway in non-myocyte cells.

Finally in the presence of β-adrenergic stimulation and concomitant PDE5 inhibition with Tadalafil 100 nM, borderline responses upon stimulation were detected in isolated cardiomyocytes carrying red cGES-DE5 (3.7 ± 0.4 %, mean± SE, n=12 cells from 3 mice, data acquired by Dr. Nikolaev).

Studies on cGMP generation were mostly performed in heart tissue and not in cardiomyocyte-enriched preparations and focused either on NO- or natriuretic peptide-mediated cGMP formation. Here, both pathways were assessed side by side and GC-B was found to be the most active guanylyl cylclase in cardiomyocytes. The role of GC-B in cardiomyocytes is poorly understood and probably underestimated, since GC-A and NO-GC are under more intensive investigation. Collectively, the data indicate that GC-B is the

predominant source of cGMP production in cardiomyocytes, while GC-A and NO-GC play much less prominent roles.

4.2.3 Analysis of basal cGMP formation

Stimulation of NO-GC did not evoke robust FRET signals, but ODQ revealed basal cGMP synthesis via NO-GC, with unstimulated cardiomyocyte cGMP levels amounted to ~10 nmol/L. Inhibition of GC-A with A71915 failed to decrease resting cGMP levels, supporting the fact that unstimulated cGMP levels are produced by NO-GC (see Fig. 21). Increased ODQ effects were observed in mice overexpressing the β_3-AR, while decreased ODQ responses were detected in β_3-AR-deficient mice (see Fig. 22). These findings indicate that cardiomyocytes from β_3-AR-TG mice showed increased basal cGMP, while the β_3-AR-KOs have decreased cGMP, thus supporting a role of the β_3-AR in the regulation of basal cGMP. However, direct pharmacological stimulation of the β_3-AR failed to increase cardiomyocyte cGMP. In conclusion, one could postulate that the β_3-adrenceptor acts as a constitutively active receptor, which maintains basal cGMP levels in myocytes of the adult mouse.[158] Given the fact that adult cardiomyocytes express little NO-GC (see Fig. 29) and basal cGMP synthesis is under control of β_3-adrenoceptors, one might speculate that the NO-GC/cGMP system is even at unstimulated state producing cGMP at its maximal capacity, which might explain the lack in NO-donor effect. To test this hypothesis, cardiomyocytes were incubated in N-Nitro-L-arginine methyl ester (L-NAME) 300 µmol/L, which is an inhibitor of NOS, to relieve NO-GC from basal cGMP production and uncouple the cyclase from the β_3-AR. Hence, endogenous NO-GC stimulation should be decreased to permit a prospective NO-donor effect. Still, there were no responses to NO donor after preincubation with L-NAME observed, suggesting that β_3-AR is not the only mechanism that controls basal cGMP levels.

4.2.4 Analysis of cGMP degradation by PDE hydrolytic activity

FRET measurements of cGMP hydrolysis revealed a strong contribution of PDE3 to total cGMP turnover at basal and prestimulated state, while inhibition of PDE1, 2 and 5 activity showed only negligible effects (see Fig. 23, 24). PDE3 dominated cGMP degradation in adult cardiomyocytes at resting state and after prestimulation with cGMP agonists. However, the presence of the competitive substrate cAMP strongly reduced cilostamide-induced FRET responses. Nevertheless, PDE3 effects were still stronger than those of the other PDEs, and PDE3 remained the major cGMP-PDE. This was also true for a model of heart failure using preincubation in BNP and angiotensin II, further confirming the central role of PDE3.

The signals evoked by all PDE blockers were small compared to CNP-induced effects, and no clear opposing effects in raw donor (T-Sapphire) and acceptor (Dimer2) single intensities could be observed online. Since T-Sapphire intensity (GFP) is vastly higher than Dimer2 (RFP) and the bleedthrough coefficient was 94 %, it is most likely that small changes in RFP intensity channel are simply overlapped by contrary changes in brighter GFP intensity which are also detected in the RFP intensity channel but must be substracted afterwards. After bleedthrough correction, the single channel intensities showed opposing effects. The mismatch in RFP and GFP intensity (GFP>>RFP) is most likely the reason why uncorrected donor and acceptor traces did not run into opposite directions after small or modest increases in cGMP content, as those seen after CNP application (see Fig. 17). In addition, a modified version of Epac1-camps, where CFP and YFP fluorescent proteins were replaced by GFP (T-Sapphire) and RFP (Dimer2), respectively, (kindly provided by Prof. Feil, Department of Biochemistry, Tübingen) showed similar behavior. Stimulation with ISO to induce a strong increase in cAMP showed a change in FRET ratio, but the uncorrected single intensity channels ran into the same direction. The original Epac1-camps containing CFP/YFP FRET pair showed opposing changes in YFP and YFP intensities even without bleedthrough correction after the same cAMP stimulus. Nevertheless, small increases in cAMP also can lead to a lack in opposing CFP and YFP intensities detected with Epac1-camps.

The finding that PDE3 is the major cGMP-PDE controlling basal cGMP levels was unexpected, since PDE3 is mainly described as a cAMP-PDE in the literature.[118, 249] Thus, PDE hydrolytic activity was assessed in homogenates of isolated cardiomyocytes using a classical PDE assay according to Thompson and Appleman. A strong contribution of PDE2 and PDE5 was found, while cilostamide-sensitive PDE3 hardly affected total cGMP degradation (see Fig. 25). These findings do not agree with opposite results detected with the FRET approach, but confirm what others have reported.[49, 259] Nevertheless, it is important to consider that established biochemical assays are carried out at 1 µmol/L cGMP as a substrate, while physiological cGMP levels in adult cardiomyocytes are far below this concentration, in the low nanomolar range. Those non-physiologically high cGMP levels most likely modulate PDE hydrolytic activity. For instance, PDE5 and PDE2 activity can be activated by binding of cGMP to regulatory GAF domains, leading to an increase in its cGMP hydrolytic activity. This might explain the strong effects of tadalafil (PDE5) and BAY (PDE2) on cGMP-induced highly active PDE5 and PDE2, which were not detectable at low cGMP with the cGMP indicator, but were overestimated in the PDE activity assay. In addition, PDE2 shows low affinity (K_m = 10 µmol/L) for cGMP compared with PDE3 (K_m = 0.02 µmol/L), but a very high catalytic turnover of cGMP (V_{max} = 123 µmol/min/mg for PDE2 vs V_{max} = 0.34

µmol/min/mg for PDE3),[118] which may also lead to strong response at high cGMP levels. Finally, the experiments were performed in lysates in the presence of detergent, which causes redistribution of PDEs from their original compartments. Thus, PDEs that normally reside in a compartment with higher or lower cGMP levels compared to the bulk cytosol, are now homogenously distributed and hydrolyze total cGMP. Therefore, FRET measurements of cGMP dynamics in living intact cardiomyocytes at endogenous cGMP levels might better reflect PDE hydrolytic activities than classical biochemical PDE activity assays.

4.2.5 Analysis of cGMP dynamics in a model of moderate pressure-overload induced hypertrophy

Transverse aortic constriction surgery was performed to induce hypertrophy and associated ventricular remodeling. PDE3 remained the major regulator of cGMP turnover and CNP effects were unchanged. Increased effects of the PDE5 inhibitor tadalafil were present in diseased cardiomyocytes, but not in control cells (see Fig. 26). It has been shown that PDE3 expression and activity was downregulated, while PDE1 was upregulated in mouse models of chronic pressure-overload using aortic banding.[138, 144] In those studies, TAC resulted in heart failure with depressed systolic performance, whereas imaging experiments of PDE3 hydrolytic activity were performed in a mild model of completely compensated hypertrophy, which most likely failed to depress PDE3 and induce PDE1 expression. Nevertheless, increased PDE5 hydrolytic activity as previously described by others.[30, 167, 260] could be recorded. Finally, responses to CNP were unaltered, which confirms a recent study that revealed unchanged strong GC-B-mediated cGMP production, in a mouse model of heart failure using aortic banding, while signaling of GC-A was significantly depressed. The authors claimed that CG-B was the major natriuretic peptide receptor in the failing heart. [261]

4.2.6 Analysis of cGMP/cAMP crosstalk in adult mouse cardiomyocytes

The interplay between the cGMP and cAMP signaling pathways was visualized using Epac1-camps mice, with a main focus on the role of PDE3. It is well known that cGMP can block PDE3 hydrolysis,[118] and act as a cAMP-PDE inhibitor. When the effects of cGMP on β-adrenergic receptor-evoked cAMP signals were investigated, natriuretic peptides potentiated β-AR-induced cAMP by cGMP-mediated inhibition of PDE3. Activation of GC-B by CNP showed significantly stronger effects than the stimulation of GC-A by ANP. These findings are in line with measurements of cGMP in red cGES-DE5 mice, where CNP induced the strongest increases in cGMP and ANP smaller responses. Furthermore, stimulation of NO-GC with SNAP in the absence of PDE5 inhibitors failed to evoke any effects in both

cyclic nucleotide signaling systems. However, SNAP induced an effect when PDE5 was blocked (see Fig. 27).

It has been demonstrated that cGMP signals induced by GC-B stimulation via CNP do interfere with β-AR-generated cAMP signaling, which leads to a positive inotropic effect in failing rat cardiomyocytes.[234] Inhibition of PDE3 was postulated as the mechanism, confirming the observations in Epac1-camps mice and providing a proof that GC-B-induced cGMP/cAMP crosstalk is highly relevant, since it can have an impact on myocyte contractility. The CNP-induced positive effect on contractilie force was only detectable in the presence of catecholamines, which supports the finding that CNP applied alone could not raise cAMP levels. Furthermore, stimulation of isolated work performing hearts or ventricular muscle strips with CNP showed a biphasic response with an initial increase in inotropy followed by a negative effect.[29, 243] The early positive inotropic effect might be explained by cGMP-mediated inhibition of PDE3, while the subsequent decrease in contraction force is due to cGMP-induced activation of cGKI activity, which blunts excitatory effects of catecholamines.[243] In addition, PDE2 hydrolytic activity was blocked, since its cAMP-hydrolytic activity can be activated by cGMP,[227] which might reduce CNP-mediated effects. However, inhibition of PDE2 could not generate a rise in CNP-induced cAMP concentrations, which was also true for inhibition of PDE5 by tadalafil. Those findings in cAMP sensor mice support the hypothesis that PDE3 dominates cytosolic GC-B-mediated cAMP/cGMP crosstalk after stimulation of β-adrenoceptors, while PDE2 and PDE 5 seem not to be involved.

ANP-induced increases in cAMP constituted less than 25 % of the maximal increase in cAMP that can be attained by total inbibition of PDE3 with cilostamide. Measurements of myocyte contractility showed no influence of ANP,[116, 262] which might go in line with the modest increase in cAMP. Nevertheless, a targeted cAMP biosensor, which resides mainly in the particulate fraction of myocyte lysates could reveal a dominant role of ANP in cAMP/cGMP interplay mediated via PDE2 hydrolytic activity in neonatal rat cardiomyocytes. The authors reported that those effects were not detectable with a biosensor, located in the soluble fraction of neonatal rat cardiomyocytes.[141] Since global cAMP levels were visualized, one has to consider that the Epac1-camps cannot resolve these local changes in cAMP. It would be interesting to see whether a targeted version of Epac1-camps sensor, probably targeted to the plasma membrane, might detect these local effects.

SNAP per se could not increase cAMP levels, but pretreatment with the PDE5 inhibitor tadalafil could reveal small responses. This is in agreement with measurements of cGMP dynamics using red cGES-DE5, where SNAP alone failed to induce cGMP generation, but in

the presence of ISO and tadalafil small responses were detected. Furthermore, it has been demonstrated that NO-GC-mediated cGMP pools are under tight regulation of PDE5 in connection with β-adrenergic stimulation.[49, 148, 262]

4.2.7 Outlook

The red cGES-DE5 transgenic mouse line harbors great promise for future investigations. As demonstrated with aortic banding experiments and for the β_3-AR, one can combine the mouse model with further genetic and experimental models of cardiovascular disease. In particular, myocardial infarction surgery to induce harsher stimuli on myocyte remodeling would greatly supplement the observations in the mild model of compensated hypertrophy. For the analysis of cGMP microdomains, it is necessary to generate targeted versions of red cGES-DE5, for instance targeted to the plasma membrane or PLB. Such targeted sensors have already been created and the mouse lines are under investigation. Here, it might be possible to detect robust ANP and NO-donor effects. In addition, the red cGES-DE5 mouse line was crossed into C57/Bl6 background, which generally shows higher increases in cGMP amounts upon stimulation, compared with the FVB/NjR mice. In addition, it is possible to combine FRET-based cGMP imaging with the scanning ion conductance microscopy (SICM) technique to further dissect the localization of various receptors. Nonetheless, an important limitation of the live cell imaging approach is the fact that cGMP signaling in single isolated cardiomyocytes might differ from cGMP dynamics under *in vivo* conditions. It is worth mentioning that red cGES-DE5 expression occurs exclusively in cardiomyocytes, and one could perform cGMP imaging of an entire heart. To do so, a living heart can be quickly removed and perfused in analogy to the working heart experiments (see *2.2.6*) for imaging experiments performed under a binocular microscope using low magnification. Finally, it is possible to generate double-transgenic mice that express Epac1-camps and red cGES-DE5 to measure cAMP and cGMP dynamics simultaneously. Such an experiment can be performed at 405 nm excitation of CFP and GFP combined with four colour imaging of CFP, YFP, GFP, and RFP emissions.[198] Such double-transgenic mice have already been created and preliminary results are available.

1. Beavo JA, Brunton LL. Cyclic nucleotide research -- still expanding after half a century. *Nat Rev Mol Cell Biol*. 2002;3:710-718
2. Ashcroft FM, Rorsman P. Diabetes mellitus and the beta cell: The last ten years. *Cell*. 2012;148:1160-1171
3. Torgersen KM, Vang T, Abrahamsen H, Yaqub S, Tasken K. Molecular mechanisms for protein kinase a-mediated modulation of immune function. *Cell Signal*. 2002;14:1-9
4. Mosenden R, Tasken K. Cyclic amp-mediated immune regulation--overview of mechanisms of action in t cells. *Cell Signal*. 2011;23:1009-1016
5. Shirshev SV. Role of epac proteins in mechanisms of camp-dependent immunoregulation. *Biochemistry (Mosc)*. 2011;76:981-998
6. Kandel ER. The molecular biology of memory: Camp, pka, cre, creb-1, creb-2, and cpeb. *Mol Brain*. 2012;5:14
7. Giese KP, Mizuno K. The roles of protein kinases in learning and memory. *Learn Mem*. 2013;20:540-552
8. Altarejos JY, Montminy M. Creb and the crtc co-activators: Sensors for hormonal and metabolic signals. *Nat Rev Mol Cell Biol*. 2011;12:141-151
9. Lee KA. Transcriptional regulation by camp. *Curr Opin Cell Biol*. 1991;3:953-959
10. Prasad KN, Cole WC, Yan XD, Nahreini P, Kumar B, Hanson A, Prasad JE. Defects in camp-pathway may initiate carcinogenesis in dividing nerve cells: A review. *Apoptosis*. 2003;8:579-586
11. Lohse MJ, Engelhardt S, Eschenhagen T. What is the role of beta-adrenergic signaling in heart failure? *Circ Res*. 2003;93:896-906
12. Biel M, Michalakis S. Cyclic nucleotide-gated channels. *Handb Exp Pharmacol*. 2009:111-136
13. de Rooij J, Zwartkruis FJ, Verheijen MH, Cool RH, Nijman SM, Wittinghofer A, Bos JL. Epac is a rap1 guanine-nucleotide-exchange factor directly activated by cyclic amp. *Nature*. 1998;396:474-477
14. Taylor SS, Buechler JA, Yonemoto W. Camp-dependent protein kinase: Framework for a diverse family of regulatory enzymes. *Annu Rev Biochem*. 1990;59:971-1005
15. Arshavsky VY, Lamb TD, Pugh EN, Jr. G proteins and phototransduction. *Annu Rev Physiol*. 2002;64:153-187
16. Nakagawa H, Oberwinkler H, Nikolaev VO, Gassner B, Umbenhauer S, Wagner H, Saito Y, Baba HA, Frantz S, Kuhn M. Atrial natriuretic peptide locally counteracts the deleterious effects of cardiomyocyte mineralcorticoid receptor activation. *Circ Heart Fail*. 2014
17. MacFarland RT, Zelus BD, Beavo JA. High concentrations of a cgmp-stimulated phosphodiesterase mediate anp-induced decreases in camp and steroidogenesis in adrenal glomerulosa cells. *J Biol Chem*. 1991;266:136-142
18. Hofmann F, Feil R, Kleppisch T, Schlossmann J. Function of cgmp-dependent protein kinases as revealed by gene deletion. *Physiol Rev*. 2006;86:1-23
19. Chusho H, Tamura N, Ogawa Y, Yasoda A, Suda M, Miyazawa T, Nakamura K, Nakao K, Kurihara T, Komatsu Y, Itoh H, Tanaka K, Saito Y, Katsuki M, Nakao K. Dwarfism and early death in mice lacking c-type natriuretic peptide. *Proc Natl Acad Sci U S A*. 2001;98:4016-4021
20. Geiselhoringer A, Gaisa M, Hofmann F, Schlossmann J. Distribution of irag and cgki-isoforms in murine tissues. *FEBS Lett*. 2004;575:19-22
21. Pfeifer A, Klatt P, Massberg S, Ny L, Sausbier M, Hirneiss C, Wang GX, Korth M, Aszodi A, Andersson KE, Krombach F, Mayerhofer A, Ruth P, Fassler R, Hofmann F. Defective smooth muscle regulation in cgmp kinase i-deficient mice. *Embo j*. 1998;17:3045-3051
22. Persson K, Pandita RK, Aszodi A, Ahmad M, Pfeifer A, Fassler R, Andersson KE. Functional characteristics of urinary tract smooth muscles in mice lacking cgmp protein kinase type i. *Am J Physiol Regul Integr Comp Physiol*. 2000;279:R1112-1120
23. Andersson KE, Wagner G. Physiology of penile erection. *Physiol Rev*. 1995;75:191-236

24. Spinas GA, Laffranchi R, Francoys I, David I, Richter C, Reinecke M. The early phase of glucose-stimulated insulin secretion requires nitric oxide. *Diabetologia*. 1998;41:292-299
25. Hofmann F, Wegener JW. Cgmp-dependent protein kinases (cgk). *Methods Mol Biol*. 2013;1020:17-50
26. Haas B, Mayer P, Jennissen K, Scholz D, Berriel Diaz M, Bloch W, Herzig S, Fassler R, Pfeifer A. Protein kinase g controls brown fat cell differentiation and mitochondrial biogenesis. *Sci Signal*. 2009;2:ra78
27. Inglis FM, Furia F, Zuckerman KE, Strittmatter SM, Kalb RG. The role of nitric oxide and nmda receptors in the development of motor neuron dendrites. *J Neurosci*. 1998;18:10493-10501
28. Feil R, Hofmann F, Kleppisch T. Function of cgmp-dependent protein kinases in the nervous system. *Rev Neurosci*. 2005;16:23-41
29. Pierkes M, Gambaryan S, Boknik P, Lohmann SM, Schmitz W, Potthast R, Holtwick R, Kuhn M. Increased effects of c-type natriuretic peptide on cardiac ventricular contractility and relaxation in guanylyl cyclase a-deficient mice. *Cardiovasc Res*. 2002;53:852-861
30. Takimoto E, Champion HC, Li M, Belardi D, Ren S, Rodriguez ER, Bedja D, Gabrielson KL, Wang Y, Kass DA. Chronic inhibition of cyclic gmp phosphodiesterase 5a prevents and reverses cardiac hypertrophy. *Nat Med*. 2005;11:214-222
31. Massberg S, Sausbier M, Klatt P, Bauer M, Pfeifer A, Siess W, Fassler R, Ruth P, Krombach F, Hofmann F. Increased adhesion and aggregation of platelets lacking cyclic guanosine 3',5'-monophosphate kinase i. *J Exp Med*. 1999;189:1255-1264
32. John SW, Veress AT, Honrath U, Chong CK, Peng L, Smithies O, Sonnenberg H. Blood pressure and fluid-electrolyte balance in mice with reduced or absent anp. *Am J Physiol*. 1996;271:R109-114
33. Kuhn M. Structure, regulation, and function of mammalian membrane guanylyl cyclase receptors, with a focus on guanylyl cyclase-a. *Circ Res*. 2003;93:700-709
34. Martinez SE, Beavo JA, Hol WG. Gaf domains: Two-billion-year-old molecular switches that bind cyclic nucleotides. *Mol Interv*. 2002;2:317-323
35. Mongillo M, Tocchetti CG, Terrin A, Lissandron V, Cheung YF, Dostmann WR, Pozzan T, Kass DA, Paolocci N, Houslay MD, Zaccolo M. Compartmentalized phosphodiesterase-2 activity blunts beta-adrenergic cardiac inotropy via an no/cgmp-dependent pathway. *Circ Res*. 2006;98:226-234
36. Biel M, Zong X, Ludwig A, Sautter A, Hofmann F. Structure and function of cyclic nucleotide-gated channels. *Rev Physiol Biochem Pharmacol*. 1999;135:151-171
37. Kushnir A, Marks AR. The ryanodine receptor in cardiac physiology and disease. *Adv Pharmacol*. 2010;59:1-30
38. Bers DM. Cardiac excitation-contraction coupling. *Nature*. 2002;415:198-205
39. Bers DM. Calcium cycling and signaling in cardiac myocytes. *Annu Rev Physiol*. 2008;70:23-49
40. Brandes R, Bers DM. Intracellular ca2+ increases the mitochondrial nadh concentration during elevated work in intact cardiac muscle. *Circ Res*. 1997;80:82-87
41. Zhao XL, Gutierrez LM, Chang CF, Hosey MM. The alpha 1-subunit of skeletal muscle l-type ca channels is the key target for regulation by a-kinase and protein phosphatase-1c. *Biochem Biophys Res Commun*. 1994;198:166-173
42. Simmerman HK, Jones LR. Phospholamban: Protein structure, mechanism of action, and role in cardiac function. *Physiol Rev*. 1998;78:921-947
43. Marx SO, Reiken S, Hisamatsu Y, Jayaraman T, Burkhoff D, Rosemblit N, Marks AR. Pka phosphorylation dissociates fkbp12.6 from the calcium release channel (ryanodine receptor): Defective regulation in failing hearts. *Cell*. 2000;101:365-376
44. Sulakhe PV, Vo XT. Regulation of phospholamban and troponin-i phosphorylation in the intact rat cardiomyocytes by adrenergic and cholinergic stimuli: Roles of cyclic nucleotides, calcium, protein kinases and phosphatases and depolarization. *Mol Cell Biochem*. 1995;149-150:103-126

45. Lehnart SE. Novel targets for treating heart and muscle disease: Stabilizing ryanodine receptors and preventing intracellular calcium leak. *Curr Opin Pharmacol*. 2007;7:225-232
46. Buxton IL, Brunton LL. Compartments of cyclic amp and protein kinase in mammalian cardiomyocytes. *J Biol Chem*. 1983;258:10233-10239
47. Jurevicius J, Fischmeister R. Camp compartmentation is responsible for a local activation of cardiac ca2+ channels by beta-adrenergic agonists. *Proc Natl Acad Sci U S A*. 1996;93:295-299
48. Perera RK, Nikolaev VO. Compartmentation of camp signalling in cardiomyocytes in health and disease. *Acta Physiol (Oxf)*. 2013;207:650-662
49. Castro LR, Verde I, Cooper DM, Fischmeister R. Cyclic guanosine monophosphate compartmentation in rat cardiac myocytes. *Circulation*. 2006;113:2221-2228
50. Lehnart SE, Wehrens XH, Reiken S, Warrier S, Belevych AE, Harvey RD, Richter W, Jin SL, Conti M, Marks AR. Phosphodiesterase 4d deficiency in the ryanodine-receptor complex promotes heart failure and arrhythmias. *Cell*. 2005;123:25-35
51. Dodge KL, Khouangsathiene S, Kapiloff MS, Mouton R, Hill EV, Houslay MD, Langeberg LK, Scott JD. Makap assembles a protein kinase a/pde4 phosphodiesterase camp signaling module. *Embo j*. 2001;20:1921-1930
52. Zalk R, Lehnart SE, Marks AR. Modulation of the ryanodine receptor and intracellular calcium. *Annu Rev Biochem*. 2007;76:367-385
53. Gyorke S, Terentyev D. Modulation of ryanodine receptor by luminal calcium and accessory proteins in health and cardiac disease. *Cardiovasc Res*. 2008;77:245-255
54. Fan GC, Yuan Q, Kranias EG. Regulatory roles of junctin in sarcoplasmic reticulum calcium cycling and myocardial function. *Trends Cardiovasc Med*. 2008;18:1-5
55. Timerman AP, Jayaraman T, Wiederrecht G, Onoue H, Marks AR, Fleischer S. The ryanodine receptor from canine heart sarcoplasmic reticulum is associated with a novel fk-506 binding protein. *Biochem Biophys Res Commun*. 1994;198:701-706
56. Wehrens XH, Lehnart SE, Reiken SR, Marks AR. Ca2+/calmodulin-dependent protein kinase ii phosphorylation regulates the cardiac ryanodine receptor. *Circ Res*. 2004;94:e61-70
57. Camors E, Valdivia HH. Camkii regulation of cardiac ryanodine receptors and inositol triphosphate receptors. *Front Pharmacol*. 2014;5:101
58. Huke S, Bers DM. Ryanodine receptor phosphorylation at serine 2030, 2808 and 2814 in rat cardiomyocytes. *Biochem Biophys Res Commun*. 2008;376:80-85
59. Yamaguchi N, Xu L, Pasek DA, Evans KE, Meissner G. Molecular basis of calmodulin binding to cardiac muscle ca(2+) release channel (ryanodine receptor). *J Biol Chem*. 2003;278:23480-23486
60. Xu L, Meissner G. Mechanism of calmodulin inhibition of cardiac sarcoplasmic reticulum ca2+ release channel (ryanodine receptor). *Biophys J*. 2004;86:797-804
61. Farrell EF, Antaramian A, Rueda A, Gomez AM, Valdivia HH. Sorcin inhibits calcium release and modulates excitation-contraction coupling in the heart. *J Biol Chem*. 2003;278:34660-34666
62. Packer M. Neurohormonal interactions and adaptations in congestive heart failure. *Circulation*. 1988;77:721-730
63. Brodde OE. Beta-adrenoceptors in cardiac disease. *Pharmacol Ther*. 1993;60:405-430
64. Bristow MR, Ginsburg R, Minobe W, Cubicciotti RS, Sageman WS, Lurie K, Billingham ME, Harrison DC, Stinson EB. Decreased catecholamine sensitivity and beta-adrenergic-receptor density in failing human hearts. *N Engl J Med*. 1982;307:205-211
65. Zhang H, Makarewich CA, Kubo H, Wang W, Duran JM, Li Y, Berretta RM, Koch WJ, Chen X, Gao E, Valdivia HH, Houser SR. Hyperphosphorylation of the cardiac ryanodine receptor at serine 2808 is not involved in cardiac dysfunction after myocardial infarction. *Circ Res*. 2012;110:831-840
66. Benkusky NA, Weber CS, Scherman JA, Farrell EF, Hacker TA, John MC, Powers PA, Valdivia HH. Intact beta-adrenergic response and unmodified progression toward heart failure in

mice with genetic ablation of a major protein kinase a phosphorylation site in the cardiac ryanodine receptor. *Circ Res*. 2007;101:819-829

67. MacDonnell SM, Garcia-Rivas G, Scherman JA, Kubo H, Chen X, Valdivia H, Houser SR. Adrenergic regulation of cardiac contractility does not involve phosphorylation of the cardiac ryanodine receptor at serine 2808. *Circ Res*. 2008;102:e65-72
68. Cotton JM, Kearney MT, Shah AM. Nitric oxide and myocardial function in heart failure: Friend or foe? *Heart*. 2002;88:564-566
69. Kojda G, Kottenberg K, Nix P, Schluter KD, Piper HM, Noack E. Low increase in cgmp induced by organic nitrates and nitrovasodilators improves contractile response of rat ventricular myocytes. *Circ Res*. 1996;78:91-101
70. Vila-Petroff MG, Younes A, Egan J, Lakatta EG, Sollott SJ. Activation of distinct camp-dependent and cgmp-dependent pathways by nitric oxide in cardiac myocytes. *Circ Res*. 1999;84:1020-1031
71. Mohan P, Brutsaert DL, Paulus WJ, Sys SU. Myocardial contractile response to nitric oxide and cgmp. *Circulation*. 1996;93:1223-1229
72. Grocott-Mason R, Anning P, Evans H, Lewis MJ, Shah AM. Modulation of left ventricular relaxation in isolated ejecting heart by endogenous nitric oxide. *Am J Physiol*. 1994;267:H1804-1813
73. Shah AM, Spurgeon HA, Sollott SJ, Talo A, Lakatta EG. 8-bromo-cgmp reduces the myofilament response to ca2+ in intact cardiac myocytes. *Circ Res*. 1994;74:970-978
74. Shah AM, MacCarthy PA. Paracrine and autocrine effects of nitric oxide on myocardial function. *Pharmacol Ther*. 2000;86:49-86
75. Layland J, Li JM, Shah AM. Role of cyclic gmp-dependent protein kinase in the contractile response to exogenous nitric oxide in rat cardiac myocytes. *J Physiol*. 2002;540:457-467
76. Gauthier C, Leblais V, Kobzik L, Trochu JN, Khandoudi N, Bril A, Balligand JL, Le Marec H. The negative inotropic effect of beta3-adrenoceptor stimulation is mediated by activation of a nitric oxide synthase pathway in human ventricle. *J Clin Invest*. 1998;102:1377-1384
77. Cawley SM, Kolodziej S, Ichinose F, Brouckaert P, Buys ES, Bloch KD. Sgc{alpha}1 mediates the negative inotropic effects of no in cardiac myocytes independent of changes in calcium handling. *Am J Physiol Heart Circ Physiol*. 2011;301:H157-163
78. Takimoto E. Cyclic gmp-dependent signaling in cardiac myocytes. *Circ J*. 2012;76:1819-1825
79. Derbyshire ER, Marletta MA. Structure and regulation of soluble guanylate cyclase. *Annu Rev Biochem*. 2012;81:533-559
80. Hammond J, Balligand JL. Nitric oxide synthase and cyclic gmp signaling in cardiac myocytes: From contractility to remodeling. *J Mol Cell Cardiol*. 2012;52:330-340
81. Balligand JL, Ungureanu-Longrois D, Simmons WW, Pimental D, Malinski TA, Kapturczak M, Taha Z, Lowenstein CJ, Davidoff AJ, Kelly RA, et al. Cytokine-inducible nitric oxide synthase (inos) expression in cardiac myocytes. Characterization and regulation of inos expression and detection of inos activity in single cardiac myocytes in vitro. *J Biol Chem*. 1994;269:27580-27588
82. Budworth J, Meillerais S, Charles I, Powell K. Tissue distribution of the human soluble guanylate cyclases. *Biochem Biophys Res Commun*. 1999;263:696-701
83. Stone JR, Marletta MA. Spectral and kinetic studies on the activation of soluble guanylate cyclase by nitric oxide. *Biochemistry*. 1996;35:1093-1099
84. Tsai EJ, Kass DA. Cyclic gmp signaling in cardiovascular pathophysiology and therapeutics. *Pharmacol Ther*. 2009;122:216-238
85. Derbyshire ER, Gunn A, Ibrahim M, Spiro TG, Britt RD, Marletta MA. Characterization of two different five-coordinate soluble guanylate cyclase ferrous-nitrosyl complexes. *Biochemistry*. 2008;47:3892-3899
86. Russwurm M, Koesling D. No activation of guanylyl cyclase. *Embo j*. 2004;23:4443-4450

87. Cary SP, Winger JA, Marletta MA. Tonic and acute nitric oxide signaling through soluble guanylate cyclase is mediated by nonheme nitric oxide, atp, and gtp. *Proc Natl Acad Sci U S A*. 2005;102:13064-13069
88. Hare JM. Nitroso-redox balance in the cardiovascular system. *N Engl J Med*. 2004;351:2112-2114
89. Mulsch A, Oelze M, Kloss S, Mollnau H, Topfer A, Smolenski A, Walter U, Stasch JP, Warnholtz A, Hink U, Meinertz T, Munzel T. Effects of in vivo nitroglycerin treatment on activity and expression of the guanylyl cyclase and cgmp-dependent protein kinase and their downstream target vasodilator-stimulated phosphoprotein in aorta. *Circulation*. 2001;103:2188-2194
90. Weber M, Lauer N, Mulsch A, Kojda G. The effect of peroxynitrite on the catalytic activity of soluble guanylyl cyclase. *Free Radic Biol Med*. 2001;31:1360-1367
91. Stasch JP, Schmidt PM, Nedvetsky PI, Nedvetskaya TY, H SA, Meurer S, Deile M, Taye A, Knorr A, Lapp H, Muller H, Turgay Y, Rothkegel C, Tersteegen A, Kemp-Harper B, Muller-Esterl W, Schmidt HH. Targeting the heme-oxidized nitric oxide receptor for selective vasodilatation of diseased blood vessels. *J Clin Invest*. 2006;116:2552-2561
92. Mingone CJ, Gupte SA, Ali N, Oeckler RA, Wolin MS. Thiol oxidation inhibits nitric oxide-mediated pulmonary artery relaxation and guanylate cyclase stimulation. *Am J Physiol Lung Cell Mol Physiol*. 2006;290:L549-557
93. Sayed N, Kim DD, Fioramonti X, Iwahashi T, Duran WN, Beuve A. Nitroglycerin-induced s-nitrosylation and desensitization of soluble guanylyl cyclase contribute to nitrate tolerance. *Circ Res*. 2008;103:606-614
94. Potter LR, Hunter T. Guanylyl cyclase-linked natriuretic peptide receptors: Structure and regulation. *J Biol Chem*. 2001;276:6057-6060
95. Kuhn M. Molecular physiology of natriuretic peptide signalling. *Basic Res Cardiol*. 2004;99:76-82
96. Potter LR. Natriuretic peptide metabolism, clearance and degradation. *Febs j*. 2011;278:1808-1817
97. Holtwick R, Gotthardt M, Skryabin B, Steinmetz M, Potthast R, Zetsche B, Hammer RE, Herz J, Kuhn M. Smooth muscle-selective deletion of guanylyl cyclase-a prevents the acute but not chronic effects of anp on blood pressure. *Proc Natl Acad Sci U S A*. 2002;99:7142-7147
98. Brenner BM, Ballermann BJ, Gunning ME, Zeidel ML. Diverse biological actions of atrial natriuretic peptide. *Physiol Rev*. 1990;70:665-699
99. Lopez MJ, Wong SK, Kishimoto I, Dubois S, Mach V, Friesen J, Garbers DL, Beuve A. Salt-resistant hypertension in mice lacking the guanylyl cyclase-a receptor for atrial natriuretic peptide. *Nature*. 1995;378:65-68
100. Steinhelper ME, Cochrane KL, Field LJ. Hypotension in transgenic mice expressing atrial natriuretic factor fusion genes. *Hypertension*. 1990;16:301-307
101. Oliver PM, John SW, Purdy KE, Kim R, Maeda N, Goy MF, Smithies O. Natriuretic peptide receptor 1 expression influences blood pressures of mice in a dose-dependent manner. *Proc Natl Acad Sci U S A*. 1998;95:2547-2551
102. Mukoyama M, Nakao K, Hosoda K, Suga S, Saito Y, Ogawa Y, Shirakami G, Jougasaki M, Obata K, Yasue H, et al. Brain natriuretic peptide as a novel cardiac hormone in humans. Evidence for an exquisite dual natriuretic peptide system, atrial natriuretic peptide and brain natriuretic peptide. *J Clin Invest*. 1991;87:1402-1412
103. van der Zander K, Houben AJ, Kroon AA, de Leeuw PW. Effects of brain natriuretic peptide on forearm vasculature: Comparison with atrial natriuretic peptide. *Cardiovasc Res*. 1999;44:595-600
104. Tamura N, Ogawa Y, Chusho H, Nakamura K, Nakao K, Suda M, Kasahara M, Hashimoto R, Katsuura G, Mukoyama M, Itoh H, Saito Y, Tanaka I, Otani H, Katsuki M. Cardiac fibrosis in mice lacking brain natriuretic peptide. *Proc Natl Acad Sci U S A*. 2000;97:4239-4244

105. Cao L, Gardner DG. Natriuretic peptides inhibit DNA synthesis in cardiac fibroblasts. *Hypertension*. 1995;25:227-234
106. Chen HH, Burnett JC, Jr. C-type natriuretic peptide: The endothelial component of the natriuretic peptide system. *J Cardiovasc Pharmacol*. 1998;32 Suppl 3:S22-28
107. Lopez MJ, Garbers DL, Kuhn M. The guanylyl cyclase-deficient mouse defines differential pathways of natriuretic peptide signaling. *J Biol Chem*. 1997;272:23064-23068
108. Doyle DD, Upshaw-Earley J, Bell EL, Palfrey HC. Natriuretic peptide receptor-b in adult rat ventricle is predominantly confined to the nonmyocyte population. *Am J Physiol Heart Circ Physiol*. 2002;282:H2117-2123
109. Wei CM, Heublein DM, Perrella MA, Lerman A, Rodeheffer RJ, McGregor CG, Edwards WD, Schaff HV, Burnett JC, Jr. Natriuretic peptide system in human heart failure. *Circulation*. 1993;88:1004-1009
110. Del Ry S, Cabiati M, Vozzi F, Battolla B, Caselli C, Forini F, Segnani C, Prescimone T, Giannessi D, Mattii L. Expression of c-type natriuretic peptide and its receptor npr-b in cardiomyocytes. *Peptides*. 2011;32:1713-1718
111. Tokudome T, Horio T, Soeki T, Mori K, Kishimoto I, Suga S, Yoshihara F, Kawano Y, Kohno M, Kangawa K. Inhibitory effect of c-type natriuretic peptide (cnp) on cultured cardiac myocyte hypertrophy: Interference between cnp and endothelin-1 signaling pathways. *Endocrinology*. 2004;145:2131-2140
112. Matsukawa N, Grzesik WJ, Takahashi N, Pandey KN, Pang S, Yamauchi M, Smithies O. The natriuretic peptide clearance receptor locally modulates the physiological effects of the natriuretic peptide system. *Proc Natl Acad Sci U S A*. 1999;96:7403-7408
113. Kalra PR, Clague JR, Bolger AP, Anker SD, Poole-Wilson PA, Struthers AD, Coats AJ. Myocardial production of c-type natriuretic peptide in chronic heart failure. *Circulation*. 2003;107:571-573
114. Dickey DM, Dries DL, Margulies KB, Potter LR. Guanylyl cyclase (gc)-a and gc-b activities in ventricles and cardiomyocytes from failed and non-failed human hearts: Gc-a is inactive in the failed cardiomyocyte. *J Mol Cell Cardiol*. 2012;52:727-732
115. Wollert KC, Yurukova S, Kilic A, Begrow F, Fiedler B, Gambaryan S, Walter U, Lohmann SM, Kuhn M. Increased effects of c-type natriuretic peptide on contractility and calcium regulation in murine hearts overexpressing cyclic gmp-dependent protein kinase i. *Br J Pharmacol*. 2003;140:1227-1236
116. Bohm M, Diet F, Pieske B, Erdmann E. H-anf does not play a role in the regulation of myocardial force of contraction. *Life Sci*. 1988;43:1261-1267
117. Lee DI, Kass DA. Phosphodiesterases and cyclic gmp regulation in heart muscle. *Physiology (Bethesda)*. 2012;27:248-258
118. Bender AT, Beavo JA. Cyclic nucleotide phosphodiesterases: Molecular regulation to clinical use. *Pharmacol Rev*. 2006;58:488-520
119. Sharma RK, Adachi AM, Adachi K, Wang JH. Demonstration of bovine brain calmodulin-dependent cyclic nucleotide phosphodiesterase isozymes by monoclonal antibodies. *J Biol Chem*. 1984;259:9248-9254
120. Hansen RS, Charbonneau H, Beavo JA. Purification of calmodulin-stimulated cyclic nucleotide phosphodiesterase by monoclonal antibody affinity chromatography. *Methods Enzymol*. 1988;159:543-557
121. Sonnenburg WK, Seger D, Kwak KS, Huang J, Charbonneau H, Beavo JA. Identification of inhibitory and calmodulin-binding domains of the pde1a1 and pde1a2 calmodulin-stimulated cyclic nucleotide phosphodiesterases. *J Biol Chem*. 1995;270:30989-31000
122. Snyder PB, Florio VA, Ferguson K, Loughney K. Isolation, expression and analysis of splice variants of a human ca2+/calmodulin-stimulated phosphodiesterase (pde1a). *Cell Signal*. 1999;11:535-544

123. Sharma RK, Wang JH. Calmodulin and ca2+-dependent phosphorylation and dephosphorylation of 63-kda subunit-containing bovine brain calmodulin-stimulated cyclic nucleotide phosphodiesterase isozyme. *J Biol Chem*. 1986;261:1322-1328
124. Bender AT, Ostenson CL, Wang EH, Beavo JA. Selective up-regulation of pde1b2 upon monocyte-to-macrophage differentiation. *Proc Natl Acad Sci U S A*. 2005;102:497-502
125. Loughney K, Martins TJ, Harris EA, Sadhu K, Hicks JB, Sonnenburg WK, Beavo JA, Ferguson K. Isolation and characterization of cdnas corresponding to two human calcium, calmodulin-regulated, 3',5'-cyclic nucleotide phosphodiesterases. *J Biol Chem*. 1996;271:796-806
126. Yan C, Zhao AZ, Bentley JK, Beavo JA. The calmodulin-dependent phosphodiesterase gene pde1c encodes several functionally different splice variants in a tissue-specific manner. *J Biol Chem*. 1996;271:25699-25706
127. Martins TJ, Mumby MC, Beavo JA. Purification and characterization of a cyclic gmp-stimulated cyclic nucleotide phosphodiesterase from bovine tissues. *J Biol Chem*. 1982;257:1973-1979
128. Rosman GJ, Martins TJ, Sonnenburg WK, Beavo JA, Ferguson K, Loughney K. Isolation and characterization of human cdnas encoding a cgmp-stimulated 3',5'-cyclic nucleotide phosphodiesterase. *Gene*. 1997;191:89-95
129. Grant PG, Colman RW. Purification and characterization of a human platelet cyclic nucleotide phosphodiesterase. *Biochemistry*. 1984;23:1801-1807
130. Harrison SA, Reifsnyder DH, Gallis B, Cadd GG, Beavo JA. Isolation and characterization of bovine cardiac muscle cgmp-inhibited phosphodiesterase: A receptor for new cardiotonic drugs. *Mol Pharmacol*. 1986;29:506-514
131. Degerman E, Belfrage P, Newman AH, Rice KC, Manganiello VC. Purification of the putative hormone-sensitive cyclic amp phosphodiesterase from rat adipose tissue using a derivative of cilostamide as a novel affinity ligand. *J Biol Chem*. 1987;262:5797-5807
132. Loughney K, Hill TR, Florio VA, Uher L, Rosman GJ, Wolda SL, Jones BA, Howard ML, McAllister-Lucas LM, Sonnenburg WK, Francis SH, Corbin JD, Beavo JA, Ferguson K. Isolation and characterization of cdnas encoding pde5a, a human cgmp-binding, cgmp-specific 3',5'-cyclic nucleotide phosphodiesterase. *Gene*. 1998;216:139-147
133. Lin CS, Lau A, Tu R, Lue TF. Expression of three isoforms of cgmp-binding cgmp-specific phosphodiesterase (pde5) in human penile cavernosum. *Biochem Biophys Res Commun*. 2000;268:628-635
134. Zoraghi R, Corbin JD, Francis SH. Phosphodiesterase-5 gln817 is critical for cgmp, vardenafil, or sildenafil affinity: Its orientation impacts cgmp but not camp affinity. *J Biol Chem*. 2006;281:5553-5558
135. Rybalkin SD, Yan C, Bornfeldt KE, Beavo JA. Cyclic gmp phosphodiesterases and regulation of smooth muscle function. *Circ Res*. 2003;93:280-291
136. Sharma RK, Wang JH. Differential regulation of bovine brain calmodulin-dependent cyclic nucleotide phosphodiesterase isoenzymes by cyclic amp-dependent protein kinase and calmodulin-dependent phosphatase. *Proc Natl Acad Sci U S A*. 1985;82:2603-2607
137. Vandeput F, Wolda SL, Krall J, Hambleton R, Uher L, McCaw KN, Radwanski PB, Florio V, Movsesian MA. Cyclic nucleotide phosphodiesterase pde1c1 in human cardiac myocytes. *J Biol Chem*. 2007;282:32749-32757
138. Miller CL, Oikawa M, Cai Y, Wojtovich AP, Nagel DJ, Xu X, Xu H, Florio V, Rybalkin SD, Beavo JA, Chen YF, Li JD, Blaxall BC, Abe J, Yan C. Role of ca2+/calmodulin-stimulated cyclic nucleotide phosphodiesterase 1 in mediating cardiomyocyte hypertrophy. *Circ Res*. 2009;105:956-964
139. Johnson WB, Katugampola S, Able S, Napier C, Harding SE. Profiling of camp and cgmp phosphodiesterases in isolated ventricular cardiomyocytes from human hearts: Comparison with rat and guinea pig. *Life Sci*. 2012;90:328-336
140. Hartzell HC, Fischmeister R. Opposite effects of cyclic gmp and cyclic amp on ca2+ current in single heart cells. *Nature*. 1986;323:273-275

141. Stangherlin A, Gesellchen F, Zoccarato A, Terrin A, Fields LA, Berrera M, Surdo NC, Craig MA, Smith G, Hamilton G, Zaccolo M. Cgmp signals modulate camp levels in a compartment-specific manner to regulate catecholamine-dependent signaling in cardiac myocytes. *Circ Res*. 2011;108:929-939
142. Mongillo M, McSorley T, Evellin S, Sood A, Lissandron V, Terrin A, Huston E, Hannawacker A, Lohse MJ, Pozzan T, Houslay MD, Zaccolo M. Fluorescence resonance energy transfer-based analysis of camp dynamics in live neonatal rat cardiac myocytes reveals distinct functions of compartmentalized phosphodiesterases. *Circ Res*. 2004;95:67-75
143. Movsesian M, Stehlik J, Vandeput F, Bristow MR. Phosphodiesterase inhibition in heart failure. *Heart Fail Rev*. 2009;14:255-263
144. Ding B, Abe J, Wei H, Huang Q, Walsh RA, Molina CA, Zhao A, Sadoshima J, Blaxall BC, Berk BC, Yan C. Functional role of phosphodiesterase 3 in cardiomyocyte apoptosis: Implication in heart failure. *Circulation*. 2005;111:2469-2476
145. Oikawa M, Wu M, Lim S, Knight WE, Miller CL, Cai Y, Lu Y, Blaxall BC, Takeishi Y, Abe J, Yan C. Cyclic nucleotide phosphodiesterase 3a1 protects the heart against ischemia-reperfusion injury. *J Mol Cell Cardiol*. 2013;64:11-19
146. Corbin J, Rannels S, Neal D, Chang P, Grimes K, Beasley A, Francis S. Sildenafil citrate does not affect cardiac contractility in human or dog heart. *Curr Med Res Opin*. 2003;19:747-752
147. Rybalkin SD, Rybalkina IG, Shimizu-Albergine M, Tang XB, Beavo JA. Pde5 is converted to an activated state upon cgmp binding to the gaf a domain. *Embo j*. 2003;22:469-478
148. Takimoto E, Champion HC, Belardi D, Moslehi J, Mongillo M, Mergia E, Montrose DC, Isoda T, Aufiero K, Zaccolo M, Dostmann WR, Smith CJ, Kass DA. Cgmp catabolism by phosphodiesterase 5a regulates cardiac adrenergic stimulation by nos3-dependent mechanism. *Circ Res*. 2005;96:100-109
149. Koss KL, Kranias EG. Phospholamban: A prominent regulator of myocardial contractility. *Circ Res*. 1996;79:1059-1063
150. Li L, Desantiago J, Chu G, Kranias EG, Bers DM. Phosphorylation of phospholamban and troponin i in beta-adrenergic-induced acceleration of cardiac relaxation. *Am J Physiol Heart Circ Physiol*. 2000;278:H769-779
151. Frey N, Katus HA, Olson EN, Hill JA. Hypertrophy of the heart: A new therapeutic target? *Circulation*. 2004;109:1580-1589
152. Frey N, Olson EN. Cardiac hypertrophy: The good, the bad, and the ugly. *Annu Rev Physiol*. 2003;65:45-79
153. Calderone A, Thaik CM, Takahashi N, Chang DL, Colucci WS. Nitric oxide, atrial natriuretic peptide, and cyclic gmp inhibit the growth-promoting effects of norepinephrine in cardiac myocytes and fibroblasts. *J Clin Invest*. 1998;101:812-818
154. Balligand JL. Beta3-adrenoreceptors in cardiovasular diseases: New roles for an "old" receptor. *Curr Drug Deliv*. 2013;10:64-66
155. Gauthier C, Rozec B, Manoury B, Balligand JL. Beta-3 adrenoceptors as new therapeutic targets for cardiovascular pathologies. *Curr Heart Fail Rep*. 2011;8:184-192
156. Moniotte S, Kobzik L, Feron O, Trochu JN, Gauthier C, Balligand JL. Upregulation of beta(3)-adrenoceptors and altered contractile response to inotropic amines in human failing myocardium. *Circulation*. 2001;103:1649-1655
157. Liggett SB, Freedman NJ, Schwinn DA, Lefkowitz RJ. Structural basis for receptor subtype-specific regulation revealed by a chimeric beta 3/beta 2-adrenergic receptor. *Proc Natl Acad Sci U S A*. 1993;90:3665-3669
158. Belge C, Hammond J, Dubois-Deruy E, Manoury B, Hamelet J, Beauloye C, Markl A, Pouleur AC, Bertrand L, Esfahani H, Jnaoui K, Gotz KR, Nikolaev VO, Vanderper A, Herijgers P, Lobysheva I, Iaccarino G, Hilfiker-Kleiner D, Tavernier G, Langin D, Dessy C, Balligand JL. Enhanced expression of beta3-adrenoceptors in cardiac myocytes attenuates neurohormone-induced hypertrophic remodeling through nitric oxide synthase. *Circulation*. 2014;129:451-462

159. Oliver PM, Fox JE, Kim R, Rockman HA, Kim HS, Reddick RL, Pandey KN, Milgram SL, Smithies O, Maeda N. Hypertension, cardiac hypertrophy, and sudden death in mice lacking natriuretic peptide receptor a. *Proc Natl Acad Sci U S A*. 1997;94:14730-14735
160. Holtwick R, van Eickels M, Skryabin BV, Baba HA, Bubikat A, Begrow F, Schneider MD, Garbers DL, Kuhn M. Pressure-independent cardiac hypertrophy in mice with cardiomyocyte-restricted inactivation of the atrial natriuretic peptide receptor guanylyl cyclase-a. *J Clin Invest*. 2003;111:1399-1407
161. Kilic A, Bubikat A, Gassner B, Baba HA, Kuhn M. Local actions of atrial natriuretic peptide counteract angiotensin ii stimulated cardiac remodeling. *Endocrinology*. 2007;148:4162-4169
162. Zahabi A, Picard S, Fortin N, Reudelhuber TL, Deschepper CF. Expression of constitutively active guanylate cyclase in cardiomyocytes inhibits the hypertrophic effects of isoproterenol and aortic constriction on mouse hearts. *J Biol Chem*. 2003;278:47694-47699
163. Wang Y, de Waard MC, Sterner-Kock A, Stepan H, Schultheiss HP, Duncker DJ, Walther T. Cardiomyocyte-restricted over-expression of c-type natriuretic peptide prevents cardiac hypertrophy induced by myocardial infarction in mice. *Eur J Heart Fail*. 2007;9:548-557
164. Soeki T, Kishimoto I, Okumura H, Tokudome T, Horio T, Mori K, Kangawa K. C-type natriuretic peptide, a novel antifibrotic and antihypertrophic agent, prevents cardiac remodeling after myocardial infarction. *J Am Coll Cardiol*. 2005;45:608-616
165. Frantz S, Klaiber M, Baba HA, Oberwinkler H, Volker K, Gabetaner B, Bayer B, Abebetaer M, Schuh K, Feil R, Hofmann F, Kuhn M. Stress-dependent dilated cardiomyopathy in mice with cardiomyocyte-restricted inactivation of cyclic gmp-dependent protein kinase i. *Eur Heart J*. 2013;34:1233-1244
166. Lu Z, Xu X, Hu X, Lee S, Traverse JH, Zhu G, Fassett J, Tao Y, Zhang P, dos Remedios C, Pritzker M, Hall JL, Garry DJ, Chen Y. Oxidative stress regulates left ventricular pde5 expression in the failing heart. *Circulation*. 2010;121:1474-1483
167. Pokreisz P, Vandenwijngaert S, Bito V, Van den Bergh A, Lenaerts I, Busch C, Marsboom G, Gheysens O, Vermeersch P, Biesmans L, Liu X, Gillijns H, Pellens M, Van Lommel A, Buys E, Schoonjans L, Vanhaecke J, Verbeken E, Sipido K, Herijgers P, Bloch KD, Janssens SP. Ventricular phosphodiesterase-5 expression is increased in patients with advanced heart failure and contributes to adverse ventricular remodeling after myocardial infarction in mice. *Circulation*. 2009;119:408-416
168. Vandenwijngaert S, Pokreisz P, Hermans H, Gillijns H, Pellens M, Bax NA, Coppiello G, Oosterlinck W, Balogh A, Papp Z, Bouten CV, Bartunek J, D'Hooge J, Luttun A, Verbeken E, Herregods MC, Herijgers P, Bloch KD, Janssens S. Increased cardiac myocyte pde5 levels in human and murine pressure overload hypertrophy contribute to adverse lv remodeling. *PLoS One*. 2013;8:e58841
169. Fisher PW, Salloum F, Das A, Hyder H, Kukreja RC. Phosphodiesterase-5 inhibition with sildenafil attenuates cardiomyocyte apoptosis and left ventricular dysfunction in a chronic model of doxorubicin cardiotoxicity. *Circulation*. 2005;111:1601-1610
170. Koka S, Kukreja RC. Attenuation of doxorubicin-induced cardiotoxicity by tadalafil: A long acting phosphodiesterase-5 inhibitor. *Mol Cell Pharmacol*. 2010;2:173-178
171. Salloum FN, Abbate A, Das A, Houser JE, Mudrick CA, Qureshi IZ, Hoke NN, Roy SK, Brown WR, Prabhakar S, Kukreja RC. Sildenafil (viagra) attenuates ischemic cardiomyopathy and improves left ventricular function in mice. *Am J Physiol Heart Circ Physiol*. 2008;294:H1398-1406
172. Das A, Ockaili R, Salloum F, Kukreja RC. Protein kinase c plays an essential role in sildenafil-induced cardioprotection in rabbits. *Am J Physiol Heart Circ Physiol*. 2004;286:H1455-1460
173. Das A, Xi L, Kukreja RC. Phosphodiesterase-5 inhibitor sildenafil preconditions adult cardiac myocytes against necrosis and apoptosis. Essential role of nitric oxide signaling. *J Biol Chem*. 2005;280:12944-12955

174. Das A, Xi L, Kukreja RC. Protein kinase g-dependent cardioprotective mechanism of phosphodiesterase-5 inhibition involves phosphorylation of erk and gsk3beta. *J Biol Chem*. 2008;283:29572-29585
175. Vandeput F, Krall J, Ockaili R, Salloum FN, Florio V, Corbin JD, Francis SH, Kukreja RC, Movsesian MA. Cgmp-hydrolytic activity and its inhibition by sildenafil in normal and failing human and mouse myocardium. *J Pharmacol Exp Ther*. 2009;330:884-891
176. Redfield MM, Chen HH, Borlaug BA, Semigran MJ, Lee KL, Lewis G, LeWinter MM, Rouleau JL, Bull DA, Mann DL, Deswal A, Stevenson LW, Givertz MM, Ofili EO, O'Connor CM, Felker GM, Goldsmith SR, Bart BA, McNulty SE, Ibarra JC, Lin G, Oh JK, Patel MR, Kim RJ, Tracy RP, Velazquez EJ, Anstrom KJ, Hernandez AF, Mascette AM, Braunwald E. Effect of phosphodiesterase-5 inhibition on exercise capacity and clinical status in heart failure with preserved ejection fraction: A randomized clinical trial. *Jama*. 2013;309:1268-1277
177. Jager R, Groneberg D, Lies B, Bettaga N, Kummel M, Friebe A. Radioimmunoassay for the quantification of cgmp levels in cells and tissues. *Methods Mol Biol*. 2013;1020:63-72
178. Sprenger JU, Nikolaev VO. Biophysical techniques for detection of camp and cgmp in living cells. *Int J Mol Sci*. 2013;14:8025-8046
179. Mullershausen F, Russwurm M, Thompson WJ, Liu L, Koesling D, Friebe A. Rapid nitric oxide-induced desensitization of the cgmp response is caused by increased activity of phosphodiesterase type 5 paralleled by phosphorylation of the enzyme. *J Cell Biol*. 2001;155:271-278
180. Russwurm M, Mullershausen F, Friebe A, Jager R, Russwurm C, Koesling D. Design of fluorescence resonance energy transfer (fret)-based cgmp indicators: A systematic approach. *Biochem J*. 2007;407:69-77
181. Mo E, Amin H, Bianco IH, Garthwaite J. Kinetics of a cellular nitric oxide/cgmp/phosphodiesterase-5 pathway. *J Biol Chem*. 2004;279:26149-26158
182. Zhang J, Campbell RE, Ting AY, Tsien RY. Creating new fluorescent probes for cell biology. *Nat Rev Mol Cell Biol*. 2002;3:906-918
183. Day RN, Davidson MW. Fluorescent proteins for fret microscopy: Monitoring protein interactions in living cells. *Bioessays*. 2012;34:341-350
184. Stryer L. Fluorescence energy transfer as a spectroscopic ruler. *Annu Rev Biochem*. 1978;47:819-846
185. Piston DW, Kremers GJ. Fluorescent protein fret: The good, the bad and the ugly. *Trends Biochem Sci*. 2007;32:407-414
186. Zaccolo M, De Giorgi F, Cho CY, Feng L, Knapp T, Negulescu PA, Taylor SS, Tsien RY, Pozzan T. A genetically encoded, fluorescent indicator for cyclic amp in living cells. *Nat Cell Biol*. 2000;2:25-29
187. Zaccolo M, Pozzan T. Discrete microdomains with high concentration of camp in stimulated rat neonatal cardiac myocytes. *Science*. 2002;295:1711-1715
188. Nikolaev VO, Bunemann M, Schmitteckert E, Lohse MJ, Engelhardt S. Cyclic amp imaging in adult cardiac myocytes reveals far-reaching beta1-adrenergic but locally confined beta2-adrenergic receptor-mediated signaling. *Circ Res*. 2006;99:1084-1091
189. Nikolaev VO, Bunemann M, Hein L, Hannawacker A, Lohse MJ. Novel single chain camp sensors for receptor-induced signal propagation. *J Biol Chem*. 2004;279:37215-37218
190. Ponsioen B, Zhao J, Riedl J, Zwartkruis F, van der Krogt G, Zaccolo M, Moolenaar WH, Bos JL, Jalink K. Detecting camp-induced epac activation by fluorescence resonance energy transfer: Epac as a novel camp indicator. *EMBO Rep*. 2004;5:1176-1180
191. Borner S, Schwede F, Schlipp A, Berisha F, Calebiro D, Lohse MJ, Nikolaev VO. Fret measurements of intracellular camp concentrations and camp analog permeability in intact cells. *Nat Protoc*. 2011;6:427-438
192. Calebiro D, Nikolaev VO, Gagliani MC, de Filippis T, Dees C, Tacchetti C, Persani L, Lohse MJ. Persistent camp-signals triggered by internalized g-protein-coupled receptors. *PLoS Biol*. 2009;7:e1000172

193. Nikolaev VO, Lohse MJ. Monitoring of camp synthesis and degradation in living cells. *Physiology (Bethesda)*. 2006;21:86-92
194. Nausch LW, Ledoux J, Bonev AD, Nelson MT, Dostmann WR. Differential patterning of cgmp in vascular smooth muscle cells revealed by single gfp-linked biosensors. *Proc Natl Acad Sci U S A*. 2008;105:365-370
195. Sato M, Hida N, Ozawa T, Umezawa Y. Fluorescent indicators for cyclic gmp based on cyclic gmp-dependent protein kinase ialpha and green fluorescent proteins. *Anal Chem*. 2000;72:5918-5924
196. Nikolaev VO, Gambaryan S, Lohse MJ. Fluorescent sensors for rapid monitoring of intracellular cgmp. *Nat Methods*. 2006;3:23-25
197. Honda A, Adams SR, Sawyer CL, Lev-Ram V, Tsien RY, Dostmann WR. Spatiotemporal dynamics of guanosine 3',5'-cyclic monophosphate revealed by a genetically encoded, fluorescent indicator. *Proc Natl Acad Sci U S A*. 2001;98:2437-2442
198. Niino Y, Hotta K, Oka K. Simultaneous live cell imaging using dual fret sensors with a single excitation light. *PLoS One*. 2009;4:e6036
199. Thunemann M, Fomin N, Krawutschke C, Russwurm M, Feil R. Visualization of cgmp with cgi biosensors. *Methods Mol Biol*. 2013;1020:89-120
200. Cawley SM, Sawyer CL, Brunelle KF, van der Vliet A, Dostmann WR. Nitric oxide-evoked transient kinetics of cyclic gmp in vascular smooth muscle cells. *Cell Signal*. 2007;19:1023-1033
201. Castro LR, Schittl J, Fischmeister R. Feedback control through cgmp-dependent protein kinase contributes to differential regulation and compartmentation of cgmp in rat cardiac myocytes. *Circ Res*. 2010;107:1232-1240
202. Saiki RK, Gelfand DH, Stoffel S, Scharf SJ, Higuchi R, Horn GT, Mullis KB, Erlich HA. Primer-directed enzymatic amplification of DNA with a thermostable DNA polymerase. *Science*. 1988;239:487-491
203. Arber W, Linn S. DNA modification and restriction. *Annu Rev Biochem*. 1969;38:467-500
204. Cho A, Haruyama N, Kulkarni AB. Generation of transgenic mice. *Curr Protoc Cell Biol*. 2009;Chapter 19:Unit 19.11
205. Ittner LM, Gotz J. Pronuclear injection for the production of transgenic mice. *Nat Protoc*. 2007;2:1206-1215
206. Louch WE, Sheehan KA, Wolska BM. Methods in cardiomyocyte isolation, culture, and gene transfer. *J Mol Cell Cardiol*. 2011;51:288-298
207. Gotz KR, Nikolaev VO. Advances and techniques to measure cgmp in intact cardiomyocytes. *Methods Mol Biol*. 2013;1020:121-129
208. Gotz KR, Sprenger JU, Perera RK, Steinbrecher JH, Lehnart SE, Kuhn M, Gorelik J, Balligand JL, Nikolaev VO. Transgenic mice for real-time visualization of cgmp in intact adult cardiomyocytes. *Circ Res*. 2014;114:1235-1245
209. Grebe C, Klingebiel TM, Grau SP, Toischer K, Didie M, Jacobshagen C, Dullin C, Hasenfuss G, Seidler T. Enhanced expression of dyrk1a in cardiomyocytes inhibits acute nfat activation but does not prevent hypertrophy in vivo. *Cardiovasc Res*. 2011;90:521-528
210. Kass-Eisler A, Falck-Pedersen E, Alvira M, Rivera J, Buttrick PM, Wittenberg BA, Cipriani L, Leinwand LA. Quantitative determination of adenovirus-mediated gene delivery to rat cardiac myocytes in vitro and in vivo. *Proc Natl Acad Sci U S A*. 1993;90:11498-11502
211. Gorelik J, Yang LQ, Zhang Y, Lab M, Korchev Y, Harding SE. A novel z-groove index characterizing myocardial surface structure. *Cardiovasc Res*. 2006;72:422-429
212. Hu P, Zhang D, Swenson L, Chakrabarti G, Abel ED, Litwin SE. Minimally invasive aortic banding in mice: Effects of altered cardiomyocyte insulin signaling during pressure overload. *Am J Physiol Heart Circ Physiol*. 2003;285:H1261-1269
213. Kirchhefer U, Neumann J, Baba HA, Begrow F, Kobayashi YM, Reinke U, Schmitz W, Jones LR. Cardiac hypertrophy and impaired relaxation in transgenic mice overexpressing triadin 1. *J Biol Chem*. 2001;276:4142-4149

214. Smith PK, Krohn RI, Hermanson GT, Mallia AK, Gartner FH, Provenzano MD, Fujimoto EK, Goeke NM, Olson BJ, Klenk DC. Measurement of protein using bicinchoninic acid. *Anal Biochem*. 1985;150:76-85
215. Thompson WJ, Appleman MM. Multiple cyclic nucleotide phosphodiesterase activities from rat brain. *Biochemistry*. 1971;10:311-316
216. Richter W, Conti M. Dimerization of the type 4 camp-specific phosphodiesterases is mediated by the upstream conserved regions (ucrs). *J Biol Chem*. 2002;277:40212-40221
217. Kuhn M, Raida M, Adermann K, Schulz-Knappe P, Gerzer R, Heim JM, Forssmann WG. The circulating bioactive form of human guanylin is a high molecular weight peptide (10.3 kda). *FEBS Lett*. 1993;318:205-209
218. Xiang Y, Kobilka BK. Myocyte adrenoceptor signaling pathways. *Science*. 2003;300:1530-1532
219. Rapoport RM, Draznin MB, Murad F. Sodium nitroprusside-induced protein phosphorylation in intact rat aorta is mimicked by 8-bromo cyclic gmp. *Proc Natl Acad Sci U S A*. 1982;79:6470-6474
220. Thunemann M, Wen L, Hillenbrand M, Vachaviolos A, Feil S, Ott T, Han X, Fukumura D, Jain RK, Russwurm M, de Wit C, Feil R. Transgenic mice for cgmp imaging. *Circ Res*. 2013;113:365-371
221. Takimoto E, Kass DA. Role of oxidative stress in cardiac hypertrophy and remodeling. *Hypertension*. 2007;49:241-248
222. Wagner S, Seidler T, Picht E, Maier LS, Kazanski V, Teucher N, Schillinger W, Pieske B, Isenberg G, Hasenfuss G, Kogler H. Na(+)-ca(2+) exchanger overexpression predisposes to reactive oxygen species-induced injury. *Cardiovasc Res*. 2003;60:404-412
223. Chan TY, Tang PL. Characterization of the antioxidant effects of melatonin and related indoleamines in vitro. *J Pineal Res*. 1996;20:187-191
224. Stasch JP, Schmidt P, Alonso-Alija C, Apeler H, Dembowsky K, Haerter M, Heil M, Minuth T, Perzborn E, Pleiss U, Schramm M, Schroeder W, Schroder H, Stahl E, Steinke W, Wunder F. No- and haem-independent activation of soluble guanylyl cyclase: Molecular basis and cardiovascular implications of a new pharmacological principle. *Br J Pharmacol*. 2002;136:773-783
225. Potter LR, Abbey-Hosch S, Dickey DM. Natriuretic peptides, their receptors, and cyclic guanosine monophosphate-dependent signaling functions. *Endocr Rev*. 2006;27:47-72
226. Chen HH, Burnett JC, Jr. The natriuretic peptides in heart failure: Diagnostic and therapeutic potentials. *Proc Assoc Am Physicians*. 1999;111:406-416
227. Zaccolo M, Movsesian MA. Camp and cgmp signaling cross-talk: Role of phosphodiesterases and implications for cardiac pathophysiology. *Circ Res*. 2007;100:1569-1578
228. Zhang L, Kelley J, Schmeisser G, Kobayashi YM, Jones LR. Complex formation between junctin, triadin, calsequestrin, and the ryanodine receptor. Proteins of the cardiac junctional sarcoplasmic reticulum membrane. *J Biol Chem*. 1997;272:23389-23397
229. Shin DW, Ma J, Kim DH. The asp-rich region at the carboxyl-terminus of calsequestrin binds to ca(2+) and interacts with triadin. *FEBS Lett*. 2000;486:178-182
230. Kirchhefer U, Neumann J, Bers DM, Buchwalow IB, Fabritz L, Hanske G, Justus I, Riemann B, Schmitz W, Jones LR. Impaired relaxation in transgenic mice overexpressing junctin. *Cardiovasc Res*. 2003;59:369-379
231. Zhang L, Franzini-Armstrong C, Ramesh V, Jones LR. Structural alterations in cardiac calcium release units resulting from overexpression of junctin. *J Mol Cell Cardiol*. 2001;33:233-247
232. Yuan Q, Fan GC, Dong M, Altschafl B, Diwan A, Ren X, Hahn HH, Zhao W, Waggoner JR, Jones LR, Jones WK, Bers DM, Dorn GW, 2nd, Wang HS, Valdivia HH, Chu G, Kranias EG. Sarcoplasmic reticulum calcium overloading in junctin deficiency enhances cardiac contractility but increases ventricular automaticity. *Circulation*. 2007;115:300-309
233. Nikolaev VO, Moshkov A, Lyon AR, Miragoli M, Novak P, Paur H, Lohse MJ, Korchev YE, Harding SE, Gorelik J. Beta2-adrenergic receptor redistribution in heart failure changes camp compartmentation. *Science*. 2010;327:1653-1657

234. Qvigstad E, Moltzau LR, Aronsen JM, Nguyen CH, Hougen K, Sjaastad I, Levy FO, Skomedal T, Osnes JB. Natriuretic peptides increase beta1-adrenoceptor signalling in failing hearts through phosphodiesterase 3 inhibition. *Cardiovasc Res*. 2010;85:763-772
235. Mika D, Bobin P, Pomerance M, Lechene P, Westenbroek RE, Catterall WA, Vandecasteele G, Leroy J, Fischmeister R. Differential regulation of cardiac excitation-contraction coupling by camp phosphodiesterase subtypes. *Cardiovasc Res*. 2013;100:336-346
236. Patten RD, Hall-Porter MR. Small animal models of heart failure: Development of novel therapies, past and present. *Circ Heart Fail*. 2009;2:138-144
237. Rockman HA, Ross RS, Harris AN, Knowlton KU, Steinhelper ME, Field LJ, Ross J, Jr., Chien KR. Segregation of atrial-specific and inducible expression of an atrial natriuretic factor transgene in an in vivo murine model of cardiac hypertrophy. *Proc Natl Acad Sci U S A*. 1991;88:8277-8281
238. Louch WE, Bito V, Heinzel FR, Macianskiene R, Vanhaecke J, Flameng W, Mubagwa K, Sipido KR. Reduced synchrony of ca2+ release with loss of t-tubules-a comparison to ca2+ release in human failing cardiomyocytes. *Cardiovasc Res*. 2004;62:63-73
239. Brette F, Orchard C. T-tubule function in mammalian cardiac myocytes. *Circ Res*. 2003;92:1182-1192
240. Haddock PS, Coetzee WA, Cho E, Porter L, Katoh H, Bers DM, Jafri MS, Artman M. Subcellular [ca2+]i gradients during excitation-contraction coupling in newborn rabbit ventricular myocytes. *Circ Res*. 1999;85:415-427
241. Chen F, Mottino G, Klitzner TS, Philipson KD, Frank JS. Distribution of the na+/ca2+ exchange protein in developing rabbit myocytes. *Am J Physiol*. 1995;268:C1126-1132
242. Rich TC, Tse TE, Rohan JG, Schaack J, Karpen JW. In vivo assessment of local phosphodiesterase activity using tailored cyclic nucleotide-gated channels as camp sensors. *J Gen Physiol*. 2001;118:63-78
243. Moltzau LR, Aronsen JM, Meier S, Nguyen CH, Hougen K, Orstavik O, Sjaastad I, Christensen G, Skomedal T, Osnes JB, Levy FO, Qvigstad E. Serca2 activity is involved in the cnp-mediated functional responses in failing rat myocardium. *Br J Pharmacol*. 2013;170:366-379
244. Brusq JM, Mayoux E, Guigui L, Kirilovsky J. Effects of c-type natriuretic peptide on rat cardiac contractility. *Br J Pharmacol*. 1999;128:206-212
245. Nir A, Zhang DF, Fixler R, Burnett JC, Jr., Eilam Y, Hasin Y. C-type natriuretic peptide has a negative inotropic effect on cardiac myocytes. *Eur J Pharmacol*. 2001;412:195-201
246. Hirose M, Furukawa Y, Kurogouchi F, Nakajima K, Miyashita Y, Chiba S. C-type natriuretic peptide increases myocardial contractility and sinus rate mediated by guanylyl cyclase-linked natriuretic peptide receptors in isolated, blood-perfused dog heart preparations. *J Pharmacol Exp Ther*. 1998;286:70-76
247. Beaulieu P, Cardinal R, Page P, Francoeur F, Tremblay J, Lambert C. Positive chronotropic and inotropic effects of c-type natriuretic peptide in dogs. *Am J Physiol*. 1997;273:H1933-1940
248. Horio T, Tokudome T, Maki T, Yoshihara F, Suga S, Nishikimi T, Kojima M, Kawano Y, Kangawa K. Gene expression, secretion, and autocrine action of c-type natriuretic peptide in cultured adult rat cardiac fibroblasts. *Endocrinology*. 2003;144:2279-2284
249. Conti M, Beavo J. Biochemistry and physiology of cyclic nucleotide phosphodiesterases: Essential components in cyclic nucleotide signaling. *Annu Rev Biochem*. 2007;76:481-511
250. Omori K, Kotera J. Overview of pdes and their regulation. *Circ Res*. 2007;100:309-327
251. Rich TC, Fagan KA, Nakata H, Schaack J, Cooper DM, Karpen JW. Cyclic nucleotide-gated channels colocalize with adenylyl cyclase in regions of restricted camp diffusion. *J Gen Physiol*. 2000;116:147-161
252. Lima B, Forrester MT, Hess DT, Stamler JS. S-nitrosylation in cardiovascular signaling. *Circ Res*. 2010;106:633-646
253. Wegener JW, Godecke A, Schrader J, Nawrath H. Effects of nitric oxide donors on cardiac contractility in wild-type and myoglobin-deficient mice. *Br J Pharmacol*. 2002;136:415-420

254. Wegener JW, Gath I, Forstermann U, Nawrath H. Activation of soluble guanylyl cyclase by yc-1 in aortic smooth muscle but not in ventricular myocardium from rat. *Br J Pharmacol*. 1997;122:1523-1529
255. Singh RJ, Hogg N, Joseph J, Kalyanaraman B. Mechanism of nitric oxide release from s-nitrosothiols. *J Biol Chem*. 1996;271:18596-18603
256. Maragos CM, Morley D, Wink DA, Dunams TM, Saavedra JE, Hoffman A, Bove AA, Isaac L, Hrabie JA, Keefer LK. Complexes of .No with nucleophiles as agents for the controlled biological release of nitric oxide. Vasorelaxant effects. *J Med Chem*. 1991;34:3242-3247
257. Keefer LK, Nims RW, Davies KM, Wink DA. "Nonoates" (1-substituted diazen-1-ium-1,2-diolates) as nitric oxide donors: Convenient nitric oxide dosage forms. *Methods Enzymol*. 1996;268:281-293
258. Saavedra JE, Southan GJ, Davies KM, Lundell A, Markou C, Hanson SR, Adrie C, Hurford WE, Zapol WM, Keefer LK. Localizing antithrombotic and vasodilatory activity with a novel, ultrafast nitric oxide donor. *J Med Chem*. 1996;39:4361-4365
259. Moltzau LR, Meier S, Aronsen JM, Afzal F, Sjaastad I, Skomedal T, Osnes JB, Levy FO, Qvigstad E. Differential regulation of c-type natriuretic peptide-induced cgmp and functional responses by pde2 and pde3 in failing myocardium. *Naunyn Schmiedebergs Arch Pharmacol*. 2014;387:407-417
260. Zhang M, Koitabashi N, Nagayama T, Rambaran R, Feng N, Takimoto E, Koenke T, O'Rourke B, Champion HC, Crow MT, Kass DA. Expression, activity, and pro-hypertrophic effects of pde5a in cardiac myocytes. *Cell Signal*. 2008;20:2231-2236
261. Dickey DM, Flora DR, Bryan PM, Xu X, Chen Y, Potter LR. Differential regulation of membrane guanylyl cyclases in congestive heart failure: Natriuretic peptide receptor (npr)-b, not npr-a, is the predominant natriuretic peptide receptor in the failing heart. *Endocrinology*. 2007;148:3518-3522
262. Takimoto E, Belardi D, Tocchetti CG, Vahebi S, Cormaci G, Ketner EA, Moens AL, Champion HC, Kass DA. Compartmentalization of cardiac beta-adrenergic inotropy modulation by phosphodiesterase type 5. *Circulation*. 2007;115:2159-2167